Aus dem Department für Augenheilkunde Tübingen
Forschungsinstitut für Augenheilkunde

Immunological impact of intracellular *Streptococcus pyogenes* Cas9 expression on human retinal pigment epithelium

Inaugural-Dissertation
zur Erlangung des Doktorgrades
der Medizin

der Medizinischen Fakultät
der Eberhard Karls Universität
zu Tübingen

vorgelegt von

Bonillo, Mario

2022

Dekan: Professor Dr. B. Pichler

1. Berichterstatter: Professor Dr. Dr. M. D. Fischer
2. Berichterstatter: Professor Dr. E. Reisinger

Tag der Disputation 16.08.2022

Meinen Eltern

Table of contents

List of abbreviations

11-*cis*-Ral	11-*cis*-retinal
11-*cis*-Rol	11-*cis*-retinol
7-AAD	7-Aminoactinomycin D
$A_{260/280}$	absorbance at 260 and 280 nm
AAV	adeno-associated virus
AGE	advanced glycation end-product
AIM2	absent in melanoma 2
AMD	age-related macular degeneration
APC	antigen-presenting cell
at-Ral	all-*trans*-retinal
at-Rol	all-*trans*-retinol
Cas9	CRISPR-associated nuclease 9
CD40	cluster of differentiation 40
CD40L	cluster of differentiation 40 ligand
cGAS	cyclic GMP-AMP synthase
CIP	alkaline phosphatase calf intestinal
*cj*Cas9	*Campylobacter jejuni Cas9*
CMV	cytomegalovirus
CpG	deoxycytidylate-phosphate-deoxyguanylate
CRALBP	cellular retinaldehyde-binding protein
CRISPR	clustered regularly interspaced short palindromic repeats
crRNA	CRISPR RNA
CSNB	congenital stationary night blindness
DAF	decay accelerating factor
DAMP	damage-associated molecular patterns
DAPI	4′,6-diamidino-2-phenylindole
DMSO	dimethyl sulfoxide
DNA	deoxyribonucleic acid
DPBS	dulbecco’s phosphate buffered saline
DSB	double-stranded DNA break
dsDNA	double-stranded DNA
dsRNA	double-stranded RNA
ELISA	enzyme-linked immunosorbent assay
EMA	European Medicines Agency
ERK1/2	extracellular signal-regulated kinase 1 and 2
FACS	fluorescence-activated cell sorting
FasL	Fas ligand
Fc	fragment crystallizable
FcRn	neonatal Fc receptor
FDA	Food and Drug Administration
FSC	forward scattered light
HDR	Homology-Directed Repair
HI-FBS	heat-inactivated fetal bovine serum
HITI	Homology-Independent Targeting Integration

HLA	human leukocyte antigen
HMW	high molecular weight
HRP	horseradish peroxidase
ICC	immunocytochemistry
IFI16	IFN-γ-inducible 16
IFN	interferon
IL	interleukin
IPM	interphotoreceptor matrix
IRBP	interphotoreceptor retinoid-binding protein
IRD	inherited retinal disease
IRF9	interferon regulatory factor 9
ITR	inverted terminal repeat
LCA	Leber congenital amaurosis
LFA-1	lymphocyte function-related antigen-1
LPS	lipopolysaccharides
LRAT	lecithin:retinol acyltransferase
Mac-1	macrophage-1 antigen
MAPK	mitogen-activated protein kinase
MCP	membrane cofactor protein
mCRP	membrane-bound complement regulatory protein
MDA5	melanoma differentiation-associated gene 5
MFI	mean fluorescence intensity
MIP3α	macrophage inflammatory protein 3 α
MPO	myeloperoxidase
mRNA	messenger RNA
MyD88	myeloid differentiation primary response 88
NC	negative control
NEB	New England Biolabs
NET	neutrophil extracellular trap
NF-κB	nuclear factor kappa-light-chain-enhancer of activated B cells
NHEJ	Non-homologous end joining
NLR	NOD-like receptor
NLRP3	NOD-like receptor pyrin domain containing 3
NOD2	nucleotide-binding and oligomerisation domain containing 2
PAM	protospacer adjacent motif
PAMP	pathogen-associated molecular pattern
PBMC	peripheral blood mononuclear cell
PBS	phosphate-buffered saline
PCR	polymerase chain reaction
PEDF	pigment epithelium-derived factor
PFA	paraformaldehyde
PMT	photomultiplier tube
Poly(I:C)	polyinosinic:polycytidylic acid
POS	photoreceptors outer segments
PRR	pattern-recognition receptor
pUC18	plasmid of University of California 18
RAGE	receptor for advanced glycation end products
RDH	all-*trans*-retinol dehydrogenase

RE	restriction endonuclease
RIG-I	retinoic acid inducible gene-I
RLRs	retinoic acid-inducible gene-I-like receptors
RNA	ribonucleic acid
RNP	ribonucleoprotein
RP	retinitis pigmentosa
RPE	retinal pigment epithelium
rRNA	ribosomal RNA
*sa*Cas9	*Staphylococcus aureus* Cas9
SDS	sodium dodecylsulfate
SEAP	secreted embryonic alkaline phosphatase
sgRNA	single-guided RNA
*sp*Cas9	*Streptococcus pyogenes* Cas9
SSC	side scattered light
ssRNA	single-stranded RNA
STAT2	signal transducers and activators of transcription 2
STAT6	signal transducer and activator of transcription 6
STING	stimulator of interferon genes
TBK-1	TANK-binding kinase 1
TGF-β	transforming growth factor-beta
THP-1	Tohoku hospital pediatrics-1
TLR	Toll-like receptor
TMB	tetramethylbenzidine
TNF-α	tumour necrosis factor α
tracrRNA	trans-activating crRNA
tRNA	transfer RNA
VEGF	vascular endothelial growth factor
w/v	weight/volume
α-MSH	alpha-melanocyte-stimulating hormone

List of figures

List of tables

1 Introduction

CRISPR/Cas9 (clustered regularly interspaced short palindromic repeats/CRISPR-associated nuclease 9) is a powerful gene editing tool that enables precise gene editing designed to cure monogenic disorders (Suzuki et al., 2016). Inherited retinal diseases (IRDs) pose attractive targets for gene therapy, as local conditions in the eye have several features advantageous for gene therapy (Peddle and MacLaren, 2017). Mutations in the retinal pigment epithelium (RPE) can cause IRDs, making the RPE a possible target for CRISPR/Cas9 gene editing (von Lintig et al., 2010). A thorough investigation of retinal Cas9 immunogenicity is crucial in ensuring the safety and efficacy of future retinal CRISPR/Cas9 gene therapies. (Bonillo et al., 2022, Pfromm et al., 2022)

1.1 IRDs

In a cross-sectional survey in the United Kingdom, 88% of participants rated sight as their most valuable sensory modality, indicating that vision impairment or loss has a tremendous negative impact on the quality of life (Enoch et al., 2019).

IRDs are a heterogeneous group of rare degenerative diseases of the retina which can ultimately lead to blindness, caused by inherited genetic mutations (Pfromm et al., 2022). Retinitis pigmentosa (RP) occurs with a prevalence of nearly 1:4000 and is the most common IRD. RP can be caused by various mutations including X-linked, autosomal dominant or autosomal recessive mutations. Those mutations result in the progressive dystrophy of photoreceptors and the RPE. These cell losses are associated with a severe concentric visual field restriction and a significant reduction in visual acuity. The disease initially affects the RPE and the rods, affecting cones later in the disease progression. With no curative therapy currently available, the fact that most patients with RP ultimately lose their sight indicates a therapeutic gap to be filled by future research (Pfromm et al., 2022). (Grehn, 2019)

Gene therapy, including CRISPR/Cas9 therapies, could facilitate the treatment of RP and help to prevent a vision loss and to improve the quality of life of patients with heritable RP (Hung et al., 2016b, Peddle and MacLaren, 2017).

1.2 Gene therapy

Gene therapy is defined as the application of nucleic acids into cells or tissues to treat genetic disorders. In contrast to gene editing, which describes the active modification of a defective gene, gene therapy is defined as the introduction of a healthy gene (Maeder and Gersbach, 2016). Viral, as well as non-viral vectors can be used to deliver therapeutic genes (Lipinski et al., 2013). There are various gene therapeutic approaches to the treatment of IRDs, depending on the causative mutation. Loss-of-function mutations lead to genetic defects which can be addressed through supplementation of the physiological gene variant. In contrast, gain-of-function mutations may induce the expression of harmful proteins, the production of which can be suppressed via gene therapy. Furthermore, gene editing can correct unfavourable mutations *in vivo*, and splicing modifications, e.g. exon skipping, can be accomplished using anti-sense oligonucleotides. (Bonillo et al., 2022, Kumaran et al., 2018, Pfromm et al., 2022) As the eye is a promising target for future gene therapies due to its immune privilege as well as its easy accessibility, the previously mentioned concepts have already been implemented in clinical trials of retinal gene therapy (Lipinski et al., 2013, Pfromm et al., 2022). For instance, in a phase 1 and phase 2a trial, the safety of a retinal gene therapy applying a therapeutic gene for wet age-related macular degeneration (AMD) has been demonstrated (Constable et al., 2016, Heier et al., 2017). In another clinical trial, anti-sense oligonucleotides were used to suppress the expression of a mutated protein causative for RP (ClinicalTrials.gov, n.d.-c). As Russell et al. (2020) have demonstrated the safety of QR-1123, which binds to a mutated ribonucleic acid (RNA) and thus ensures adequate splicing, a phase 2/3 study is currently underway to assess its efficacy in treating Leber congenital amaurosis (LCA) (Bonillo et al., 2022, ClinicalTrials.gov, n.d.-b). Moreover, Luxturna, a gene-supplementing therapy for LCA, has recently received the approval of the Food and Drug Administration (FDA) and European Medicines Agency (EMA), emphasising the relevance of gene therapy for IRDs (Bonillo et al., 2022, European Medicines Agency, 2018, Pfromm et al., 2022, Russell et al., 2017, U.S. Food and Drug Administration, 2017).

1.3 CRISPR/Cas9 as an important gene therapy tool

1.3.1 Mechanism

CRISPR/Cas9 represents a powerful tool for modifying deoxyribonucleic acid (DNA) sequences and has rapidly gained popularity in the emerging field of gene therapy (Cong et al., 2013, Pfromm et al., 2022). CRSPR/Cas9 is a naturally occurring system used by bacteria and archaea to protect against viral infection (Bonillo et al., 2022, Li et al., 2013, Peddle and MacLaren, 2017).

CRISPR is a small DNA region found in the genomes of bacteria and archaea. Foreign DNA sequences such as viral DNA are integrated as spacer sequences between short CRISPR regions. These CRISPR and spacer sequences are then transcribed into CRISPR RNA (crRNA), which is converted from its original form into a mature and functional molecule by RNase III and the trans-activating crRNA (tracrRNA). The mature crRNA contains a copy of the CRISPR sequence and the integrated foreign DNA. (Max Planck Gesellschaft, n.d.)

Cas9 is a bacterial DNA endonuclease which can induce double-stranded DNA breaks (DSBs) (Wu et al., 2017). Single-guided RNA (sgRNA), an artificial merge of crRNA and tracrRNA, binds to target DNA sequences and guides Cas9 to the desired sequence by complexing with Cas9 (Bonillo et al., 2022, Cong et al., 2013, Jinek et al., 2012). In addition to the simple design and efficient manufacturing, sgRNA ensures a high cleaving efficacy; the use of sgRNAs increases the advantageous capability of CRISPR/Cas9 systems to ensure sequence-specific DSBs (He et al., 2016, Wu et al., 2017). (Pfromm et al., 2022)

In addition to sgRNAs, Cas9 requires a protospacer adjacent motif (PAM) site to recognise its target region. The PAM site is a short DNA sequence 3 to 8 bp long, adjacent to the target region (Bonillo et al., 2022, Jinek et al., 2012). PAM sequences differ between Cas9 orthologs. Cas9 isolated from *Streptococcus pyogenes* (*sp*Cas9), for example, is the most commonly utilized Cas9 ortholog (Jo et al., 2019a). Its PAM sequence 5'-NGG-3' is shorter than that of other Cas9 orthologs (Kim et al., 2017). Its binding site is able to recognize multiple sequences, as the first position, “N”, represents any nucleotide. The short length of the *sp*Cas9 PAM sequence establishes the ability to potentially target various

genomic loci (Chew et al., 2016). This makes *sp*Cas9 a very promising Cas9 ortholog and is the reason that the experiments described in this thesis were carried out using *sp*Cas9. In contrast, though, longer PAM sequences may reduce unwanted off-target effects (Müller et al., 2016). Additionally, as the *sp*Cas9 gene is larger than the *Staphylococcus aureus* Cas9 (*sa*Cas9) and *Campylobacter jejuni* Cas9 (*cj*Cas9), the delivery of *sp*Cas9 into cells may be more challenging. (Kim et al., 2017, Peddle and MacLaren, 2017, Ran et al., 2015)

In response to viral DNA complementary to pre-existing crRNA, the Cas9 endonuclease cleaves and inactivates the viral DNA, preventing further transcription. The lack of PAM sequences in the bacterial genome prevents self-destruction via bacterial CRISPR/Cas9. (Cong et al., 2013, Jinek et al., 2012, Peddle and MacLaren, 2017)

A Cas9-induced DSB can either be repaired by a non-homologous end joining (NHEJ) or homology-directed repair (HDR) process. If no complementary DNA sequence is available NHEJ is employed. NHEJ is an error-prone repair mechanism, which often leads to random insertions and deletions at the site of the DNA break. As insertions and deletions may cause frame-shift mutations in an exon region, gene expression after NHEJ is often dysfunctional. In contrast, DSB may be repaired through HDR if a complementary DNA sequence is available leading to a precise DSB correction. HDR enables researchers to insert specific mutations and edit the genome precisely, by inserting a DNA sequence into the cell which contains the desired mutation and exhibits a high degree of homology to the DSB site. The presence of the HDR pathway increases the probability of the successful integration of artificially inserted DNA sequences into the cellular genome. Consequently, using the CRISPR/Cas9 systems with following HDR repair, precise correction of the DSB is performed, making CRISPR/Cas9 an attractive gene editing tool. (Fishman-Lobell et al., 1992, Lino et al., 2018, Peddle and MacLaren, 2017, Rouet et al., 1994)

1.3.2 Off-target mutations

In addition to the numerous advantages of CRISPR-Cas9 technology, potential challenges exist, which require further investigation to secure the safety and efficiency of future gene editing therapies (Bonillo et al., 2022, Peddle and MacLaren, 2017).

Besides modification at the target region, Cas9 is able to non-specifically cleave DNA sites containing sequences similar to the target region. Non-specific, off-target DSB created by erroneous Cas9 cleavage within an exon region of a tumour suppressor gene, for example, could induce the development of cancer. (Cho et al., 2014, Hung et al., 2016b)

It remains unclear how much discrepancy between the sgRNA and target sequence prevents unspecific gene editing (Fu et al., 2013, Smith et al., 2015). However, the frequency of unspecific DNA modifications post Cas9 editing is classified as very rare (Iyer et al., 2015). Several adjustments to existing CRISPR/Cas9 systems, such as the adaption of the Cas9 concentration (Hsu et al., 2013) and the development of artificial Cas9 molecules (Kleinstiver et al., 2016, Ran et al., 2013), have been developed in recent years to improve the specificity, and therefore safety, of the CRISPR/Cas9 system. (Bonillo et al., 2022)

1.3.3 Cas9 delivery

Cas9 can be transferred into cells in a variety of forms including messenger RNA (mRNA) or a plasmid expressing Cas9. Preformed complexes of Cas9 protein and sgRNA, so-called ribonucleoproteins (RNPs), pose an alternative approach to Cas9 delivery (Cromer et al., 2018). Efficient Cas9 delivery is feasible with several methods including viral vectors, such as lentiviruses, adenoviruses or adeno-associated viruses (AAVs). Additionally, electroporation, microinjection, and non-viral vectors, such as nanoparticles and cationic lipids, are alternative transfer methods. (Bonillo et al., 2022, Liu and Shui, 2016, Pfromm et al., 2022)

AAVs, small single-stranded DNA viruses, are a promising delivery technique *in vivo*, but their packaging capacity is limited (Wu et al., 2010). Due to the relatively

large size of the *sp*Cas9 gene sequence, approximately 4.1 kbp, it is difficult to package *sp*Cas9 together with an sgRNA in a single AAV vector, whose carrying capacity is around 5 kbp (Kim et al., 2017, Ran et al., 2015). Alternative transduction methods include a split-*sp*Cas9 systems which utilise two AAV vectors to increase the overall packaging capacity (Truong et al., 2015, Zetsche et al., 2015). Additionally, Reichel et al. (2017) demonstrated that AAVs trigger innate and adaptive immune responses *in vivo*. (Bonillo et al., 2022)

Cationic lipid transfection is a common efficient, and reproducible method often applied *in vitro* (Liu and Shui, 2016), which is why cationic lipid transfection was chosen for us in this project. *Sp*Cas9 plasmids have been used to transfect and edit retinal cells in several retinal gene therapy studies, indicating the high clinical relevance of the investigation of potential immune responses to these developing therapies (Bakondi et al., 2016, Pfromm et al., 2022, Wang et al., 2014a). The potentially toxic and immunological effects of intracellular plasmids remain unclear; this investigative gap was addressed in part by the work presented in this thesis.

1.3.4 Retinal CRISPR/Cas9 gene therapy

Since pathological mutations causative to RP, such as *rhodopsin* (RHO) or *RPE65* mutations, are attractive targets for gene therapy, current developments in ocular gene therapy are illustrated using the example of RP (Booij et al., 2005, Sung et al., 1991). The knock-down of dominant pathogenic mutations using NHEJ is currently one of the most promising approaches to retinal CRISPR/Cas9 gene therapy for IRDs (Pfromm et al., 2022). Since HDR occurs mainly in mitotically active cells, photoreceptor and RPE cells have a low HDR rate, making retinal gene editing via the HDR pathway fundamentally difficult. (Duan et al., 2016, Iyama and Wilson III, 2013, Peddle and MacLaren, 2017)

However, Jo et al. (2019a) were recently able to demonstrate the induction of HDR in RPE cells. Latella et al. (2016) reported the successful knock-down of a dominant mutation of the *RHO* gene via NHEJ. A combination of an sgRNA and an *sp*Cas9 plasmid were able to eliminate 70 - 82% of mutated alleles *in vitro*.

Furthermore, gene editing was also achieved *in vivo*, but with a significantly lower editing-rate (Latella et al., 2016).

An additional challenge to treating IRDs are autosomal recessive mutations causative for RP and other IRDs. Treatment of these mutations requires the restoration of wild type allele function, which is challenging but still feasible using CRISPR/Cas9 systems (Pfromm et al., 2022). Generally, the HDR pathway is used for this purpose, but, as mentioned above, it is not highly active in photoreceptors and RPE cells making the treatment of autosomal recessive mutations in these cell lines more challenging. (Peddle and MacLaren, 2017)

Homology-independent targeting integration (HITI) is a promising alternative for HDR. In HITI Cas9 cleaves the genomic DNA target site once and additionally cleaves the DNA insert at both ends. Afterwards, the insert is incorporated into the genomic target region using NHEJ. If the DNA insert is integrated incorrectly, Cas9 will cleave the incorrect integration site, as this incorrect integration generates a new cleaving site. The insert is thusly removed from the target region until it is correctly integrated. HITI thereby circumvents the HDR pathway by using the NHEJ pathway to enable high efficacy knock-in edits in dividing and non-dividing cells. Suzuki et al. (2016) demonstrated the effectivity of a HITI-mediated gene editing model *in vitro* and *in vivo* using a rat model of RP. In 2019, a clinical trial began in which a gene was edited *in vivo* using CRISPR/Cas9 technology to correct an LCA-causative point mutation (Bonillo et al., 2022, ClinicalTrials.gov, n.d.-a, Pfromm et al., 2022). The fact that CRISPR/Cas9 can be used to knock-down dominant pathogenic mutations as well as to correct mutations *in vivo* to restore wild type function makes it a promising component of future gene therapies. (Peddle and MacLaren, 2017)

1.4 Cas9 immunogenicity

Due to the intracellular nature of the *sp*Cas9 protein, sufficient investigation of the reactions of the adaptive and innate immune systems to *sp*Cas9 must be undertaken to assess its potential immunogenicity. Recently, the relative lack of investigation into this topic has prompted researchers to explore whether pre-

existing immunity to *sp*Cas9 is present in humans. Several publications were able to demonstrate the existence of pre-existing immune reactivity to *sp*Cas9 (Charlesworth et al., 2019, Pfromm et al., 2022, Simhadri et al., 2018, Wagner et al., 2019). Charlesworth et al. (2019) tested for the presence of anti-*sp*Cas9 antibodies in human serum and anti-*sp*Cas9 T cells in human peripheral blood. They demonstrated the presence of IgG-ABs against *sp*Cas9 in 58 % and against *sa*Cas9-ABs in 78% of all samples (Bonillo et al., 2022, Charlesworth et al., 2019). Furthermore, anti-*sp*Cas9 T cells and anti-*sa*Cas9 T cells were detected in 67% and 78% of the blood specimens, respectively (Bonillo et al., 2022, Charlesworth et al., 2019). In contrast, Simhadri et al. (2018) only detected *sp*Cas9 specific antibodies in 2.5% of all samples. Differing test modalities, however, may explain the varying prevalence of *sp*Cas9 specific antibodies seen between studies (Charlesworth et al., 2019, Simhadri et al., 2018).

Wagner et al. (2019) demonstrated that such pre-existing adaptive immunity could impact the efficacy of Cas9 gene therapy. *Sp*Cas9 plasmids were injected into lymphoblastoid B cells via electroporation and incubated in the presence of *sp*Cas9 specific T cells (Wagner et al., 2019). Wagner et al. (2019) showed that *sp*Cas9-expressing cells were likely preferably eliminated by cytotoxic T cells. Moreno et al. (2019) also observed that cells presenting Cas9 epitopes were targeted and eliminated by anti-Cas9 T cells. The results shown by Wagner et al. (2019) and Moreno et al. (2019) emphasise the relevance of Cas9-specific immunogenicity to the safety and efficacy of gene therapy, as both pre-existing and induced adaptive immunity can lead to the elimination of genetically modified cells (Pfromm et al., 2022). However, *sp*Cas9 regulatory T cells could potentially be used to impair the function of *sp*Cas9 effector T cells and thus counteract the problem of pre-existing Cas9 immunity (Wagner et al., 2019). (Bonillo et al., 2022) Chew et al. (2016) dealt with the question of how the immune system reacts to intramuscularly expressed *sp*Cas9. *Sp*Cas9 was transduced into the murine muscle using viral vectors such as AAV. The intramuscular expression of *sp*Cas9 leads to CD45+ cell activation, including antigen-specific T cell activation and *sp*Cas9 specific ABs (Bonillo et al., 2022). This study further demonstrated that

*sp*Cas9 could induce cellular and humoral immune responses. (Chew et al., 2016)

Not only the presence of Cas9-modified cells may be immunogenic. Extracellular Cas9 may potentially trigger varying proinflammatory pathways and must also be taken into consideration when assessing the immune-modulating effects of Cas9 therapies. Kang et al. (2018) demonstrated that extracellular Cas9 protein induces proinflammatory cytokine secretion (Bonillo et al., 2022, Pfromm et al., 2022).

The effect of proinflammatory cytokines and immune responses on the efficacy of CRISPR/Cas9 needs to be assessed. However, Machitani et al. (2017) showed that interferon α (IFN α), the production of which can be induced by non-viral and viral vectors, significantly reduces the expression of sgRNA. Thereby, an IFN α-mediated immune response significantly impairs the cleaving efficacy of CRISPR/Cas9-mediated gene editing (Machitani et al., 2017). (Bonillo et al., 2022, Pfromm et al., 2022)

In contrast to Cas9, CRISPR sequences vary depending on potential gene therapy targets (Jinek et al., 2012), which is why the present study only assesses immune responses to Cas9 and not CRISPR. Cas9 DNA, RNA and/or a subsequent Cas9 protein could each initiate immune responses, which may attenuate the effects of gene therapies (Bonillo et al., 2022, Cromer et al., 2018). According to current research, Cas9 is a weak immunogen, but retinal Cas9 immunogenicity remains to be precisely characterised. (Crudele and Chamberlain, 2018, Pfromm et al., 2022)

1.5 Ocular immune privilege

Since immune responses to gene therapy vary between the target cells (Chew et al., 2016, Cromer et al., 2018), an understanding of the eye’s unique immunological microenvironment is crucial to assessing potential immune responses to ocular gene therapy. Local immune reactions as well as inflammatory responses to external stimuli are often suppressed, which means that the eye rarely rejects foreign tissues (Medawar, 1948). This phenomenon is

referred to as the ocular immune privilege. It is commonly believed that the eye suppresses local immune responses to prevent excessive immune reactions that might cause photoreceptor damage and long-term vision impairment (Perez and Caspi, 2015, Streilein, 2003, Zhou and Caspi, 2010). (Bonillo et al., 2022)

Several aspects combine to form the foundation of the ocular immune privilege. The absence of adequate lymph drainage plays a decisive role, as antigens are presented to B and T cells in lymph nodes via lymphatic drainage pathways. The venous drainage of ocular antigens consequently minimises B and T cell sensitisation. (Bonillo et al., 2022, Streilein, 1997)

Likewise, both membrane-bound and soluble immunosuppressive factors are present intraocularly (Holtkamp et al., 1998). For example, transforming growth factor-beta (TGF-β) (Cousins et al., 1991) and alpha-melanocyte-stimulating hormone (α-MSH) (Taylor et al., 1992) inhibit immunocompetent cells. In addition, the constitutive expression of Fas ligand (FasL) on the surface of ocular cells is believed to contribute decisively to the immune privilege of the eye (Streilein, 1997). Griffith et al. (1995) showed that Fas-FasL interaction induces apoptosis in inflammatory cells which enter the eye. Additionally, the entry of blood-borne cells into the ocular tissue is strictly regulated by the blood-retina barrier, which protects the eye from systemic influences (Streilein, 1997). One major component of this blood-retina barrier is the RPE (Ban and Rizzolo, 2000). (Bonillo et al., 2022)

1.6 RPE

The RPE plays a vital role in the ocular immune system as it contributes significantly to the immune privilege of the eye and interacts with the innate and adaptive immune system (Ban and Rizzolo, 2000, Detrick and Hooks, 2020, Holtkamp et al., 2001). Since the RPE is involved in the pathogenesis of several IRDs, it also represents an attractive gene therapy target, but may additionally function as local Cas9 sensor (von Lintig et al., 2010). (Bonillo et al., 2022, Pfromm et al., 2022)

1.6.1 Structure and localisation

The RPE consists of a monolayer of pigmented cells found between the photoreceptor outer segments (POS) and the Bruch's membrane that shields the inner eye from the fenestrated endothelium of the choriocapillaris. The RPE represents the outermost layer of the retina. It is polarised and encloses the POS, with its 5-7 µm long microvilli on its apical side. The basolateral membrane of the RPE is characterised by deep folding with many mitochondria in its vicinity. The RPE cells are linked by tight junctions that generate a high grade of paracellular resistance (Ban and Rizzolo, 2000). Consequently, a barrier between the subretinal space and the choriocapillaris is established by the RPE, which is why it represents a key component of the blood-retina barrier. (Ban and Rizzolo, 2000, Boulton and Dayhaw-Barker, 2001, Strauss, 2005)

1.6.2 Functions

RPE cells are responsible for absorbing scattered light focused on the retina through the lens. Additionally, RPE cells contain various pigments that filter and absorb light of specific wavelengths to improve the optical quality. Furthermore, due to the high concentrations of antioxidants such as superoxide dismutase (Newsome et al., 1990) and catalase (Miceli et al., 1994), the RPE reduces the oxidative damage caused by phagocytosis. Lipids or proteins, which have been damaged by reactive oxygen species, for example, are identified and restored by RPE cells. (Strauss, 2005)

RPE cells also play a crucial role in the visual cycle as they absorb vitamin A (all-*trans*-retinol) from the blood of the choriocapillaris as well as from the photoreceptors. Photoreceptors produce all-*trans*-retinol (*at*-Rol) during the visual cycle, which cannot be entirely isomerised to 11-*cis*-retinal (11-*cis*-Ral) by the photoreceptors themselves. The RPE takes over this function and transports 11-*cis*-Ral back to the photoreceptors. There it binds to opsin to induce a phototransduction cascade. (Baehr et al., 2003)

Fig. 1 displays an overview of the visual cycle and the associated retinal diseases.

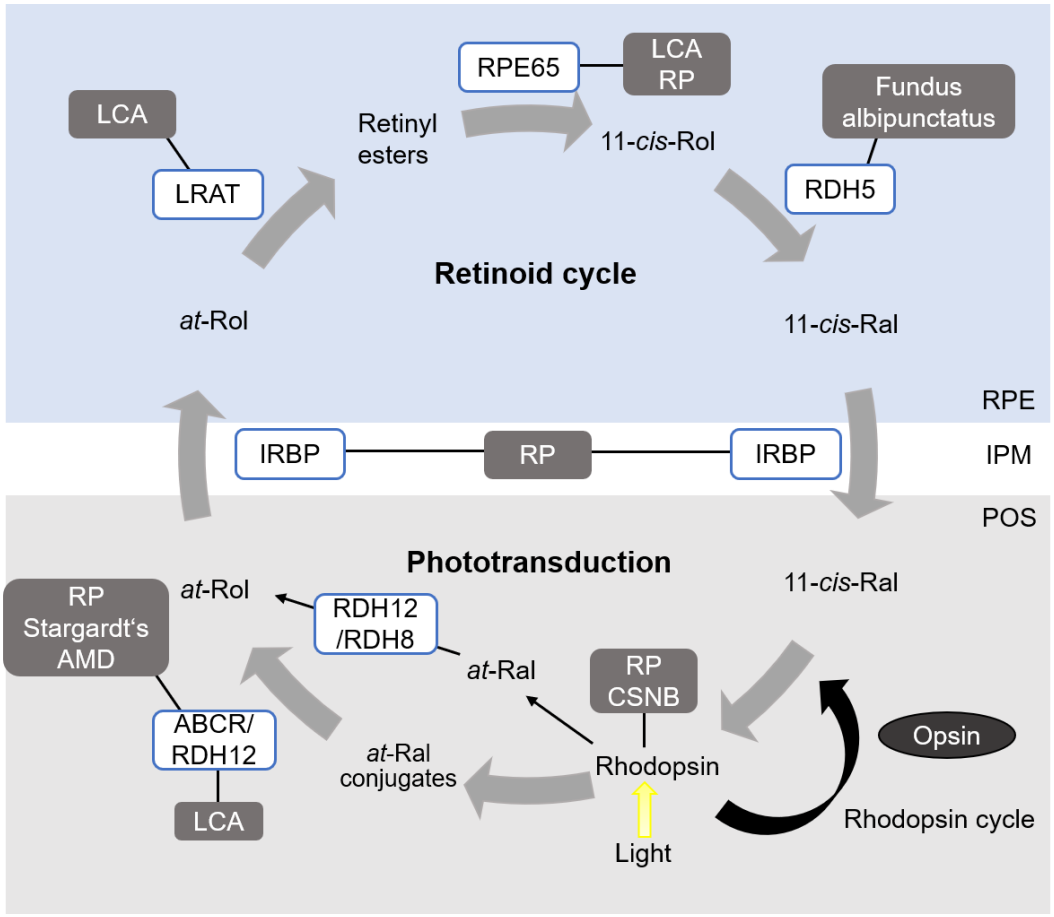

Fig. 1: Visual cycle and associated retinal diseases.

A simplified representation of the visual cycle depicting key enzymes and their associated retinal diseases: 11-*cis*-retinal (11-*cis*-Ral); all-*trans*-retinal (*at*-Ral); all-*trans*-retinol dehydrogenase (RDH); all-*trans*-retinol (*at*-Rol); interphotoreceptor retinoid-binding protein (IRBP); interphotoreceptor matrix (IPM); lecithin:retinol acyltransferase (LRAT); 11-*cis*-retinol (11-*cis*-Rol); Defective proteins caused by mutations to these enzymes can lead to retinal diseases, which are displayed in the grey boxes: age-related macular degeneration (AMD), congenital stationary night blindness (CSNB), Fundus albipunctatus, Leber congenital amaurosis (LCA) and Stargardt's disease (Kiser et al., 2012). Adapted from von Lintig et al. (2010).

Additionally, the RPE serves a transport function in the eye. Hughes et al. (1984) demonstrated that the RPE transports ions and water from the subretinal space towards the choriocapillaris, thereby ensuring the adhesion of photoreceptors to the retina (Frambach et al., 1989). Moreover, the removal of the metabolic end products of the photoreceptors by the RPE, including lactate, provides a constant retinal pH value (Hamann et al., 2000). The RPE also supplies the photoreceptors

with glucose and other nutrients via the GLUT1 transporter present on the apical and basolateral RPE membranes (Harik et al., 1990, Kwon and Freeman, 2020). In order to ensure optimal functioning of the photoreceptors, the POS is regularly renewed (Hall et al., 1969) and phagocytised by the RPE (Bibb and Young, 1974). The RPE also serves a secretory role in the healthy eye, as RPE cells secrete growth factors, such as pigment epithelium-derived factor (PEDF) (Dawson et al., 1999) and vascular endothelial growth factor (VEGF) (Adamis et al., 1993). It has been demonstrated that PEDF serves a neurotrophic function by protecting photoreceptors from light damage and minimising ischemic injuries (Cao et al., 2001, Ogata et al., 2001). Blaauwgeers et al. (1999) stated that RPE cells secrete VEGF mainly basolaterally in the direction of the choriocapillaris, where it influences neovascularisation and the integrity of the choroidal epithelium's fenestrations (Roberts and Palade, 1995). (Strauss, 2005)
Furthermore, the RPE shields the inner eye from exposure to the systemic bloodstream, which contributes to the maintenance of the ocular immune privilege (see chapter 1.5) (Bonillo et al., 2022, Ishida et al., 2003).

1.6.3 Interaction with the innate immune system

The innate immune system does not require antigen imprinting or adaption to eliminate pathogens. It becomes active immediately after pathogen contact leading to activation of both cellular and humoral defence mechanisms. Since no pathogen-specific adaptation takes place during the innate immune response, the innate immune system functions non-specifically. Innate immune components include microbial sensors, the complement system, cytokines, and chemokines. Monocytes, macrophages, dendritic cells, granulocytes, mast cells and NK cells also serve as key components of the innate immune system. (Detrick and Hooks, 2020)

1.6.3.1 Pattern-recognition receptors (PRR)

PRRs are responsible for the detection of microbial pathogen-associated molecular patterns (PAMPs) and damage-associated molecular patterns (DAMPs). Pathogen recognition often results in proinflammatory chemo- and cytokine secretion. Examples of cell-associated PRRs are NOD-like receptors (NLRs), receptor for advanced glycation end products (RAGE), cytosolic DNA sensors, retinoic acid-inducible gene-I-like receptors (RLRs), and Toll-like receptors (TLRs). (Bonillo et al., 2022, Kauppinen et al., 2016)

TLRs are microbial sensors that detect pathogens including bacteria or viruses. Different TLR types are classified by differing ligand specificity and cellular localisation. Human RPE cells express many TLRs (1 through 10), demonstrating their importance as a rapid defence system for the retina (Kumar et al., 2004, Mai et al., 2014, Pfromm et al., 2022). TLR3 is one of the most frequently expressed TLR on human RPE cells, and is essential for the recognition of and response to a viral infection (Kumar et al., 2004). TLR3 recognises double-stranded RNA (dsRNA) motifs, such as the dsRNA analogue polyinosinic:polycytidylic acid (Poly(I:C) or intermediates of viral replication (Alexopoulou et al., 2001, Pfromm et al., 2022). The cellular endosome is the locus of TLR3 as well as TLR9. TLR9 acts as an intracellular DNA sensor that detects double-stranded DNA (dsDNA). In particular, bacterial deoxycytidylate-phosphate-deoxyguanylate (CpG) DNA activates TLR9. Activation of TLRs can lead to the secretion of various cytokines, which can trigger a rapid immune response. (Bauer et al., 2001, Bonillo et al., 2022, Detrick and Hooks, 2020)

1.6.3.2 Cytokines

Cytokines are a heterogeneous group of proteins that primarily act as signal transducers between cells. They are involved in proinflammatory and anti-inflammatory processes as well as facilitating the interaction between the innate and adaptive immune systems. In the retina, the RPE plays a prominent role, as RPE cells produce numerous cytokines, some of which are highlighted below (Pfromm et al., 2022). (Bonillo et al., 2022, Detrick and Hooks, 2020)

Interleukin 1 (IL-1) is a proinflammatory cytokine and one of the most potent cytokines in terms of cellular activation and immune cell stimulation. Therefore, IL-1 plays a decisive role in modulating the innate immune response. The cell-associated IL-1α and the secreted IL-1β are the most common variants of IL-1, and both cytokines bind to the same receptor. Jaffe et al. (1992) showed that unstimulated RPE cells express neither IL-1α mRNA nor IL-1α protein. Both IL-1α mRNA and IL-1α protein are inducible by IL-1, tumour necrosis factor α (TNF-α), or lipopolysaccharides (LPS) (Jaffe et al., 1992, Planck et al., 1993). These studies also reported that RPE cells do not constitutively express IL-1β, but IL-1α, IL-1β, or TNF-α exposure are capable of inducing IL-1β gene expression (Jaffe et al., 1992, Planck et al., 1993). Based on these studies, the role of RPE-produced IL-1 in inflammatory reactions in the posterior region of the eye was found to be marginal. Nevertheless, IL-1 plays a fundamental role in the induction of other cytokines. (Holtkamp et al., 2001)

Interleukin 6 (IL-6) can have similar and partly synergistic effects to IL-1. IL-6 activates B and T cells and induces T cell and macrophage activation. IL-6 is primarily produced by immune cells, but may also be produced by endothelial and epithelial cells. (Holtkamp et al., 2001, Neta et al., 1988) Planck et al. (1992) demonstrated that human RPE cells are capable of IL-6 secretion *in vitro* after stimulation with IL-1α or IL-1β (Bonillo et al., 2022). TNF-α represents an additional IL-6 inducer (Benson et al., 1992). Chen et al. (2018) showed that IL-6 release from ARPE-19 cells is mediated through the same signaling molecules as IL-8 release (Pfromm et al., 2022). Furthermore, IL-6 is secreted in a polarised manner, meaning that RPE cells release IL-6 mainly basolaterally towards the choroid (Holtkamp et al., 1998). Thus, IL-6 plays a pivotal role in the ocular inflammatory response of the posterior segment of the eye. (Holtkamp et al., 2001)

Another crucial proinflammatory cytokine is TNF-α, which is particularly relevant to the initiation of an inflammatory immune response (Beutler and Cerami, 1989). TNF-α is mainly produced by macrophages and monocytes. Tanihara et al. (1992) revealed that IL-1β stimulation of RPE cells leads to expression of the *TNFα* gene but does not result in the secretion of the protein. However, it is

unclear whether human RPE cells are able to secrete TNF-α. (Holtkamp et al., 2001)

Immune cells, as well as endothelial cells or fibroblasts, can attract and activate neutrophil granulocytes using Interleukin 8 (IL-8). IL-8 is a highly chemotactic agent for neutrophil granulocytes and plays a role in neovascularisation as well as in the induction of adhesion molecules (Baggiolini et al., 1989, Pfromm et al., 2022, Strieter et al., 1992). Elner et al. (1990) found that human RPE cells secret IL-8 in response to IL-1β, TNF-α, and LPS stimulation (Bonillo et al., 2022). They also demonstrated that IL-1β is the most potent inducer of IL-8 in the human RPE. Elner et al. (1997) showed that IL-8 is rarely cell-associated, indicating an efficient secretion, predominantly on the basolateral side of the RPE. It was suggested that RPE cells could regulate the activity of neutrophil granulocytes in the posterior eye via IL-8 secretion (Elner et al., 1997, Smith et al., 1994). (Holtkamp et al., 2001)

Type 1 IFNs, such as IFN-α and IFN-β, represent a pivotal group of mediators of the unspecific immune response and are mainly involved in the immune response to viral pathogens (Muller et al., 1994). RPE cells have been proven to produce IFN-β, which has an immunomodulatory function (Hooks et al., 2008). Hooks et al. (2008) showed that IFN-β plays an anti-inflammatory role in the retina by inhibiting adhesion molecules and chemokines to prevent severe retinal immune responses and destruction. The production of type 1 IFNs were assessed in this thesis, as Muerdter et al. (2018) and Mann et al. (2012) detected a type 1 IFN release in response to DNA plasmids. (Bonillo et al., 2022, Pfromm et al., 2022)

INF-γ is another immunologically relevant cytokine for the innate but also the adaptive immune response. T lymphocytes and NK cells are the main producers of IFN-γ, but professional antigen-presenting cells (APCs) such as B cells can secrete IFN-γ as well. IFN-γ secretion triggers the activation of macrophages and the upregulation of MHC I, which induces cell-associated immunity. Furthermore, MHC II can be upregulated in both professional and unprofessional APCs such as RPE cells (Kanuga et al., 2002, Pfromm et al., 2022). MHC II upregulation may result in the activation of CD4+ T cells. (Frucht et al., 2001, Schroder et al., 2004)

Cluster of differentiation 40 ligand (CD40L) is an inflammatory mediator that is expressed by activated T cells and other immune and non-immune cells such as epithelial cells (Schönbeck and Libby, 2001). The interaction of CD40L and its receptor, cluster of differentiation 40 (CD40), which is present on APCs, is necessary for the activation of APCs (Bian et al., 2018). Human RPE cells have been shown to express the CD40L receptor, and CD40L, as well as its receptors, are involved in various ocular inflammatory processes (Bian et al., 2018, Portillo et al., 2008, Portillo et al., 2017).

Fig. 2 gives a simplified overview of the role of cytokines in selected immune cells relevant for this thesis.

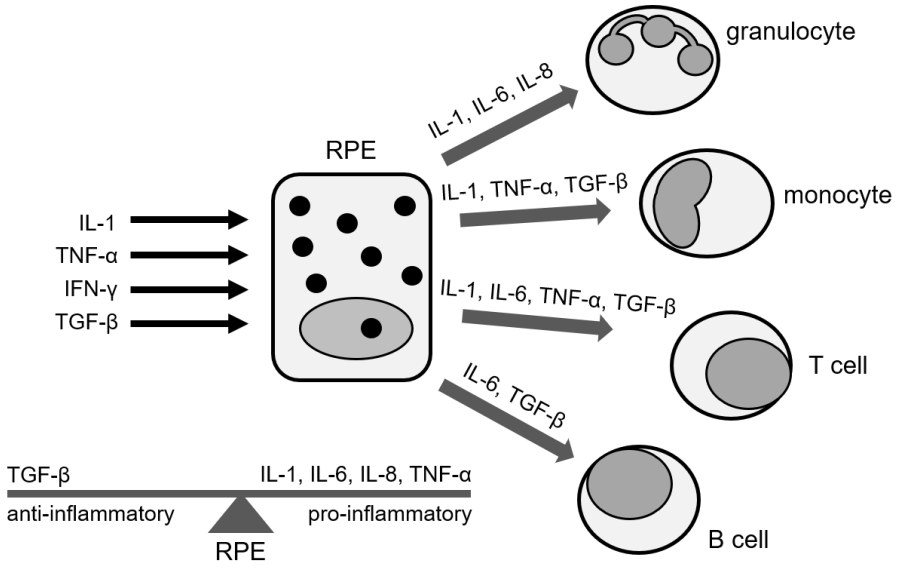

Fig. 2: RPE cytokine production and downstream immune cell modulation.

Simplified scheme of the relevant cytokines that influence cytokine secretion in RPE cells. Immune cells which are modulated by RPE-produced cytokines are shown. Some cytokines are classified as anti-inflammatory or proinflammatory. Adapted from Holtkamp et al. (2001).

1.6.3.3 Complement system

The complement system belongs to the humoral component of the innate immune system and serves to eliminate cellular pathogens. RPE cells express complement system components, like C3a and C5a receptors (Brandstetter et al., 2015). The C5a receptor is activated via binding C5a, leading to an inflammatory reaction (Fukuoka et al., 2003). Host tissue must be protected from

the damage caused by the activation of the complement system, which is ensured by the presence of complement regulating proteins. Bora et al. (1993) showed that the following membrane-bound complement regulatory proteins (mCRPs) are expressed in the eye: CD59, membrane cofactor protein (MCP) and decay accelerating factor (DAF). CD59 is present in all layers of the retina (Bora et al., 1993). Yang et al. (2009) found that human RPE cells express CD59, which is induced by proinflammatory cytokines like TNF-α and IL-1β. Furthermore, Hahn et al. (1992) stated that CD59 plays a role in T cell activation by RPE cells. The presence of mCRPs demonstrates that a regulatory system exists in the eye to protect ocular cells from the complement system. (Detrick and Hooks, 2020)

1.6.3.4 Leukocyte adhesion and transmigration

In addition to antigen processing and presentation, leukocyte adhesion is another feature of an immune response. Intercellular adhesion molecule-1 (ICAM-1 or CD54) is a surface marker that mediates both the adhesion and transmigration of leukocytes through the vascular endothelium. Upregulation of ICAM-1 by inflammatory cytokines promotes extravasation of leukocytes, such as neutrophil granulocytes, monocytes, and B and T lymphocytes, leading to a localised immune response (Kishimoto et al., 1990). (Liversidge et al., 1990)

Extravasation is facilitated by the binding of ICAM-1 to the integrins lymphocyte function-related antigen-1 (LFA-1) or macrophage-1 antigen (Mac-1) (Springer, 1994). ICAM-1 is present on human RPE cells and is induced by IL-1β, IFN-γ, and TNF-α (Pfromm et al., 2022, Platts et al., 1995). Activated lymphocytes bind to human RPE cells predominantly via ICAM-1 and alternatively via other adhesion molecules (Liversidge et al., 1990). The expression of adhesion molecules such as ICAM-1 on RPE cells is essential to enable leukocyte migration across the blood-retina barrier (Crane and Liversidge, 2008, Pfromm et al., 2022). The increased expression of ICAM-1 is thereby a further indicator of an immune response in the retina. (Holtkamp et al., 2001)

1.6.4 Interaction with the adaptive immune system

In contrast to the innate immune response, the adaptive immune system is highly specific and able to develop an immunological memory. It usually takes hours to days to generate an adequate adaptive immune response. However, in the case of renewed antigen contact, a rapid and targeted immune response is initiated. Cellular immunity is embodied by T lymphocytes, whereas antibodies produced by B lymphocytes and plasma cells represent humoral immunity. Antigen presentation by immunological surface markers is vital to activate the adaptive immune system. (Chaplin, 2010, Detrick and Hooks, 2020)

Antigens must be processed and prepared for the recognition by T lymphocytes. The products of antigen processing are short peptides which are presented to T cells with assistance of specialized cell surface molecules, also called major histocompatibility complex (MHC). MHCs can be divided into two classes: MHC I and MHC II. There are three types of MHC I molecules: human leukocyte antigen A (HLA-A), HLA-B and HLA-C. They are expressed by nucleated cells and provide peptides for CD8+ T cell recognition. Through MHC I presentation, cytoplasmic antigens, such as endogenous proteins or viral proteins, are presented to immune cells. (Bröker et al., 2019)

Kanuga et al. (2002) demonstrated that IFN-γ modulates the expression of MHC I molecules (Pfromm et al., 2022). MHC II molecules serve as important surface markers for the initiation and maintenance of an adaptive immune response by presenting antigenic peptides to CD4+ T cells. Hence, MHC II expression links the innate and the adaptive immune systems. Human MHC II molecules are called HLA-DR, HLA-DP, and HLA-DQ, and mainly present extracellular antigens, such as exogenous peptides, bacteria, and toxins. The expression of MHC II molecules is restricted to APCs, in particular dendritic cells, monocytes, macrophages, and B cells. (Bröker et al., 2019)

Liversidge et al. (1988) showed that MHC II is expressed by human RPE cells after stimulation with IFN-γ or conditioned lymphocytes medium. MHC II expression demonstrates the prominent position of RPE cells within the ocular immune system, as they can function as retinal APCs. (Bonillo et al., 2022, Detrick and Hooks, 2020, Pfromm et al., 2022)

1.6.5 *In vitro* cell model

ARPE-19 is a human non-primary adherent cell line, which immortalised spontaneously (ATCC, n.d.). Previous studies confirmed that ARPE-19 cells have functional and structural similarities to *in vivo* RPE cells, making them applicable for *in vitro* experiments investigating the RPE (Dunn et al., 1996). Nevertheless, other researchers have described ARPE-19 cells as non-pigmented (Biesemeier et al., 2010, Luo et al., 2006) and there are contradictory studies on the presence of RPE-specific proteins, such as RPE65 and cellular retinaldehyde-binding protein (CRALBP) in ARPE-19 cells (Ahmado et al., 2011, Dunn et al., 1996, Vugler et al., 2008). Despite these differences to native RPE cells, it was concluded that ARPE-19 cells are still suitable to mimic aged and pathologic *in vivo* RPE cells, which represent potential retinal gene therapy targets (Ablonczy et al., 2011).

1.7 Aim of the study

IRDs are severe diseases with a major impact on the quality of life with limited therapeutic options. Gene therapy is a promising field of research in the search for definitive cures for IRDs. Additionally, the eye is an attractive gene therapeutic target due to its easy accessibility as well as its immune-privileged characteristics. (Peddle and MacLaren, 2017)

Nevertheless, studies have showed that Cas9 has at least a slight immunogenic effect (Kang et al., 2018) and a pre-existing Cas9 immunity may exist in humans (Charlesworth et al., 2019). An ocular immune response could both reduce the gene editing efficiency of Cas9 and potentially lead to vision impairment (Machitani et al., 2017, Zhou and Caspi, 2010). (Bonillo et al., 2022, Pfromm et al., 2022)

As the immunological effects of intracellular Cas9 expression on the human RPE are poorly understood, the objectives of this *in vitro* project were to investigate whether intracellular Cas9 induces a proinflammatory cytokine release and/or the upregulation of immunological surface markers in human RPE (1) (Pfromm et al., 2022). Additionally, the present study assessed whether plasmid transfection is

a suitable method for retinal gene therapy from an immunological perspective (2). The final aim was to conclude whether intracellularly expressed Cas9 in ARPE-19 cells can induce a retinal proinflammatory immune response *in vitro*. This thesis is one of the first to investigate the retinal immunogenicity of Cas9, a topic of high clinical relevance.

2 Material

2.1 Devices and laboratory equipment

Table 1: Instruments

Product	Number	Company
8-channel pipette 100 µl	3125000036	Eppendorf, Hamburg, Germany
8-channel pipette 300 µl	3125000052	Eppendorf, Hamburg, Germany
BD FACSCanto™ II	N/A	BD biosciences, Heidelberg, Germany
Bench	51025413	Thermo Fisher Scientific, Dreieich, Germany
Cell culture flask 25 cm^2	690160	Greiner, Frickenhausen, Germany
Cell culture flask 75 cm^2	658170	Greiner, Frickenhausen, Germany
Cell culture flask 175 cm^2	660160	Greiner, Frickenhausen, Germany
Centrifuge Mega Star 3.0R	5211752	VWR International, Bruchsal, Germany
Chamber slides	154534	Thermo Fisher Scientific, Dreieich, Germany
Circular cover glasses, 13 mm diameter	10073691	Thermo Fisher Scientific, Dreieich, Germany
Cryo tubes	368632	Thermo Fisher Scientific, Dreieich, Germany
Electrophoresis power supply E835	N/A	Consort, Turnhout, Belgium
Eppendorf tubes 5 ml	13748	Omnilab, Essen, Germany
FACS tube 5 ml	352235	Corning, Bodenheim, Germany
Falcon tube 15 ml	T1818500EA	Greiner, Frickenhausen, Germany
Falcon tube 50 ml	T2193300EA	Greiner, Frickenhausen, Germany
Fluorescence microscope Axio Observer 5	4919160001000	Carl Zeiss, Jena, Germany
Incubator HERACELL	51026331	Thermo Fisher Scientific, Dreieich, Germany
Infinite M200 microplate reader	IN-MNANO	Tecan, Crailsheim, Germany
LI-COR Odyssey® Infrared Imaging System	2800	LI-COR, Bad Homburg, Germany

Microcentrifuge Micro Star	5211647	VWR International, Bruchsal, Germany
MilliporeSigma™ Milli-Q™ Direct Water Purification System	ZR0Q008US	Thermo Fisher Scientific, Dreieich, Germany
NanoQuant Plate™	N/A	Tecan, Crailsheim, Germany
Neubeuer cell counting chamber	718620	BRAND, Wertheim, Germany
PCR cycler	N/A	VWR International, Bruchsal, Germany
PCR microfuge tubes 0.2 ml 8-stripes	040230600	Nerbe plus, Winsen, Germany
Petri dishes	632180	Greiner, Frickenhausen, Germany
Pipette controller pipetboy acu2	155000	Integra, Fernwald, Germany
Pipettes (10µl, 100µl, 200µl, 1,000µl)	31230000-20; -46;-54;-62;	Eppendorf, Hamburg, Germany
Pipette tips (10µl, 100µl, 200µl, 1,000µl) sterile	S11213810; S11231840; S11208810; S11221830	Starlab, Hamburg, Germany
Plate shaker ST5	602810000	CAT, M. Zipperer GmbH, Staufen, Germany
Reagent reservoir 50ml, sterile	73224	neoLab Migge, Heidelberg, Germany
Rocking platform shaker S26	603860000	CAT, M. Zipperer GmbH, Staufen, Germany
Shaking incubator	N/A	Infors, Bottmingen, Switzerland
SmartBlue Transilluminator	170042	JoJo Life Science, Giengen an der Brenz, Germany
Stirrer	D6610	neoLab Migge, Heidelberg, Germany
Serological pipette 5 ml	4051	Corning, Bodenheim, Germany
Serological pipette 10 ml	4101	Corning, Bodenheim, Germany
Serological pipette 25 ml	4251	Corning, Bodenheim, Germany
Tissue culture plate 6 well, standard	657160	Greiner, Frickenhausen, Germany
Tissue culture plate 24 well, standard	662160	Greiner, Frickenhausen, Germany
Tissue culture plate 96 well, half area	675161	Greiner, Frickenhausen, Germany
Tissue culture plate 96 well, standard	655162	Greiner, Frickenhausen, Germany
ThermoMixer C	4600223	VWR International, Bruchsal, Germany
UniThermix 2 pro	6263484	Lab Logistics Group, Meckenheim, Germany

Water bath	HAKATSGP02	VWR International, Bruchsal, Germany

2.2 Reagents

Table 2: Reagents used for molecular cloning.

Product	Number	Company
100 bp DNA ladder	15628019	Thermo Fisher Scientific, Dreieich, Germany
Alcaline phosphatase, calf intestinal	M0290S	New England Biolabs, Frankfurt am Main, Germany
BspEI (Restriction enzyme)	R0540S	New England Biolabs, Frankfurt am Main, Germany
DNA gel loading dye, purple (6x)	R0611	Thermo Fisher Scientific, Dreieich, Germany
MluI-HF (Restriction enzyme)	R3198S	New England Biolabs, Frankfurt am Main, Germany
NsiI-HF (Restriction enzyme)	R3127S	New England Biolabs, Frankfurt am Main, Germany
SYBR® Safe DNA gel stain	S33102	Thermo Fisher Scientific, Dreieich, Germany
T4 DNA ligase	M0202S	New England Biolabs, Frankfurt am Main, Germany

2.3 Chemicals

Table 3: Chemicals

Product	Number	Company
2-propanol	109634	Merck, Darmstadt, Germany
4′,6-diamidino-2-phenylindole	18860	SERVA Electrophoresis, Heidelberg, Germany
Agar	05040250G	Sigma-Aldrich, Seelze, Germany
Agarose	17850	Life Technologies, Darmstadt, Germany
Albumin (BSA) Fraction V (pH 7.0)	A1391	PanReac AppliChem, Darmstadt, Germany
Dako Antibody Diluent	S3022	Agilent Technologies, Waldbronn, Germany
Dimethyl sulfoxide	D2650	Sigma-Aldrich, Seelze, Germany

Donkey serum	D9663	Sigma-Aldrich, Seelze, Germany
Ethanol absolute p.A.	131086	AppliChem, Darmstadt, Germany
Ethanol 99%	ETOS1000991	SAV Liquid Production, Flintsbach am Inn, Germany
Fluoromount-G™	00495802	Thermo Fisher Scientific, Dreieich, Germany
H_2SO_4	93161	Carl Roth, Karlsruhe, Germany
KCl	104936	Merck, Darmstadt, Germany
KH_2PO_4	104873	Sigma-Aldrich, Seelze, Germany
LB broth (Miller)	L3522	Sigma-Aldrich, Seelze, Germany
NaCl	27810295	VWR International, Bruchsal, Germany
Na_2CO_3	106392	Merck, Darmstadt, Germany
$NaHCO_3$	106329	Sigma-Aldrich, Seelze, Germany
Na_2HPO_4	106586	Sigma-Aldrich, Seelze, Germany
QUANTI-Blue™	rep-qb2	InvivoGen, San Diege, USA
Paraformaldehyde	P6148	Sigma-Aldrich, Seelze, Germany
Triton-X 100	2104100	bioVision, Ilmenau, Germany
Trypan blue solution	T8154	Sigma-Aldrich, Seelze, Germany
Trypsin-EDTA Solution (1X)	25200072	Thermo Fisher Scientific, Dreieich, Germany
Tween20	39796.01	SERVA Electrophoresis, Heidelberg, Germany

2.4 Buffer solutions

Table 4: Buffer solutions

Buffer solution	Number	Company
Antibody dilution buffer (ICC) - Dulbecco's phosphate buffered saline (DPBS) (1X) - 1% (v/v) donkey serum - 0.05% (v/v) Triton-X 100		
Assay Diluent (ELISA)		

- Phosphate-buffered saline (PBS) - 1% Bovine serum albumin (BSA)		
Blocking buffer (ICC) - DPBS (1X) - 10% donkey serum - 0.05% Tween20		
Brilliant Stain Buffer (FACS)	566349	BD biosciences, Heidelberg, Germany
Coating buffer (ELISA) - 8.4 g $NaHCO_3$ - 3.56 g Na_2CO_3		
CutSmart-Buffer	B7204S	New England Biolabs, Frankfurt am Main, Germany
DPBS (1X)	14190169	Thermo Fisher Scientific, Dreieich, Germany
Endotoxin-Free Ultra-Pure Water	TMS011	Sigma-Aldrich, Seelze, Germany
FACS buffer - PBS - 2% BSA		
NEBuffer™ 3.1	B7203S	New England Biolabs, Frankfurt am Main, Germany
PBS - 8.0 g NaCl - 1.16 g Na_2HPO_4 - 0.2 g KH_2PO_4 - 0.2 g KCl		
Stop solution (ELISA) - 2N H_2SO_4		
T4 DNA ligase reaction buffer	B0202S	New England Biolabs, Frankfurt am Main, Germany
TAE buffer (50X)	10399519	Thermo Fisher Scientific, Dreieich, Germany
UltraPure™ distilled water DNase/ RNase free	10977015	Life Technologies, Darmstadt, Germany
Wash buffer (ELISA) - PBS - 0.05% Tween20		
Wash buffer (ICC) - 1X DPBS - 1% donkey serum - 0.05% Tween20		

2.5 Antibiotics

Table 5: Antibiotics

Antibiotic	Number	Company
Ampicillin sodium salt	A95185G	Sigma-Aldrich, Seelze, Germany
Normocin	ant-nr-1	Invivogen, San Diego, USA
Penicillin/streptomycin	156140122	Thermo Fisher Scientific, Dreieich, Germany

2.6 Kits

Table 6: Kits

Kit	Number	Company
ARPE-19 transfection kit	6130	Altogen, Las Vegas, USA
ELISA MAX™ Standard Set Human TNF-α	430201	BioLegend, Koblenz, Germany
EndoFree® plasmid mega kit	12381	Qiagen, Hilden, Germany
GenElute™ plasmid miniprep kit	PLN701KT	Sigma-Aldrich, Seelze, Germany
Human CD40 Ligand Quantikine ELISA Kit	DCDL40	R&D Systems, Minneapolis, USA
Human IFN-α2 DuoSet ELISA	DY9345-05	R&D Systems, Minneapolis, USA
Human IFN-β DuoSet ELISA	DY814-05	R&D Systems, Minneapolis, USA
Human IL-1β DuoSet ELISA	DY201	R&D Systems, Minneapolis, USA
Human IL-6 DuoSet ELISA	DY206	R&D Systems, Minneapolis, USA
Human IL-8 DuoSet ELISA	DY208	R&D Systems, Minneapolis, USA
KOD hot start DNA polymerase	710863	Merck, Darmstadt, Germany
Lipofectamine LTX	15338030	Thermo Fisher Scientific, Dreieich, Germany
Lipofectamine 3000	L3000001	Thermo Fisher Scientific, Dreieich, Germany
Mix2Seq kit	30SK000MSK	Eurofins Genomics, Ebersberg, Germany
Pierce™ TMB Substrate Kit	34021	Thermo Fisher Scientific, Dreieich, Germany

Proteome Profiler Human XL Cytokine Array Kit	ARY022B	R&D Systems, Minneapolis, USA
PureLink™ Expi Endotoxin-Free Maxi Plasmid Purification Kit	K210016	Life Technologies, Darmstadt, Germany
QIAquick® gel extraction kit	28704	Qiagen, Hilden, Germany
Venor®GeM Classic	111050	Minerva Biolabs, Berlin, Germany

2.7 Antibodies

Table 7: Antibodies

Antibody	**Number**	**LOT**	**Company**
FACS antibody			
- 7-Aminoactinomycin D (7-AAD**)**	559925	8352536	BD biosciences, Heidelberg, Germany
- Anti-HLA-DR APC-Cy™7	335831	9294724	BD biosciences
- Anti-Mouse Ig, κ/Negative Control Compensation Particles Set	552843	9093966	BD biosciences
- APC Mouse Anti-Human HLA-ABC	555555	9143711	BD biosciences
- BV510 Mouse Anti-Human CD59	742937	9330973	BD biosciences
- Human BD Fc Block™	564219	9284147	BD biosciences
- PE Mouse Anti-Human CD54	555511	9240255	BD biosciences
Primary antibody			
- Cas9 (7A9-3A3) mouse mAb	14697	3	Cell Signaling Technology, Danvers, USA
Secondary antibody			
- Donkey Anti-mouse IgG H&L, (Alexa Fluor® 568)	ab175472	GR23400811	Abcam, Cambridge, UK
- IRDye 800CW streptavidin	9632230	96-32230	LI-COR, Bad Homburg, Germany

2.8 Synthetic oligonucleotides

Table 8: Synthetic oligonucleotides

Primer's name	Sequence 5'-3'	Annealing temperature
Backbone 1400	5'GCGATCTGTCTATTTCGTTCATCC'3	56 °C
Backbone 2300	5'GGTTCCGCGCACATTTCCCCGAA'3	69 °C
Backbone 500	5'CCACAGAATCAGGGGATAACGCA'3	60 °C
CAG 3700 rev	5'CCAACCAACCATCCCTTAAACCCTT'3	61 °C
Cas9 1824 F	5'TGATCTATCTGGCCCTGGCCCACATGA'3	68 °C
Cas9 2736 F	5'GGGAAACAGCAGATTCGCCTGGAT'3	63 °C
Cas9 3600 F	5'CGAGCTCGTGAAAGTGATGG'3	53 °C
Cas9 4500 F	5'CGAGCAGGAAATCGGCAAGGCTA'3	63 °C
Cas9 5400 F	5'GTACTTTGACACCACCATCGA'3	50 °C
Cas9_RC 2 rev	5'GGAATTCGGCAGTGGTCCGGACC'3	64 °C
c-β-Act-Prom-F	5'AATCAGAGCGGCGCGCTCCGAAA'3	69 °C
Downstream FW2	5'GTCCGGAAAAAGGCCGGCGGCCAC'3	73 °C
hU6-F	5'GAGGGCCTATTTCCCATGATT'3	54 °C
U6P_FW #2	5'CCACGCGTGACGGCCTATTTCCCATGATTC'3	70 °C
Upstream Rev 2	5'GTCCGGAGCTGGGACTCCGTGGAT'3	67 °C

2.9 Plasmids and bacteria strains

Table 9: Plasmids and bacteria strains

Plasmid bacteria / strain	Number	Origin
cjCas9 backbone plasmid	N/A	Gift from Julia Pfromm
NC plasmid	N/A	self-designed
EGFP-*sp*Cas9 plasmid	48138	Addgene, Watertown, USA
*sp*Cas9 plasmid	N/A	self-designed
XL10-Gold® ultracompetent cells	200314	Agilent, Waldbronn, Germany

2.10 Stimulants

Table 10: Stimulants

Stimulant	Number	Company
dsDNA-EC	tlrlecdna	Invivogen, San Diego, USA
Poly(I:C) HMW	tlrlpic	Invivogen, San Diego, USA
Recombinant Human IFN-γ	285IF100	Bio-Techne, Wiesbaden, Germany

2.11 Services

Table 11: Services

Service	Number	Service provider
TubeSeq Service	30SK000MSK	Eurofins Genomics, Ebersberg, Germany

2.12 Culture media

Table 12: Culture media

Culture medium	Number	Company
ARPE-19 culture medium		
89% DMEM Glutamax	61965059	Thermo Fisher Scientific, Dreieich, Germany
- 10% HI-FBS		Thermo Fisher Scientific
- 1% P/S		Thermo Fisher Scientific
HEK-Blue™ IFN-α/β culture medium		
89% DMEM Glutamax	61965059	Thermo Fisher Scientific
- 10% HI-FBS		Thermo Fisher Scientific
- 1% P/S		Thermo Fisher Scientific
- 100 µg/ml normocin		Invivogen
Ampicillin agar medium		
- 3.12 g LB medium		
- 1.8 g agar		
- 125 ml Milli-Q water		
- 125 µl ampicillin		
OptiMEM reduced serum medium	31985047	Thermo Fisher Scientific
SOC medium	S1797	Sigma-Aldrich, Seelze, Germany

2.13 Cell lines

Table 13: Cell lines

Cell line	Number	Provider
ARPE-19	CRL2302	ATCC®, Manassas, USA
HEK-Blue™ IFN-α/β	hkbifnab	Invivogen, San Diego, USA

2.14 Software

Table 14: Software

Software	Provider
BD FACSDiva™ version 8.0.2	BD biosciences, Heidelberg, Germany
FlowJo version 10.6.1	BD biosciences, Heidelberg, Germany
Geneious version 2019.0.1	Biomatters Inc., Auckland, New Zealand
GraphPad Prism 8 version 8.0.2	GraphPad software Inc., San Diego, USA
Image Studio Lite version 5.2	LI-COR, Bad Homburg, Germany
SPSS version 25.0	SPSS Inc., Chicago, USA
ZEN pro imaging software version 2.6	Carl Zeiss, Jena, Germany

3 Methods

3.1 Molecular cloning

An experimental *sp*Cas9 plasmid without other potentially immunogenic sequences was generated to precisely assess immune responses to Cas9. The EGFP-*sp*Cas9 plasmid (see Fig. 3), which contains an AAV2, an inverted terminal repeat (ITR) and an enhanced green fluorescent protein (EGFP) sequence, served as the initial template for the experimental *sp*Cas9 plasmid (Pfromm et al., 2022). The AAV2 (Li et al., 2008) and ITR sequences (Chikhlikar et al., 2004) are immunogenic. Moreover, Ansari et al. (2016) detected both toxicity and an immune response to EGFP (Pfromm et al., 2022). It is possible to assess Cas9 immunogenicity more accurately by removing these three potentially immunogenic sequences from the EGFP-*sp*Cas9 plasmid. A non-coding control plasmid (NC plasmid) was created using the *sp*Cas9 plasmid as a template and used to obtain an appropriate control (Pfromm et al., 2022). The *sp*Cas9 sequence of the *sp*Cas9 plasmid was removed to create the NC plasmid, so that differences in the cytokine production of *sp*Cas9 or NC plasmid-transfected cells could be ascribed as being attributed to Cas9 expression (Pfromm et al., 2022).

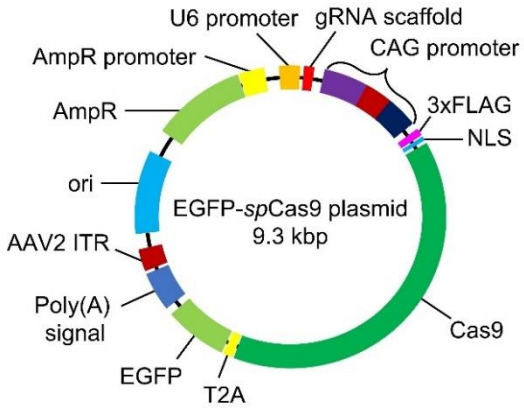

Fig. 3: Plasmid map of EGFP-*sp*Cas9 plasmid.

The figure depicts a plasmid map of the EGFP-*sp*Cas9 plasmid. A transfection with this plasmid should result in a co-expression of enhanced green fluorescent protein (EGFP) and *sp*Cas9. Besides, the plasmid contains other potentially immunogenic sequences such as adeno-associated virus 2 (AAV2) and inverted terminal repeat (ITR). Adapted from Pfromm et al. (2022).

3.1.1 Hot start polymerase chain reaction (PCR)

PCR was performed to amplify DNA fragments of the template plasmids. This technique has evolved into a unique technology enabling easy DNA synthesis (Mullis et al., 1986). Along with the template DNA, two primers are required, which correspond to the two accompanying DNA fragments' sequences. The primers must be oriented in opposing directions. Primers are single-stranded DNA sequences with a length of 20 to 30 base pairs (bp) which act as initiators of the PCR reaction. The DNA polymerase KOD Hot Start Polymerase synthesises a corresponding copy of the template DNA. The DNA polymerase uses deoxynucleotide triphosphate (dNTPs) to construct the new DNA strand. The reaction buffer ensures optimal reaction conditions. PCR occurs in three steps. First, the DNA is denatured at a temperature of around 90 °C which creates single-stranded templates. After reducing the reaction temperature, primers anneal to the template DNA and serve as initiators for the synthesis of a new DNA strand at 70 °C by a thermostable DNA polymerase. This cycle is repeated 25 to 40 times to obtain billions of DNA copies. (Stephenson, 2003)
Gel electrophoresis was performed to visualise generated DNA fragments. Instead of a conventional PCR, a hot start PCR was performed which includes an additional heat activation step to improve PCR specificity and precision. This is accomplished by preventing DNA polymerase from extending non-specific primer binding sequences (Lebedev et al., 2008).

3.1.1.1 Primer design

Primers for PCR and sequencing were self-designed with the bioinformatics software Geneious. Geneious is used for molecular cloning including primer design, restriction digest, and DNA ligation, as it can display the restriction sites of a plasmid. (Geneious, n.d.)

3.1.1.2 *sp*Cas9 and NC fragment amplification

A sequence of the EGFP-*sp*Cas9 plasmid was amplified using hot start PCR (Pfromm et al., 2022). The amplified sequence comprises the *sp*Cas9 sequence and additional sequences, such as cytomegalovirus (CMV) enhancer, chicken beta-actin promoter, and hybrid intron, which are obligatory for the Cas9 expression. The PCR amplification was carried out according to the manufacturer's instructions (Merck Millipore, n.d.). Table 15 shows the components added to each reaction tube. During PCR optimisation, the volume of $MgSO_4$ was increased up to 4 µl and dimethyl sulfoxide (DMSO) up to 4% v/v to increase the amount of DNA produced and to enhance reproducibility. The optimisation of the $MgSO_4$ concentration is crucial, as specificity and DNA yield may decrease due to insufficient Mg^{2+} concentration (Markoulatos et al., 2002). Additionally, DMSO prevents inter- and intrastrand re-annealing (Frackman et al., 1998). The activation temperature was set at 95 °C once for 2 min followed by 25 cycles of denaturation at 95 °C for 20 s, with annealing at 63.1 °C for 10 s and elongation at 70 °C for 2:30 min.

To generate the NC plasmid, the *sp*Cas9 gene sequence of the *sp*Cas9 plasmid was flanked by a forward-facing downstream and a reversed upstream primer. As a result, all sequences except the Cas9 sequence were amplified. Both primers had a BspEI restriction site at their 5' end allowing later restriction digestion. PCR was performed according to the manufacturer's instructions (Merck Millipore, n.d.). (Pfromm et al., 2022)

Table 15 shows the components added to each reaction tube. Activation temperature was set at 95 °C once for 2 min followed by 25 cycles of denaturation at 95 °C for 20 s, with annealing at 68 °C for 10 s and elongation at 70 °C for 1:40 min.

Table 15: PCR of *sp*Cas9 and NC fragment: volumes and reagents.

Reagent	Volume (*sp*Cas9 fragment)	Volume (NC fragment)
Reaction buffer	5 µl	5 µl
dNTPs	5 µl	5 µl
KOD Hot Start Polymerase	1 µl	1 µl
DNA template (concentration: 10 ng/µl)	1 µl	1 µl
Forward primer	1.5 µl (U6P_FW #2)	1.5 µl (downstream FW2)
Reverse primer	1.5 µl (Cas9_RC 2 rev)	1.5 µl (upstream rev 2)
$MgSO_4$	4 µl	4 µl
DMSO	2 µl	2.5 µl
Sterile water	29 µl	28.5 µl

3.1.2 Agarose gel electrophoresis

Agarose gel electrophoresis is an efficient method for discriminating DNA fragments according to their size. Due to non-covalent binding, agarose polymers form a network consisting of pores that separate DNA molecules by their size. The DNA is placed in separate wells of an electric field and moves towards the positively charged anode due to its negatively charged phosphate backbone. Consequently, DNA sequences are separated by length, as small fragments move through the gel faster and therefore cover more distance in the same amount of time as larger fragments. It is essential to include a DNA ladder containing DNA fragments of known sizes in a separate well for size approximation of unknown DNA fragments. (Aaij and Borst, 1972, Lee et al., 2012)

Gel electrophoresis was performed to assess the size of PCR products and generated plasmids. 1 % w/v agarose gel was prepared from 200 ml TAE buffer and 2 g of agarose gel powder. The mixture was placed in an Erlenmeyer flask and heated in a microwave for approximately 2 min. It was ready to use soon

after the powder dissolved and the fluid turned clear. Subsequently, the gel was cooled at room temperature to approximately 50 °C. Then 2 µl SYBR® Safe DNA gel stain was added and gently stirred. Afterwards, the gel was poured into a gel chamber, and well forms were inserted. The gel cooled at room temperature for 40 min. After solidification, the gel was placed into an electrophoresis unit and additional TAE buffer was added to the electrophoresis unit to cover the gel with liquid. After PCR was done, 50 µl PCR samples were mixed with 8 µl loading dye through gentle centrifugation. 5 µl DNA weight ladder was filled into the first and last wells. 30 µl of PCR sample/dye-mix were loaded into the remaining wells. The power supply was turned on and gel ran at 100 V for 1 h and 45 min. The DNA was stained with SYBR® Safe DNA gel stain. (Addgene, n.d.-a)
Ethidium bromide was not used due to its high mutagenicity (Kirsanov et al., 2010). The DNA was visualised using a blue-light as it is established that UV-light can damage DNA (Kielbassa et al., 1997). After proper distribution of the DNA bands was proven using the SmartBlue Transilluminator, the gel was removed from the power source. The images of the distributed DNA bands were captured using the LI-COR Odyssey® Infrared Imaging System.

3.1.3 Gel extraction

After gel electrophoresis, DNA bands were excised from the gel. The Gel Extraction Kit provided by Qiagen was used to purify DNA, as this kit is suitable for 70 bp to 10 kb long PCR products. The method was performed according to the recommended protocol of the manufacturer. Step 9 in this protocol, DNA elution, was performed twice to increase the final DNA concentration. UniThermix 2 was used to heat samples. Finally, DNA was eluted in 30 µl Buffer EB and DNA concentration and purity were examined using the Infinite M200 microplate reader. (Qiagen, 2018, Sambrook et al., 1989)

3.1.4 Measuring DNA concentration and purity

The Infinite M200 microplate reader was used to assess DNA concentration and purity (Pfromm et al., 2022). For blanking, 2 µl of elution solution was added to the NanoQuant plate, and DNA solution was placed on the corresponding positions. Blanking and analysis were performed using the same settings. Finally, a precise result of the DNA concentration and purity was obtained (Tecan, 2008, Tecan, 2011).

The absorbance of the solution was measured photometrically at 260 nm and 280 nm. The absorbance at 260 nm indicates the amount of nucleic acids, while the measurement at 280 nm displays DNA purity as it measures phenols and proteins. The ratio of absorbance at 260 nm and 280 nm should be between 1.8 and 2.0, indicating a pure DNA concentrate. (Armbrecht, 2013)

3.1.5 Restriction digest

Restriction digest was performed with the amplified DNA fragments to generate corresponding ends for DNA ligation. Restriction endonucleases (REs) cleave DNA precisely at target regions, which mainly contain palindromes. Palindromes are sequences in which the 5'-to-3' sequence of the sense strand corresponds to the 3'-to-5' of the antisense strand. In cleaving DNA, REs produce either sticky or blunt ends which are defined by the presence of overhangs. Consequently, DNA fragments were prepared for the subsequent ligation by creating compatible termini through REs. (Stephenson, 2003)

3.1.5.1 Preparation for *sp*Cas9 plasmid ligation

The insert (*sp*Cas9 fragment) and the vector (the backbone of the *cj*Cas9 plasmid) were prepared for *sp*Cas9 plasmid ligation. A double restriction digest with REs MluI-HF and NsiI-HF was performed prior to ligation. Each RE has a 6 bp specific recognition site and cleaved the backbone of the *cj*Cas9 plasmid and the *sp*Cas9 fragment only once. As a result, compatible ends were produced to ensure proper directional insertion. (New England Biolabs, n.d.-e, Pfromm et al., 2022)

The backbone fragment was additionally treated with alkaline phosphatase calf intestinal (CIP), which dephosphorylates the 5' and 3' ends of the DNA, to prevent recirculation (New England Biolabs, n.d.-a, Røkke et al., 2014). The protocol was calculated using NEBcloner and was performed as per the manufacturer's instructions (see Table 16). One negative control contained no restriction enzymes, and another contained only the restriction enzymes.

Table 16: Restriction digest of *sp*Cas9 and backbone fragment: volume and reagents.

Reagent	Volume (*sp*Cas9 fragment)	Volume (backbone fragment)
DNA template	1 µg	1 µg
10X NEBuffer CutSmart	5 µl	5 µl
Mlul-HF (RE)	1 µl	1 µl
Nsil-HF (RE)	1 µl	1 µl
nuclease-free water	42 µl	42 µl
CIP	0 µl	0.5 µl

Tubes containing *sp*Cas9 fragment were incubated for 2 h at 37 °C and subsequently inactivated with 10 µl of 6x gel loading dye (New England Biolabs, n.d.-b). The backbone fragments' samples were incubated at 37 °C for 1 h. Subsequently, 0.5 µl CIP was added to the reaction tubes and incubated for another 60 min at 37 °C. To inactivate the REs, 10 µl of 6x gel loading dye was added, and the DNA was subsequently purified using gel electrophoresis. (New England Biolabs, n.d.-a)

Agarose gel preparation and gel electrophoresis were performed as described in chapter 3.1.2. The QIAquick® Gel Extraction Kit was used for DNA extraction and purification (see chapter 3.1.3). Purity and concentration of the DNA were analysed using the Infinite M200 microplate reader (see chapter 3.1.4).

3.1.5.2 Preparation for NC plasmid ligation

The NC fragment was flanked by two restriction sites for the RE BspEI. As the NC fragment sequence includes a backbone, recirculation was not prevented. For this reason, only one RE and no CIP treatment was used. The protocol was calculated using NEBcloner (see Table 17). (Pfromm et al., 2022)

Table 17: Restriction digest of NC fragment: volume and reagents.

Reagent	Volume
DNA template	769.6 ng
10X NEBuffer 3.1	5 µl
BspEI (RE)	1 µl
nuclease-free water	43 µl

A sample containing no REs was used as a negative control. The samples were incubated at 37 °C for 2 h and heat-inactivated at 80 °C for 20 min (New England Biolabs, n.d.-c).

Analysis of DNA purity and concentration was performed as described in chapter 3.1.4.

3.1.5.3 Assessing generated plasmid size

Before sequencing, a double (*sp*Cas9 plasmid) and single (NC plasmid) restriction digest was conducted to estimate the size of both plasmids. As a control, a separate single restriction digest of *sp*Cas9 plasmid was performed. A second negative control sample for both plasmids contained no REs. The protocols were carried out according to the manufacturer's instructions (see Table 18) (New England Biolabs, n.d.-b, New England Biolabs, n.d.-c). Only plasmids with an appropriate size were sent for sequencing.

Table 18: Restriction digest of *sp*Cas9 and NC plasmid: volume and reagents.

Reagent	Volume (*sp*Cas9 plasmid)	Volume (NC plasmid)
DNA template	1 µg	1 µg
10X NEBuffer CutSmart	5 µl	5 µl
Mlul-HF (RE)	1 µl	0 µl
Nsil-HF (RE)	1 µl	0 µl
BspEI (RE)	0 µl	1 µl
nuclease-free water	42 µl	43 µl

3.1.6 DNA ligation

After amplification and cleavage by REs, the DNA fragment was merged with a vector. This method, in which an enzyme catalyses the covalent binding of 5'-phosphate and 3'-hydroxy ends of both reaction partners, is called ligation. Once a vector and an insert are ligated, a plasmid has been successfully generated. (Stephenson, 2003)

T4 DNA ligase was used to connect insert and vector (Pfromm et al., 2022). The amount of vector and insert to be used in the ligation was calculated in advance using the Addgene ligation calculator. The vector:insert ratio was varied from 1:1 to 1:3 for *sp*Cas9 plasmid ligation. The protocol was carried out according to the manufacturer's instructions (see Table 19) (New England Biolabs, n.d.-d). As negative controls, either no insert (*sp*Cas9 plasmid) or no T4 DNA ligase (NC plasmid) were added to the reaction tube. The tubes were incubated overnight at 4 °C and subsequently heat-inactivated at 65 °C for 10 min. Afterwards, samples were chilled on ice and transformed into appropriate cells for bacterial transformation (Addgene, n.d.-b, New England Biolabs, n.d.-d).

Table 19: DNA ligation of *sp*Cas9 and NC fragment: volume and reagents.

Reagent	Volume (*sp*Cas9 fragment)	Volume (NC fragment)
DNA insert (1:1 / 1:3)	68.3 ng / 86.44 ng	50 ng
DNA vector (1:1 / 1:3)	32 ng / 13.5 ng	0 ng
T4 DNA ligase reaction buffer (10X)	1 µl	2 µl
T4 DNA ligase	1 µl	1 µl
endonuclease-free water	up to 10 µl in total	12 µl

3.1.7 Bacterial transformation

Bacterial transformation was used to introduce DNA into bacteria, as artificial pores in the bacterial cell membrane facilitate DNA delivery. The generated plasmid was transferred into bacteria and was then replicated. Since the *sp*Cas9 plasmid and NC plasmid contain an ampicillin resistance gene, bacteria that had successfully taken up one of these plasmids survived cultivation on an ampicillin-containing agar plate. This ensured the selection of appropriately transformed bacteria. (Mandel and Higa, 1970, Sambrook et al., 1989, Stephenson, 2003)

XL10-Gold® ultracompetent cells that are tetracycline- and chloramphenicol-resistant were used (Pfromm et al., 2022). The cells did not express any REs that could potentially cleave a delivered plasmid, making them suitable for large plasmids that are difficult to clone. The bacterial transformation was carried out according to the manufacturer's recommended protocol. However, instead of NZY$^+$ broth, SOC medium was used. 200 µl of the transformation mixture were applied to agar plates and incubated overnight at 37 °C. A total of three plates were plated. The first agar plate was an experimental plate and contained a ligation mixture. The second plate served as a negative control as no insert DNA was added during ligation. The third plate functioned as a positive control for transfection. pUC18 plasmid was used as a control plasmid for this procedure, and approximately 250 colonies would grow on the agar plate according to the protocol. Agar plates were evaluated the day after incubation. (Stratagene, n.d.)

3.1.8 Isolation of plasmid DNA

For plasmid DNA isolation, the GenElute™ Plasmid Miniprep Kit was utilised according to the manufacturer's protocol. This kit minimised RNA contamination, making plasmids suitable for sequencing (Sigma-aldrich, 2014).

Highly purified endotoxin-free plasmids were used to assess innate immune responses and to increase transfection efficacy. Therefore, the EndoFree® Plasmid Mega Kit and PureLink™ Expi Endotoxin-Free Maxi Plasmid Purification Kit were used (Pfromm et al., 2022). For both kits, the manufacturer's recommended protocol was used (Qiagen, n.d.-b, Sigma-aldrich, n.d.).

Bacterial cell membranes were lysed in NaOH-sodium dodecylsulfate (SDS). Additional RNase treatment degrades every contaminating RNA in the sample and thus prevents RNA contamination. Due to an optimised incubation period, the majority of plasmid DNA is released, whereas chromosomal DNA remains within the nuclear membrane. Acidic potassium acetate neutralises the lysate. SDS forms insoluble complexes due to high salt concentrations, which lead to the precipitation of chromosomal DNA. Plasmid DNA remains in the supernatant, ensuring a precise separation of these two components. Cartridges were used to remove the precipitated sequences. Subsequently, the remaining RNAs and proteins were removed in several washing steps. Additional washing steps with isopropanol and ethanol were performed to improve DNA purity. Finally, the plasmid DNA was diluted in TE buffer. (Birnboim and Doly, 1979, Qiagen, n.d.-a) DNA purity and quantity were assessed as described in chapter 3.1.4.

3.1.9 Sequencing

The *sp*Cas9 and NC plasmids were sequenced using the Sanger method to assess their precise sequences (Sanger et al., 1977).

The Mix2Seq Kit from Eurofins was used to prepare the generated plasmids for sequencing (Pfromm et al., 2022). According to the manufacturer's protocol, 15.76 µl of template DNA (75 ng/µl) per reaction tube were combined with 2.1 µl of 10 pmol/µl primer (Eurofins, n.d.-b). Table 20 lists primers, which were used for *sp*Cas9 and NC plasmid sequencing.

Table 20: Primers used for *sp*Cas9 and NC plasmid sequencing.

***sp*Cas9 plasmid**	**NC plasmid**
hU6-F	hU6-F
c-β-Act-Prom-F	c-β-Act-Prom-F
Cas9 1824 F	downstream FW2
Cas9 2736 F	backbone 500
Cas9 3600 F	backbone 1400
Cas9 4500 F	backbone 2300
Cas9 5400 F	CAG 3700 rev
backbone 500	
backbone 1400	
backbone 2300	
CAG 3700 rev	

Premixed samples were transferred into Mix2Seq tubes and sealed. The tubes were sent to Eurofins for Sanger sequencing (Eurofins, n.d.-b).

Results were evaluated with Geneious by analysing consensus identity between the sample and the projected plasmid sequence. Due to G/C-rich regions in the CAG-promoter sequence (Kieleczawa, 2006), a Power Read Upgrade with TubeSeq Service was required making complex template sequencing more successful (Eurofins, n.d.-a). For the experimental *sp*Cas9 and NC plasmid, primer CAG 3700 rev was used for Power Read analysis. Settings and protocols were similar to the described protocol above and were provided by Eurofins (Eurofins, n.d.-b).

3.2 ARPE-19 cells

ARPE-19 cells were maintained in 20 ml ARPE-19 culture medium in a 175 cm^2 flask at 37 °C and 5 % CO_2 (Pfromm et al., 2022). The medium was replaced every three days (ATCC, n.d.).

3.2.1 Passaging

Cells were subcultured (1:5 ratio) as soon as they reached 90 % confluency. ARPE-19 cells were washed with 15 ml DPBS (1X) after the culture medium was removed. DPBS (1X) was then discarded, and ARPE-19 cells were detached using 7 ml Trypsin-EDTA solution (1X) for 5 min and neutralised with 14 ml complete growth medium. The cells were aspirated through gentle pipetting and transferred into a 50 ml falcon suitable for centrifugation, which was performed at 300 x g for 5 min. The supernatant was discarded, and the cell pellet was resuspended in 5 ml complete growth medium and transferred to a new 175 cm^2 flask containing 15 ml culture medium. Cells in passages 11 to 18 were used for cell experiments. (ATCC, n.d.)

3.2.2 Cell counting

The Neubauer cell counting chamber was used to calculate the cells per ml of cell suspension. 10 µl cell suspension was mixed with 10 µl trypan blue solution to discriminate between viable and dead cells. Trypan blue visualises dead cells by penetrating through damaged membrane as the cell membrane of viable cells is intact (Fang and Trewyn, 2012).
10 µl of this diluted cell suspension was added to the counting chamber. The cell count per ml was calculated by averaging four representative counting fields multiplied by the volume factor 10^4. The result was multiplied by 2 as the suspension was diluted 1:1 with the trypan blue solution.

$$a = \frac{b}{4} x2x10^4$$

$$a = cells\ per\ ml; b = cell\ number\ of\ four\ representative\ counting\ fields$$

3.2.3 Cryopreservation and thawing

Cryopreservation was performed using freezing medium containing complete growth medium and 10% (v/v) DMSO. $2x10^6$ cells per ml were frozen, and the cryovials were stored at -180 °C in a liquid nitrogen tank.
For thawing, cryovials were first thawed in a 37 °C water bath until the ice had completely melted. Afterwards, the contents of the vial were transferred into a 15 ml falcon containing 12 ml preheated complete growth medium. This falcon was centrifuged at 300 x g for 5 min. The supernatant was discarded, and the cell suspension was resuspended with 5 ml complete growth medium and transferred into a 175 cm^2 flask containing 15 ml culture medium. (ATCC, n.d.)

3.3 HEK-Blue™ IFN-α/β cells

HEK-Blue INF -α/β cells are modified HEK293 cells that can detect IFN type 1. HEK293 cells were transfected with *signal transducers and activators of transcription 2* (*STAT2*) and *interferon regulatory factor 9* (*IRF9*) genes, leading to a complete IFN 1 pathway in HEK-Blue™ IFN-α/β cells. HEK-Blue™ IFN-α/β cells were transfected with a secreted embryonic alkaline phosphatase (SEAP) gene linked to a reporter gene. Consequently, the presence of interferons type 1 triggers the production of SEAP in HEK-Blue™ IFN-α/β, which is then measured using the Quanti-Blue™ medium. (InvivoGen, n.d.-c, Pfromm et al., 2022)

3.3.1 Passaging

HEK-Blue™ IFN-α/β cells were maintained in HEK-Blue™ IFN-α/β culture medium (Pfromm et al., 2022). The cells were passaged at a 1:10 ratio once they reached 90% confluency. The cells were washed and detached using 10 ml DPBS (1X) after removal of the culture medium. Once the cells separated, 10 ml complete growth medium was added. HEK-Blue cells were aspirated through gentle pipetting and transferred into a 50 ml falcon suitable for centrifugation, which was performed at 300 x g for 5 min. The supernatant was discarded, and the cell pellet was resuspended with 5 ml complete fresh growth medium. The

suspension was placed in a new 75 cm^2 flask containing 7 ml of culture medium. For further cell experiments, cell passages between 7 and 9 were used. (InvivoGen, n.d.-c)

3.3.2 Cryopreservation and thawing

Cryopreservation was carried out with freezing medium containing DMEM + GlutaMax, 20% (v/v) heat-inactivated fetal bovine serum (HI-FBS) and 10% (v/v) DMSO. $2x10^6$ cells per ml were frozen, and cryovials were stored at -180 °C in a liquid nitrogen tank.

Cryovials were thawed in a 37 °C water bath, and the vial content was transferred into a 15 ml falcon containing 12 ml of preheated complete growth medium. The falcon was centrifuged at 300 x g for 5 min. The supernatant was discarded, and the cell suspension was resuspended in 5 ml complete growth medium. The cells were transferred into a 75 cm^2 flask containing 7 ml of culture medium. (InvivoGen, n.d.-c)

3.4 PAMP stimulation

3.4.1 Poly(I:C) HMW stimulation

ARPE-19 cells were stimulated with PAMPs to assess whether they can produce inflammatory cytokines. Poly(I:C) high molecular weight (HMW) is a synthetic agonist of the TLR3 receptor, which mainly detects dsRNA and is expressed on human RPE cells (InvivoGen, n.d.-b, Kumar et al., 2004). ARPE-19 cells were stimulated with Poly(I:C) HMW to establish a cytokine release control as Mai et al. (2014) demonstrated RPE cytokine production in response to Poly(I:C) stimulation.

ARPE-19 cells were seeded into 96-well plates 24 h prior to stimulation with 10 µg/ml Poly(I:C) HMW (Pfromm et al., 2022). The cells' supernatants were sampled at 3 h, 12 h, 18 h, 24 h, 48 h post-stimulation and samples were stored at -80 °C. The experiment was run in triplicates with separate wells for each time point. As a negative control, no reagent was added to the cells. (InvivoGen, n.d.-b)

The supernatants' cytokine concentration was measured with an enzyme-linked immunosorbent assay (ELISA).

3.4.2 Ds-DNA stimulation

DsDNA-EC served as second PAMP. Once dsDNA, such as plasmids, is transfected into cells, it can be recognised by TLR9 and other cytosolic DNA sensors resulting in cytokine release (Wang et al., 2014b). This potential immunogenicity applies to the *sp*Cas9 plasmid, which consists of dsDNA and could be detected by TLR9. As Kumar et al. (2004) found that human RPE cells express TLR9, a TLR9-response to dsDNA could be relevant for further *in vivo* experiments.

The stimulation was performed according to the manufacturer's provided protocol. 1 µg/ml dsDNA were transfected using 0.2 µl Lipofectamine LTX and compared with a transfection control in which cells were treated with Lipofectamine LTX transfection reagent only (Pfromm et al., 2022). Supernatants were collected 3 h, 12 h, 18 h, 24 h, and 48 h post-stimulation and stored at -80 °C. (InvivoGen, n.d.-a)

The supernatant's cytokine concentration was measured using an ELISA.

3.5 Cationic lipid transfection

Large DNA particles like plasmids can be transfected with a moderate cytotoxicity rate using cationic lipid transfection (Felgner et al., 1987, Romano et al., 2000). Due to their ambivalent molecular structures, cationic lipids support the intracellular uptake of DNA plasmids by forming DNA-lipid complexes (Rädler et al., 1997). The positively charged head group of cationic lipids is crucial for the interaction with the negatively charged phosphate backbone of nucleic acids as well as for fusion with the negatively charged cell membrane. Labat-Moleur et al. (1996) found that DNA-lipid complexes enter cells primarily via endocytosis. (Chesnoy and Huang, 2000, Thermo Fisher Scientific, n.d.-b)

Cationic lipids serve as non-viral vectors (Bennett et al., 1992). Liang et al. (2015) found that cationic lipids are valuable for transfecting different cell lines with Cas9 plasmids. Therefore, plasmids were delivered into ARPE-19 cells via cationic lipid

transfection to obtain a high transfection efficacy and a low cytotoxicity rate. Studies demonstrated that Lipofectamine 3000 (Lin et al., 2014) and Lipofectamine LTX (Sakuma et al., 2016) are well suited to transfect cells with complexes or plasmids, which is why these reagents were chosen. An optimised transfection protocol was established to obtain a high ARPE-19 transfection efficacy. Hence, three different transfection reagents were compared: Lipofectamine 3000, Lipofectamine LTX and an ARPE-19 transfection Kit from Altogen Biosystems. For all transfection reagents, the manufacturer's recommended protocol was followed (Altogen, n.d., Thermo Fisher Scientific, n.d.-c, Thermo Fisher Scientific, n.d.-e).

An EGFP-tagged *sp*Cas9 plasmid was used for transfection optimisation. The fluorescence-tag allows quantification of transfection efficacy via a fluorescence microscope. Moreover, the size of the EGFP-tagged *sp*Cas9 plasmid (9,288 bp) is comparable to the experimental *sp*Cas9 plasmid (8,069 bp). Three different transfection reagents were compared to identify the most promising transfection reagent.

150,000 cells/well were seeded in triplicates in a 24-well plate 24h prior to transfection. The cells were seeded densely to achieve high confluency and to minimise the number of dividing cells. High confluency relates the experiment to the *in vivo* situation, as mature retinal pigmented epithelium consists of a monolayer of non-dividing cells (Boulton and Wassell, 1998). The manufacturer's instructions were followed, and the amounts of plasmid DNA and transfection reagent added to the cells were modified to optimise transfection efficacy (see Table 21).

Table 21: Combination of transfection reagent and amount of DNA plasmid.

Transfection reagent	Amount of plasmid DNA
Lipofectamine 3000 (1.5 µl)	250 ng, 375 ng
Lipofectamine LTX (1.5 µl)	125 ng, 250 ng, 375 ng
Altogen transfection reagent (1 µl; 5 µl)	750 ng, 1,500 ng

As a negative control, cells were either treated with the transfection reagent or with plasmid DNA only. Non-stimulated ARPE-19 cells were cultured in parallel

to be able to exclude autofluorescence of any component. An established transfection protocol of HEK-Blue™ IFN-α/β served as a positive control.
Transfection efficacies were assessed at 24 h and 48 h post-transfection using fluorescence microscopy. Images were captured with a fluorescence microscope, and the number of EGFP-positive cells were calculated in four images per well by research group members, who did not know which combinations were used for each well. Therefore, the evaluation was blinded. After successful transfection protocol optimisation, $1.5*10^5$ ARPE-19 cells per well were seeded in a 24-well plate in complete growth medium 24 h before transfection. 1.5 µl Lipofectamine LTX was diluted with 23.5 µl OptiMEM and the reaction tube was mixed thoroughly. To prepare the DNA master mix, 375 ng plasmid DNA were combined 1:1 with Plus™ reagent and supplemented with OptiMEM to a total volume of 25 µl. The solution was mixed by resuspending and was incubated at room temperature for 10 min. Afterwards, the DNA master mix was added to diluted Lipofectamine LTX and incubated for a further 20 min at room temperature. Meanwhile, the medium was removed and replaced with OptiMEM. Finally, 60 µl of transfection mixture was added to each well. Transfection efficacy was evaluated 24 h later via fluorescence microscopy. (Pfromm et al., 2022)

3.6 Fluorescence microscopy

Proteins can be detected and localised through fluorescence microscopy, which makes use of the property of certain substances, known as fluorophores, which absorb ultraviolet or short-wave visible light. As a result, fluorophores emit a part of this energy as longer-wave radiation, which is visualised via fluorescence microscopy. Visualisation is possible within living cells as the fluorescent image capturing is not associated with any significant physiological stress for viable cells. (Lakowicz, 1999, Majtner, 2015)
Fig. 4 shows the principle of a fluorescence microscope as well as its image capturing. The fluorescence images were captured with Axio Observer 5 fluorescence microscope and processed with ZEN 2.6 pro software program. The fluorescence settings were adjusted to the individual fluorophore.

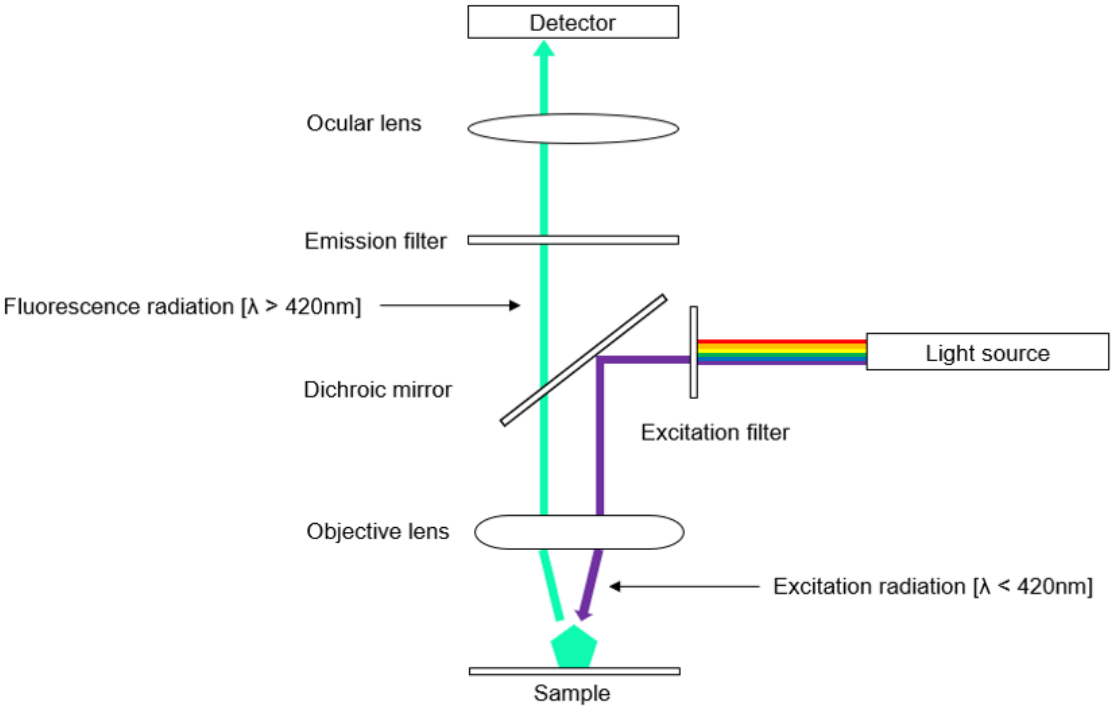

Fig. 4: Principle of a fluorescence microscope.

The required excitation radiation is filtered by an excitation filter. The dichroic mirror directs the short-wave excitation radiation to the sample/fluorophore, which absorbs the excitation radiation. The fluorophore consequently emits low-energy fluorescence radiation, which passes through the dichroic mirror without changing its direction as it differs from the excitation radiation wavelength. Thereby, the dichroic mirror separates the fluorescence radiation and excitation radiation. The fluorescence radiation then passes through an emission filter to the detector where an image is captured. Adapted from Majtner (2015).

3.7 Immunocytochemistry (ICC)

ICC enables researchers to detect and localise intracellular proteins using antibodies. A primary antibody (AB) specifically binds to a protein such as Cas9. A secondary AB, which is labelled with a fluorophore, then attaches to the primary AB. In this manner, Cas9 expression can be finally assessed with a fluorescence microscope. (Renshaw, 2017)

Thus, ICC was performed 24 h after *sp*Cas9 plasmid transfection to prove intracellular Cas9 expression. ICC was carried out in three experimental groups. ARPE-19 cells were transfected with either the EGFP-*sp*Cas9 plasmid (1), the

*sp*Cas9 plasmid (2) or the NC plasmid (3). EGFP-*sp*Cas9 plasmid transfected ARPE-19 cells served as a positive control since plasmid uptake could be proven via fluorescence microscopy. The NC plasmid functioned as a negative control since NC plasmid transfection does not lead to Cas9 expression (Pfromm et al., 2022). An established staining protocol was used (Abcam, n.d.).

Before transfection, coverslips were sterilised with UV-light for 30 min and placed into a 24-well plate. 24 h after transfection, the culture medium was removed, and the cells were fixed using 4 % PFA for 10 min at room temperature. Subsequently, they were washed three times in wash buffer for 5 min per rinse. Since Cas9 is an intracellular target, a permeabilization step is crucial. Hence, coverslips were incubated in DPBS (1X) with 0.05 % (v/v) Triton-X 100 for 10 min, followed by three washes in wash buffer for 5 min per rinse. For blocking, the cells were incubated in blocking buffer for 60 min at room temperature with two subsequent wash cycles at 5 min per wash. The primary Cas9 (7A9-3A3) mouse mAb was diluted 1:600 in antibody dilution buffer. The cells were incubated with the primary AB at 4 °C overnight. The solution was then removed, and the cells were washed twice. They were subsequently washed once with DPBS (1X) for 5 min. Secondary AB, Donkey Anti-mouse IgG H&L (Alexa Fluor® 568), was diluted 1:600 in Dako Diluent, and cells were incubated with secondary AB in the dark for two hours at room temperature. Any exposure to light was avoided. After removal of the secondary AB solution, the cells were washed in the dark with wash buffer twice for 5 min per wash. Afterwards, another washing cycle with DPBS (1X) for 5 min was carried out. The cells were then incubated with 4′,6-diamidino-2-phenylindole (DAPI) for 2 min and washed once with 1X DPBS for 5 min. The coverslips were air-dried for 20 min and mounted with a drop of Fluoromount-G™. Finally, the slides were examined with a fluorescence microscope for Cas9 expression and stored in the dark at 4 °C for long-term storage. (Abcam, n.d., Pfromm et al., 2022)

3.8 Cas9 stimulation

ARPE-19 cells were transfected with the *sp*Cas9 plasmid and Lipofectamine LTX, as described in chapter 3.5, to evaluate immune responses to Cas9. The cytokine concentrations of their supernatants were compared using four different control groups, as shown in Fig. 5.

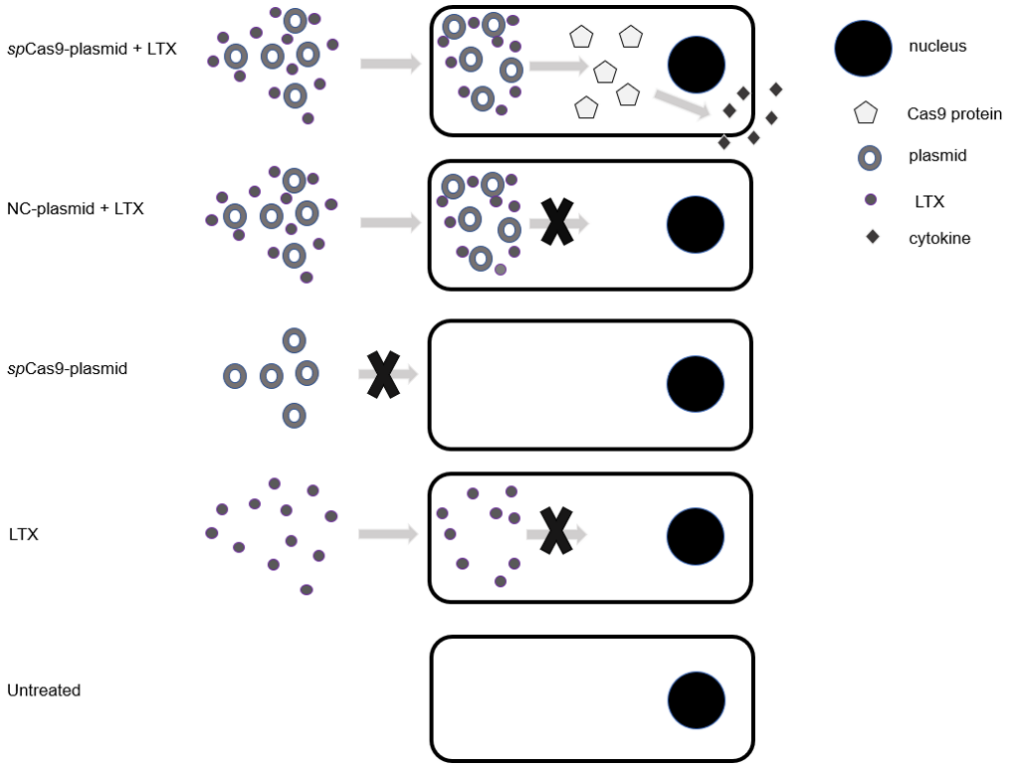

Fig. 5: Experimental and control groups for Cas9 stimulation.

Cytokine concentrations of supernatant from Cas9 expressing ARPE-19 cells were compared with non-Cas9 expressing ARPE-19 cells after NC plasmid transfection. Treatment only with *sp*Cas9 plasmid or Lipofectamine LTX served as controls. Additionally, non-stimulated ARPE-19 cells functioned as a negative control.

ARPE-19 cells were seeded in 96-well plates 24 h before transfection. Cell supernatants were collected at 3 h, 12 h, 18 h, 24 h, and 48 h after transfection (Pfromm et al., 2022). Separate wells were prepared for each time point and experimental group, and the experiment was run in triplicates. Simultaneously, the Cas9 expression in ARPE-19 cells transfected with *sp*Cas9 plasmid was confirmed with ICC, as described in chapter 3.7. The supernatants were stored at -80 °C and the Proteome Profiler Array and ELISAs were used to detect cytokine release.

3.9 Proteome Profiler Array

The production of various cytokines was examined to evaluate whether intracellular Cas9 induces a cytokine release. The Proteome Profiler Array Kit allows simultaneous detection of 105 cyto- and chemokines in Cas9-stimulated cells' supernatant. This kit assesses the production of both inflammatory and anti-inflammatory cytokines and was used by Kang et al. (2018) to detect immune responses to extracellular Cas9. Before using the Proteome Profiler Array, ARPE-19 cells were transfected with the *sp*Cas9 plasmid using Lipofectamine LTX. The supernatants' cytokine concentrations were compared with those of NC plasmid transfected ARPE-19 cells. The supernatants of both groups were collected 24 h after stimulation (Pfromm et al., 2022). The samples were stored at -80 °C.

The array membranes were incubated with 500 µl of supernatant, allowing proper binding of target analytes to their specific AB. The design and image acquisition of the Proteome Profiler Array is illustrated in Fig. 6. Instead of the horseradish peroxidase (HRP)-conjugated streptavidin, IRDye 800CW streptavidin was used. IRDye 800CW streptavidin binds directly to the detection ABs enabling near-infrared fluorescence detection by the LI-COR Odyssey® Infrared Imaging System (Pfromm et al., 2022). According to the manufacturer's protocol (R&D systems, n.d.-b), infrared imaging ensures protein detection over a broader dynamic range.

Finally, the membranes were analysed using the LI-COR reading machine and a 2 min exposure time at 800 nm wavelength. An image was acquired showing capture AB spotted dots with their pixel density representing the concentration of the respective cyto- or chemokine. The pixel densities were measured using Image Studio Lite (version 5.2). Cytokine concentration differences were calculated by comparing the pixel densities of cyto- and chemokines between both groups. (Pfromm et al., 2022, R&D systems, n.d.-a, R&D systems, n.d.-b)

The Proteome Profiler Array was carried out once, and the results were verified with several ELISAs.

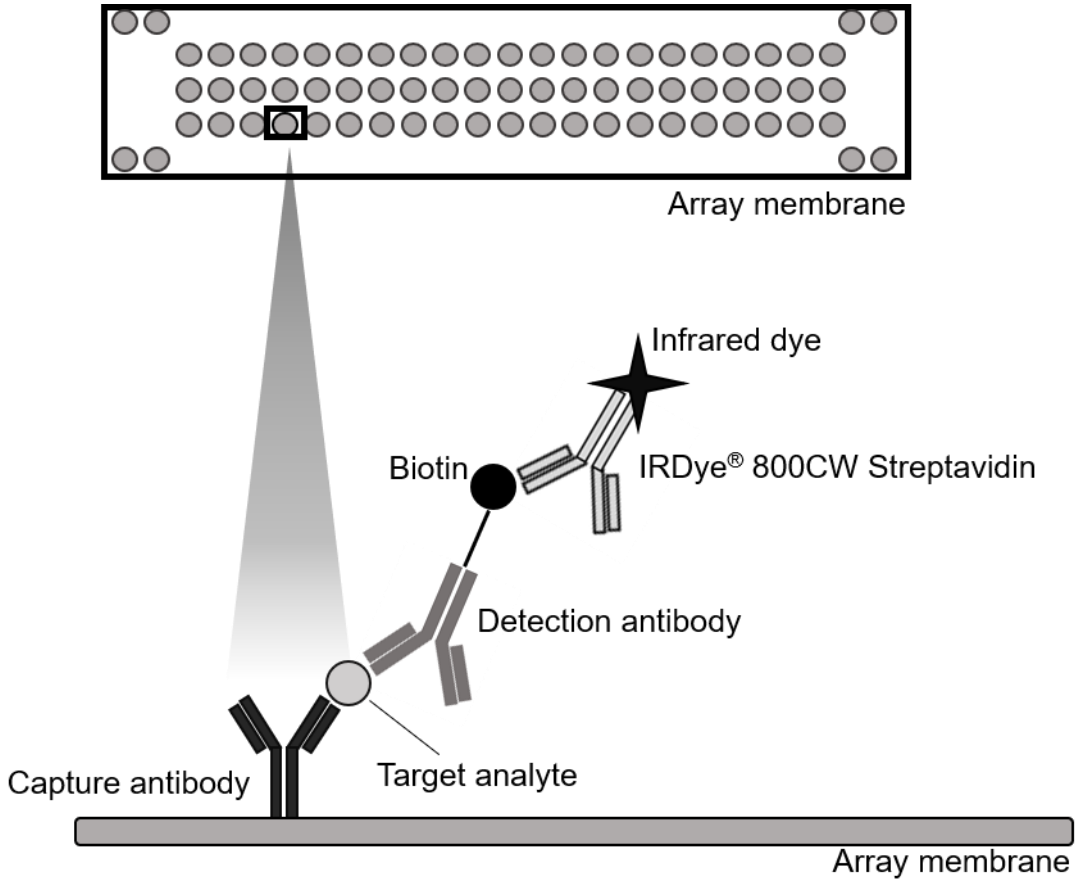

Fig. 6: Principle of the Proteome Profiler Array.

Array membranes are spotted in duplicates with 105 different capture ABs of chemo- and cytokines. The target analytes bind to their specific AB. After exposure to a detection AB mixture, detection ABs bind to their corresponding target analyte. IRDye 800CW streptavidin binds directly to the detection ABs. The pixel density of target analytes can be determined with LI-COR Odyssey® Infrared Imaging Systems. Adapted from R&D systems (n.d.-b).

3.10 ELISA

Human CD40L, IFN-α, IFN-β, IL-1β, IL-6, IL-8 and TNF-α ELISAs were carried out according to the manufacturers' recommended protocols (Pfromm et al., 2022). ELISA is an immune assay that detects cyto- and chemokines in the cells' supernatant (Engvall and Perlmann, 1971). 96-well half area plates were used instead of 96-well plates (except for CD40L ELISA) to reduce the amount of required ABs. The volumes were adjusted appropriately, and the half-area plates were spotted with the capture ABs targeting a specific cyto- or chemokine.

However, there are some uncoated spots on the well surface, which can bind proteins and antibodies other than the corresponding antigen. Therefore, the wells were incubated with blocking buffer, a mix of proteins, to prevent unspecific AB binding on the uncoated surfaces. This results in lower background noise and increases the specificity and sensitivity of the ELISA. The wells were then incubated with the sample to ensure binding of the capture AB to the respective antigen. Once the antigen had bound to the capture AB, a biotinylated detection AB was added to the sample, which attaches to the antigen and forms an antibody-antigen-antibody-sandwich. As the number of avidin-horseradish peroxidase enzymes bound to biotin is proportional to the antigen concentration, the supplementation of these enzymes ensures a precise cytokine calculation. (Thermo Fisher Scientific, n.d.-a)

Tetramethylbenzidine (TMB) and peroxide solution were added to detect horseradish peroxidase activity, which hydrolyses hydrogen peroxide. The resulting oxygen radicals oxidises TMB, which generates blue light. (Thermo Fisher Scientific, n.d.-d)

Finally, a stop solution containing sulfuric acid was supplemented, which turns the solution colour to yellow. The wells were washed between steps to prevent false-positive results. Analysis was performed using an Infinite M200 microplate reader. The absorbance was assessed at 450 nm with wavelength correction at 570 nm. The experiments were run in duplicates and repeated twice to obtain a total of three independent experiments for each cytokine. (BioLegend, n.d., Thermo Fisher Scientific, n.d.-a)

3.11 Flow cytometry

In addition to cytokine release, Cas9 and plasmid-mediated gene transfer may trigger immunological surface marker expression and might lead to reduced cell viability. Fluorescence-activated cell sorting (FACS) was performed to assess cell viability rates as well as the immune surface marker expression of ARPE-19 cells.

3.11.1 Background

Cells are sorted by size, granularity, and protein expression through the use of flow cytometry (Schumann et al., 1971). For flow cytometric assessment, cells were assessed in suspension to facilitate cell acceleration and hydrodynamic sorting by sheath fluids, which forces cells into a single-file stream at the interrogation point. A laser beam with a wavelength of 488 nm (blue laser), 633 nm (red laser), or 405 nm (violet laser) excites each cell at the interrogation point (BD biosciences, n.d.-b). The light is scattered characteristically, dependent on the size and granularity of the passing cell. The forward scattered light (FSC) detected by the FSC channel indicates the cell size. A stronger FSC signal is produced by larger cells. Simultaneously, the side scattered light (SSC) displays the cells' granularity and complexity. FSC and SSC characterisation facilitates the distinction of different cell populations and discrimination of living and dead cells. Additionally, cells can be distinguished based on the expression of certain surface markers, as fluorescent-labelled ABs can bind to surface markers. During measurement, fluorophores absorb the excitation radiation of the laser beam and subsequently emit light of a specific wavelength. (Sack et al., 2006)

Photomultiplier tubes (PMT) detect the scattered light and fluorescence signal. BD FACSCanto™ II has five PMTs for the blue laser and two PMTs each for the violet and red laser (BD biosciences, n.d.-b). FSC, SSC, and the varying fluorescent signals are detected by separate PMTs, ensuring surface molecule distinction. The detected light signals are converted into electrical signals, which were calibrated using BD FACSDiva™ software (version 8.0.2). The data was analysed using FlowJo (version 10.6.1) by recording FSC and SSC linearly in density plots and displaying the fluorescence signal logarithmically in histograms (Pfromm et al., 2022). BD FACSCanto™ II was used for all FACS experiments (Pfromm et al., 2022). (BD biosciences, n.d.-b, Frey, 2019, Sack et al., 2006)

FACS was carried out to assess viability rates and to investigate the immunological surface marker expression of Cas9 stimulated ARPE-19 cells (see chapter 3.8) in comparison to the control groups (Pfromm et al., 2022).

3.11.2 Establishing a positive control and AB titration

Several publications demonstrated that ARPE-19 cells express immunological surface markers, including HLA-DR, HLA-ABC, CD54 and CD59, in response to IFN-γ stimulation (Jørgensen et al., 2001, Kanuga et al., 2002, Makhoul et al., 2012). Therefore, IFN-γ was used as a positive control for immunological activation. A FACS AB titration was performed prior to evaluation of Cas9-induced surface marker expression to reduce background noise caused by unspecific AB binding as well as false-positive results (Biorad, n.d.). In addition to ARPE-19 cells, HEK-Blue™ IFN-α/β cells were used as a second cell population. Both cell lines were seeded in 6-well plates, with $9*10^5$ cells per well, containing complete growth medium. 24 h later, both cell lines were stimulated with 1,000 IU/ml human recombinant IFN-γ in complete growth medium for 48 h (Kanuga et al., 2002). (Pfromm et al., 2022)

48 h later, the supernatant was discarded, and the cells were washed with 2 ml DPBS (1X). After that, ARPE-19 cells were incubated in Trypsin-EDTA solution (1X) for 5 min, which was then inactivated with 3 ml of complete growth medium. In contrast, HEK-Blue™ IFN-α/β were detached through rinsing with DPBS (1X). Both cell lines were transferred into 50 ml falcon tubes in which ARPE-19 and HEK-Blue™ IFN-α/β cells were mixed. The samples were centrifuged at 300 x g for 10 min at 4 °C. After discarding the supernatant, the cell pellet was resuspended in 50 µl FACS buffer containing 2.5 µl fragment crystallizable (Fc) block and incubated for 5 min on ice. Since it has been described that ARPE-19 cells express Fc receptors, such as CD16, CD64, and neonatal Fc receptor (FcRn), Fc blocking is crucial to avoid unspecific AB binding as Fc receptors can bind to the Fc region of ABs (Van Bilsen et al., 2011, Wang et al., 2010). Fc blocking was followed by AB staining (50µl) for another 15 min on ice. An AB titration with varying AB concentrations was carried out to ascertain the appropriate AB dilution. Table 22 displays an overview of tested FACS AB dilutions. For each FACS AB, a single-staining titration was performed. An unstained control was run in a separate tube to assess the cells' autofluorescence. After incubation, the samples were washed with 1 ml of FACS buffer followed by further centrifugation at 300 x g for 10 min at 4 °C. The

supernatants were aspirated, and the cell pellets were resuspended in 200 µl FACS buffer. Finally, the cell suspensions were transferred into separate FACS tubes. The samples and ABs were always shielded from light. The protocol was performed according to the manufacturer's recommendations. (BD biosciences, n.d.-a)

The FACS analysis was executed with BD FACSCanto™ II (BD biosciences, n.d.-b). The stain index, which represents the ratio of the mean fluorescence intensity (MFI) between positive and negative controls, was used to determine the most promising dilution of FACS AB (Biorad, n.d.):

$$Stain\ index\ = \frac{MFI\ pos\ - MFI\ neg}{2\ SD}$$

Table 22: FACS AB titration.

FACS AB	Dilution
Anti-HLA-DR APC-Cy™7	1:1; 1:2; 1:4; 1:6; 1:8
APC Mouse Anti-Human HLA-ABC	1:1; 1:2; 1:4; 1:6; 1:8; 1:16; 1:25; 1:100; 1:400; 1:1.000; 1:4.000
BV510 Mouse Anti-Human CD59	1:1; 1:2; 1:4; 1:6; 1:8; 1:64
PE Mouse Anti-Human CD54	1:1; 1:2; 1:4; 1:6; 1:8; 1:16; 1:25; 1:32; 1:64; 1:100; 1:400; 1:1.000

3.11.3 Surface marker expression of Cas9-stimulated ARPE-19 cells

ARPE-19 cells were stimulated with Cas9, as described in chapter 3.5 and 3.8. The cells were seeded into 6-well plates with all volumes adjusted accordingly. ARPE-19 cell collection and FACS staining were performed, as described in chapter 3.11.2, with some minor adjustments. A multi-AB-staining was executed instead of a single-AB-staining. Table 23 lists the most promising AB dilutions for multi-staining, as assessed using the performed AB titration experiments (see chapter 3.11.2). 7-AAD, a viability dye, was added to the multi-dye cocktail to evaluate cell viability (Gaforio et al., 2002, Schmid et al., 1994). Fluorescent minus one (FMO) control was carried out with each of the five FACS ABs to assess fluorescence spillover, since fluorescent signals can overlap in different

channels. Gating was adjusted to discriminate between positively and negatively stained cells (Maecker and Trotter, 2006). The protocol was performed according to the manufacturer's recommendations (BD biosciences, n.d.-a). Analysis of the FACS tubes was performed using the BD FACSCanto™ II and data was analysed using FlowJo (version 10.6.1) (BD biosciences, n.d.-b). (Pfromm et al., 2022)

Table 23: Dilution of FACS ABs for multi-staining.

FACS AB	Dilution for multi-staining
Anti-HLA-DR APC-Cy™7	1:1
APC Mouse Anti-Human HLA-ABC	1:100
BV510 Mouse Anti-Human CD59	1:8
PE Mouse Anti-Human CD54	1:100

3.12 Statistical analysis

All statistical analyses were performed with SPSS, version 25.0 (SPSS Inc. Chicago, IL). Data was analysed with a one-way ANOVA, linear regression models or *t*-tests once a normal distribution was proven with the Shapiro-Wilk test. Non-normally distributed data was analysed using the Kruskal-Wallis-test or Mann-Whitney *U* test. The Bonferroni test was performed for all significant one-way ANOVA results, and pairwise comparisons were carried out for significant Kruskal-Wallis-test results. Results with a p-value < 0.05 were considered statistically significant and were marked (*) in graphics. P-values < 0.01 (**) and < 0.001 (***) were highlighted in graphics as well. (Pfromm et al., 2022)

Fig. 1 to Fig. 6 and Fig. 14 were created in Microsoft PowerPoint (version 2005), and Fig. 23 using Microsoft Excel (version 2005). Fig. 20 and Fig. 22 were captured with ZEN pro imaging software (version 2.6). Image Studio Lite (version 5.2) was used to capture images, which are displayed in Fig. 7 to Fig. 10, Fig. 12 and Fig. 13. Fig. 29 was acquired with BD FACSDiva™ (version 8.0.2) and Fig. 31 with FlowJo (version 10.6.1). All other figures and supplements were designed using GraphPad Prism 8 (version 8.0.2) (Pfromm et al., 2022).

4 Results

4.1 Generation of *sp*Cas9 plasmid and control plasmid

4.1.1 PCR

The AAV2, ITR, and EGFP sequences were removed from the template plasmid, EGFP-*sp*Cas9 plasmid, to generate an *sp*Cas9 plasmid whose remaining sequence has a low immunogenic potential. The expected *sp*Cas9 fragment length was 5.5 kbp. Fig. 7 illustrates an amplified DNA fragment of the appropriate size. In addition, the generation of a second plasmid, NC plasmid, was necessary to assess the immunogenicity of Cas9. The entire *sp*Cas9 plasmid, except the Cas9 sequence, was amplified to ensure that NC plasmid transfection does not result in Cas9 expression, so that differences between cellular responses seen in cells transfected with *sp*Cas9 plasmid or the NC plasmid could be ascribed to responses to intracellular Cas9 DNA, RNA, and/or protein (Pfromm et al., 2022). The NC fragment had a size of 4 kbp, which corresponds to the amplified fragment shown in Fig. 8.

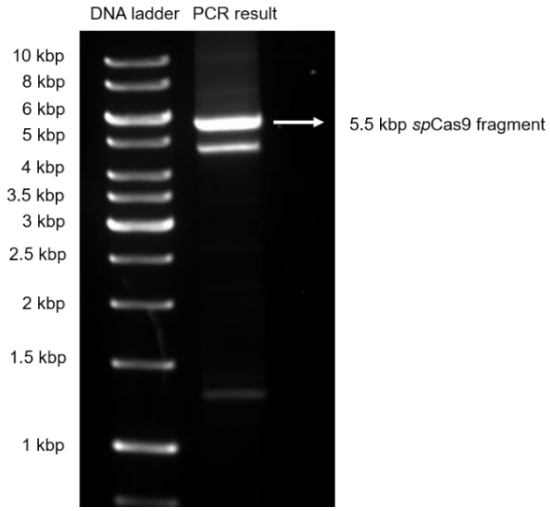

Fig. 7: PCR result of *sp*Cas9 fragment amplification.

The EGFP-*sp*Cas9 plasmid, excluding the AAV2, ITR, and EGFP sequences, was amplified via PCR and run through an agarose gel. The left track represents a DNA ladder, and PCR results are shown on the right track. Two PCR products were amplified with sizes of approximately 5.5 kbp and 4.7 kbp. The 5.5 kbp PCR product indicates successful *sp*Cas9 fragment amplification.

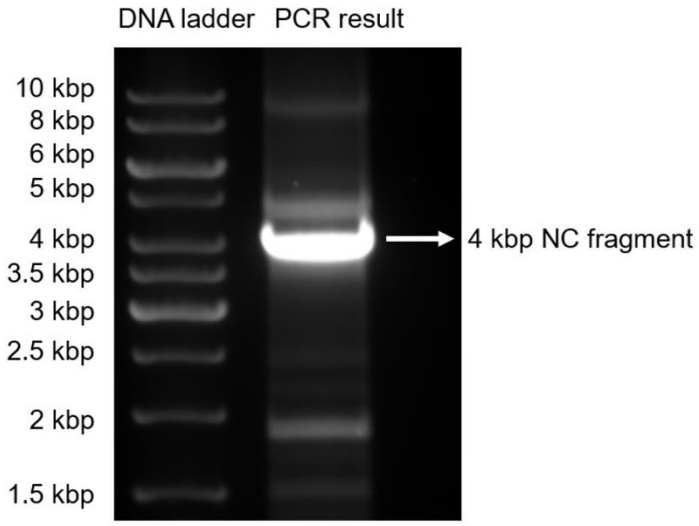

Fig. 8: PCR result of NC fragment amplification.

*Sp*Cas9 plasmid, excluding the *sp*Cas9 sequence, was amplified via PCR and run through an agarose gel. The left track represents the DNA ladder, and PCR results are displayed on the right track. A 4 kbp DNA fragment and minimal byproducts were amplified. The 4 kb fragment corresponds to the expected size and thus indicates successful NC fragment amplification.

Both fragments were then extracted, purified and their DNA concentration as well as their ratio of absorbance at 260 and 280 nm ($A_{260/280}$) was determined using an Infinite M200 microplate reader. The results of this analysis are shown in Table 24. Both DNA fragments had a satisfactory degree of DNA purity, as the $A_{260/280}$ ratios were 1.935 (*sp*Cas9 fragment) and 2.09 (NC fragment). For this reason, both fragments were used for the next step of molecular cloning, the restriction digest.

Table 24: DNA concentration and ratio of $A_{260/280}$ of *sp*Cas9 fragment and NC fragment.

	DNA concentration	**Ratio of $A_{260/280}$**
***sp*Cas9 fragment**	64.1 ng / µl	1.935
NC fragment	29.6 ng / µl	2.09

4.1.2 Restriction digest of PCR fragments

The *sp*Cas9 fragment was ligated to the backbone of the *cj*Cas9 plasmid to obtain an *sp*Cas9 plasmid. Prior to this ligation, the backbone fragment was removed from the *cj*Cas9 plasmid with two REs, NsiI-HF and MluI-HF. Fig. 9 represents the result of this double restriction digest and shows that the plasmids were cleaved into 2.5 kbp and 3.7 kbp DNA fragments. The smaller fragment possessed the expected size of the backbone fragment, whose size was calculated using Geneious software prior to restriction digest. Fig. 9 indicates that suitable REs were selected, and that restriction digest was adequately performed. The 2.5 kbp backbone fragment was extracted from the agarose gel and used for subsequent DNA ligation.

In a further restriction digest, the amplified *sp*Cas9 fragment was also treated with the RE's NsiI-HF and MluI-HF to generate suitable ends for ligation with the backbone fragment. Fig. 10 shows the restriction digest result of two 5.5 kbp DNA fragments, whose size corresponds to the amplified *sp*Cas9 fragment. These results indicate that the fragments were cleaved by NsiI-HF and MluI-HF only at their ends, as the primer sequences for the PCR integrated a cleaving site of both REs. The absence of byproducts indicates that no additional cleaving sites were created. Consequently, it could be assumed that this restriction digest generated the required DNA fragments, which were then extracted from the agarose gel.

The NC plasmid was prepared for ligation with a BspEI restriction digest (gel electrophoresis not shown).

Table 25 displays the DNA concentrations and the $A_{260/280}$ ratio of the extracted DNA fragments. The backbone fragment had sufficient DNA purity, indicated by its $A_{260/280}$ ratio of 2.19. The $A_{260/280}$ ratio of the *sp*Cas9 fragment (2.64) and the NC fragment (2.42) was higher, but still sufficient for subsequent DNA ligation.

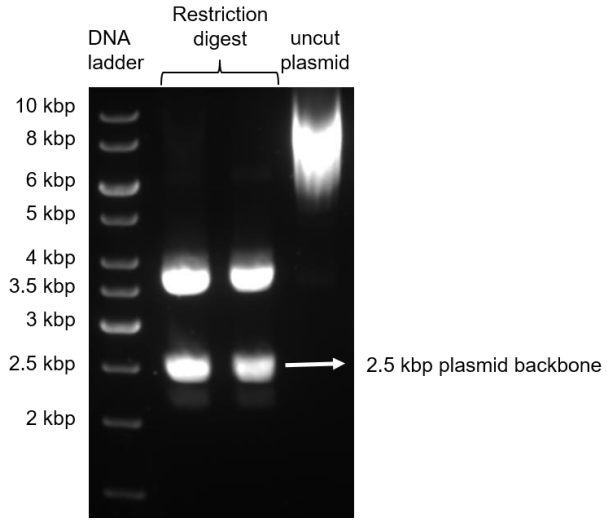

Fig. 9: Restriction digest of *cj*Cas9 plasmid.

The *cj*Cas9 plasmid was treated with NsiI-HF, MluI-HF, and CIP, and the reaction mixture was run through an agarose gel. The left track represents a DNA ladder and the two middle tracks display restriction digest results showing DNA fragments with a size of approximately 2.5 kbp. The 2.5 kbp DNA fragments have an appropriate size indicating restriction digest was performed properly. In contrast, the right track shows an uncut plasmid, which was not treated with any RE.

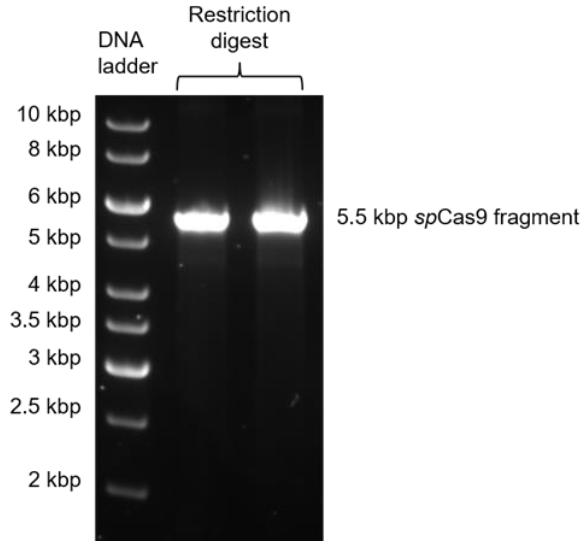

Fig. 10: Restriction digest of *sp*Cas9 fragment.

The *sp*Cas9 fragment was treated with NsiI-HF and MluI-HF, and was run through an agarose gel. The left track represents the DNA ladder. The restriction digest results, two 4 kbp DNA fragments, are displayed by the two right tracks. Both DNA fragments have the appropriate size indicating restriction digest was performed properly.

Table 25: DNA concentration and ratio of $A_{260/280}$ of *sp*Cas9 fragment, NC fragment and backbone fragment after restriction digest.

	DNA concentration	Ratio of $A_{260/280}$
***sp*Cas9 fragment**	20.2 ng / µl	2.64
NC fragment	17.85 ng / µl	2.42
Backbone fragment	13.5 ng / µl	2.19

4.1.3 DNA ligation and bacterial transformation

4.1.3.1 *sp*Cas9 plasmid

The *sp*Cas9 fragment (insert) was ligated to the *cj*Cas9 plasmid backbone (vector) and delivered into *E. coli* bacteria. More *E. coli* colonies grew on the ampicillin agar plate after treatment with a vector:insert ratio of 1:1 compared to a vector:insert ratio of 1:3 and a control group, in which no insert was added to the ligation mixture (Data not shown). *E. coli* colonies could only grow on an ampicillin agar plate once they took up a plasmid containing an *ampicillin resistance* gene. As the vector contained such a gene, *E. coli* colonies which took up a *sp*Cas9 plasmid should have survived on the ampicillin agar plate. Therefore, 16 *E. coli* colonies of the ampicillin agar plate with the highest density of *E.coli* colonies were used for further plasmid DNA isolation to obtain a *sp*Cas9 plasmid.

4.1.3.2 NC plasmid

After the NC fragment was amplified and digested with the RE BspEI, it was self-ligated using a T4 DNA ligase. As a control, a separate reaction mixture containing no T4 DNA ligase was created. Fig. 11 shows grown *E. coli* colonies after treatment with and without T4 DNA ligase on two separate ampicillin agar plates. On the left plate, considerably more *E. coli* colonies grew as, in contrast to the control group, T4 DNA ligase was added to the reaction mixture. The high number of *E. coli* colonies indicates that many *E. coli* integrated plasmids containing an *ampicillin resistance* gene into their genome. Thus, plasmid DNA

isolation was performed using eight *E. coli* colonies from the ampicillin agar plate containing more *E. coli* colonies.

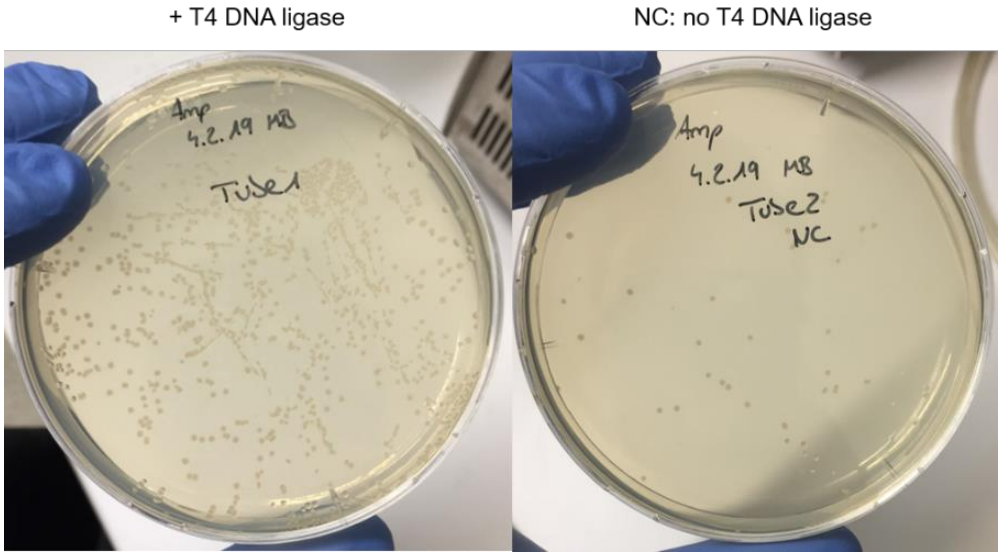

Fig. 11: DNA ligation and bacterial transformation of NC plasmid.

DNA ligation of the NC plasmid and subsequent bacterial transformation was performed. The figure displays two ampicillin agar plates with cultivated *E. coli* colonies after bacterial transformation. The left agar plate shows the DNA ligation result with T4 DNA ligase and the right agar plate without T4 DNA ligase. More *E. coli* colonies grew on the left ampicillin agar plate, indicating successful DNA ligation.

4.1.4 Isolation of plasmid DNA

4.1.4.1 Miniprep of *sp*Cas9 and NC plasmid

The GenElute™ Plasmid Miniprep Kit was used to assess if the grown *E. coli* colonies on the ampicillin agar plates had incorporated a plasmid of the appropriate size. The DNA concentration and purity (ratio of $A_{260/280}$) of both plasmids which were sent in for sequencing are shown in Table 26. DNA concentration and purity were adequately assessed for both plasmids.

Table 26: Miniprep: DNA concentration and ratio of $A_{260/280}$ of *sp*Cas9 and NC plasmid.

	DNA concentration	Ratio of $A_{260/280}$
***sp*Cas9 plasmid**	61.3 ng / µl	1.675
NC plasmid	255.75 ng / µl	1.85

4.1.4.2 Plasmid size calculation

The size of the isolated plasmids was determined prior to sequencing via a further restriction digest. Fig. 12 displays the result of a double and single *sp*Cas9 plasmid restriction digest. The plasmid size was approximately 8 kbp. This indicates that the *sp*Cas9 plasmid contains one recognition site for each of the REs, NsiI-HF and MluI-HF. Fig. 13 displays the result of a BspEI single restriction digest of the NC plasmid. The size of the plasmid was approximately 4 kbp. The reported results indicate that both isolated plasmids have the required size, which is why both the *sp*Cas9 and the NC plasmid were sent in for sequencing.

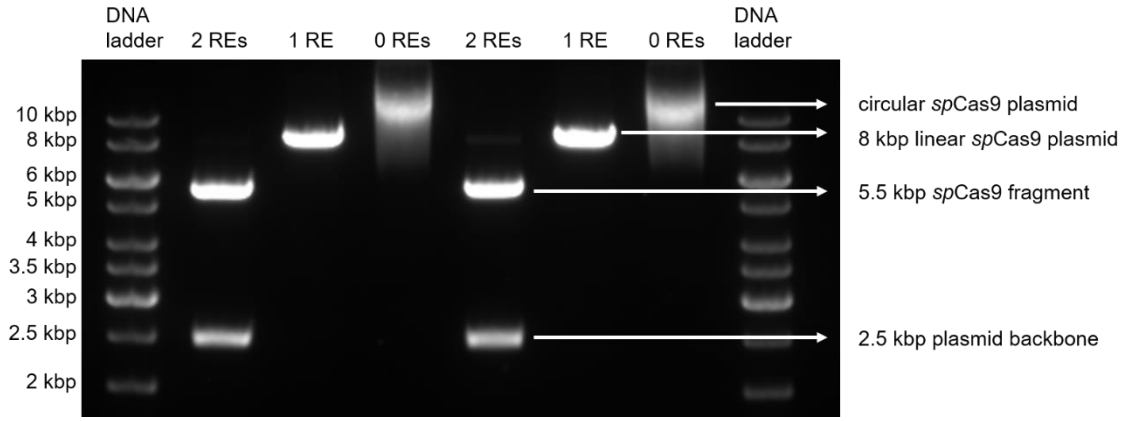

Fig. 12: Restriction digest of *sp*Cas9 plasmid.

The *sp*Cas9 plasmid was digested with the REs NsiI-HF, MluI-HF and was subsequently run through an agarose gel. The left and right track represent the DNA ladder. The second track from the left and the fourth track from the right show the restriction digest with two REs. In these tracks, two DNA fragments are displayed with 2.5 kbp (plasmid backbone) and 5.5 kbp (*sp*Cas9 fragment). The third track from the left and the third track from the right present single restriction digests leading to a plasmid linearisation, indicating that 8 kbp is the size of the entire plasmid. The fourth track from the left and the second track from the right represent the control groups in which no restriction digest was performed. This figure demonstrates that a plasmid with the required size and restriction sites was generated. Consequently, this plasmid was sequenced.

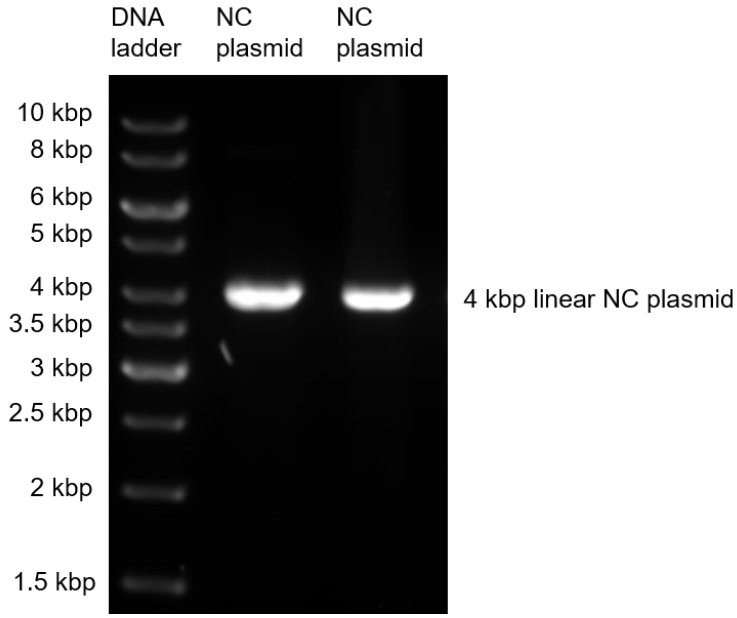

Fig. 13: Restriction digest of NC plasmid.

The NC plasmid was linearised via BspEI restriction digest and was run through an agarose gel. The left track represents the DNA ladder. The two right tracks show the single restriction digests with the RE BspEI. In each of these two tracks, one DNA fragment is displayed with a size of 4 kbp, indicating the plasmid's full size, which corresponds to the NC plasmid size.

4.1.5 Plasmid sequencing

The *sp*Cas9 and NC plasmid were sequenced to exclude the occurrence of mutations during molecular cloning. The sequences of the designed *sp*Cas9 and NC plasmid were compared to the digital plasmid sequences created using Geneious. Consensus identities of 100% for both designed plasmids were calculated, indicating that no mutation occurred during molecular cloning (Data not shown). The sequencing results confirmed that the required *sp*Cas9 and NC plasmid were properly generated. Fig. 14 presents the plasmid map of both the *sp*Cas9 and NC plasmid. The size between both plasmids differs by 4 kbp due to the absence of the Cas9 gene in the NC plasmid. Thus, *sp*Cas9 plasmid transfection should lead to Cas9 expression, whereas NC plasmid transfection should not. In this way, an altered cytokine secretion in *sp*Cas9 plasmid transfected cells when compared to NC plasmid transfected cells may be ascribed to the presence of Cas9 DNA, RNA and/or protein. (Pfromm et al., 2022)

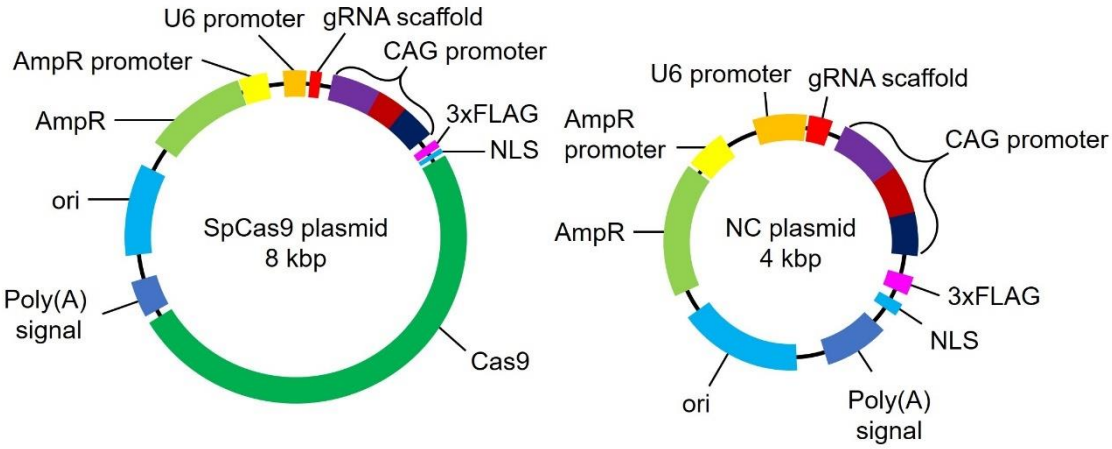

Fig. 14: Plasmid map of *sp*Cas9 plasmid and NC plasmid.

The figure shows a plasmid map of both plasmids. The two plasmids only differ in the presence of the Cas9 gene, leading to a reduced NC plasmid size of 4 kbp compared to the *sp*Cas9 plasmid size of 8 kbp. As no Cas9 gene is present in the NC plasmid, a transfection should not lead to intracellular Cas9 expression. Adapted from (Pfromm et al., 2022).

4.1.6 Plasmid preparation

The EndoFree® Plasmid Mega Kit was used prior to plasmid transfection and ICC to obtain endotoxin-free plasmids. DNA concentration and plasmid purity (ratio of $A_{260/280}$) were evaluated using the Infinite M200 microplate reader. Table 27 shows these results and confirms that all three plasmids have an adequate DNA concentration as well as a high degree of purity, since the ratios of $A_{260/280}$ are between 1.8 and 2.0 (see chapter 3.1.4).

Table 27: Megaprep - DNA concentration and ratio of $A_{260/280}$ of EGFP-*sp*Cas9, *sp*Cas9 and NC plasmid.

	DNA concentration	Ratio of $A_{260/280}$
EGFP-*sp*Cas9 plasmid	2,046 ng / µl	1.87
***sp*Cas9 plasmid**	2,340 ng / µl	1.86
NC plasmid	2,586 ng / µl	1.855

4.2 Cytokine secretion of ARPE-19 cells after PAMP stimulation

4.2.1 Poly(I:C) HMW stimulation

ARPE-19 cells were stimulated with Poly(I:C) HMW, a TLR3 agonist, to establish robust technical controls for cytokine production and to characterise ARPE-19 cytokine response to external stimuli. The cytokine concentrations of the supernatants were measured via ELISAs. Fig. 15, Fig. 16, and Fig. 17 display the concentrations of IL-8, IL-6 and TNF-α released by ARPE-19 cells in response to Poly(I:C) stimulation. Poly(I:C) induced a significant IL-8 release compared to an unstimulated control group at 12 h ($p < 0.001$), 18 h ($p = 0.006$), 24 h ($p = 0.001$), and 48 h ($p = 0.004$) (Pfromm et al., 2022). In addition, Poly(I:C) triggered a strong IL-6 release ($p < 0.001$) and a slight TNF-α release ($p = 0.041$) when compared to an unstimulated control group (Pfromm et al., 2022). IL-8 was the cytokine with the highest absolute supernatant concentration (1,009 pg/ml), reached at 12 h post-stimulation, in comparison to IL-6 (764 pg/ml) and TNF-α (44 pg/ml). This suggests that ARPE-19 produce proinflammatory cytokines in response to external stimuli. In contrast, Poly(I:C) stimulation did not lead to IL-1β, IFN-β, IFN-α, or CD40L release in ARPE-19 cells (see Suppl. 1, Suppl. 2, Suppl. 3 and Suppl. 4).

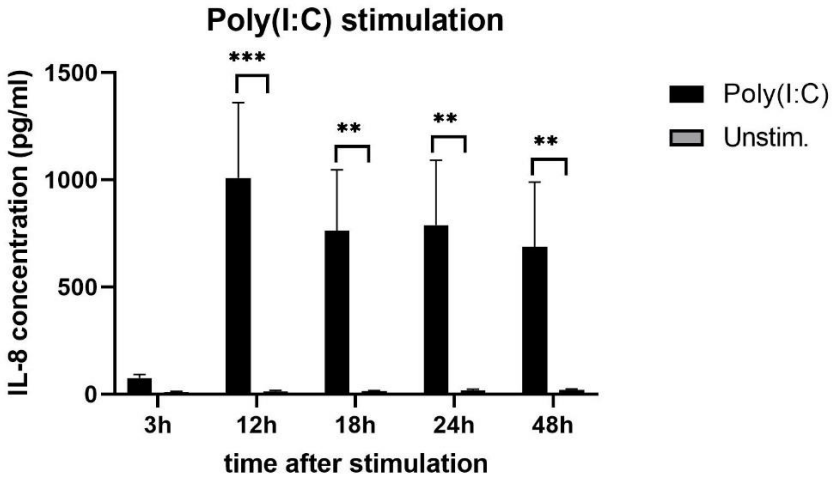

Fig. 15: IL-8 concentration after Poly(I:C) stimulation on ARPE-19 cells.

The IL-8 concentration of ARPE-19 cells' supernatant was measured at five time points (3 h, 12 h, 18 h, 24 h, 48 h) after Poly(I:C) stimulation using ELISA. The figure displays a significantly increased IL-8 secretion in response to Poly(I:C) stimulation compared to unstimulated ARPE-19 cells. The bars represent mean values, and the error bars represent standard deviations of four independent experiments. (n=4, one-way ANOVA, Bonferroni, **=p<0.01, ***=p<0.001)

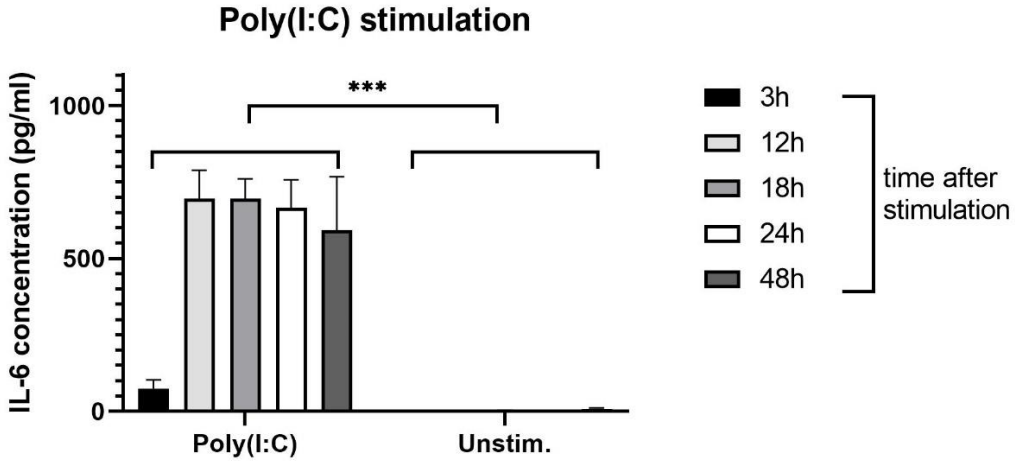

Fig. 16: IL-6 concentration after Poly(I:C) stimulation on ARPE-19 cells.

ARPE-19 cells were stimulated with Poly(I:C) and the IL-6 concentration of the cells' supernatant was measured at five time points (3 h, 12 h, 18 h, 24 h, 48 h) using ELISA. The figure displays a significant increase in IL-6 secretion in response to Poly(I:C) stimulation when compared to unstimulated ARPE-19 cells. The bars represent mean values, and the error bars represent standard deviations of three independent experiments. (n=3, Mann-Whitney *U* test, ***=p<0.001)

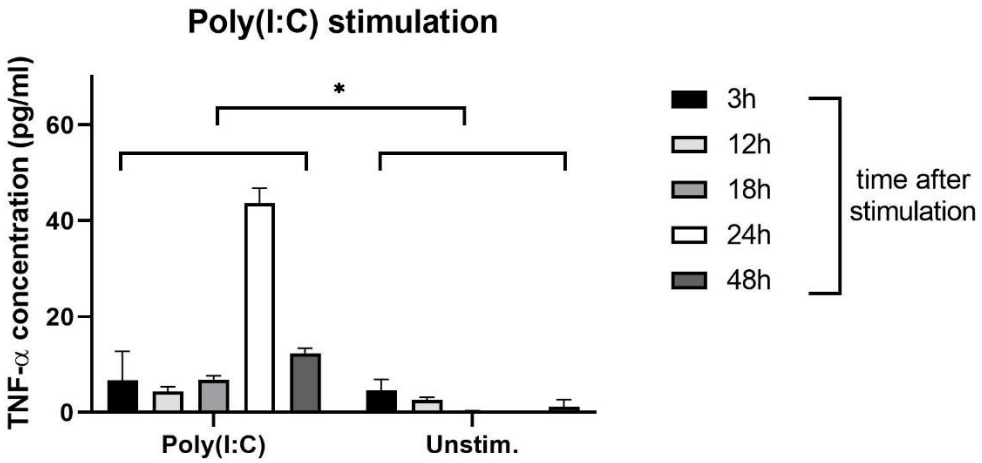

Fig. 17: TNF-α concentration after Poly(I:C) stimulation on ARPE-19 cells.

ARPE-19 cells were stimulated with Poly(I:C) and the cells' TNF-α supernatant concentration was measured at five time points (3 h, 12 h, 18 h, 24 h, 48 h) via ELISA. The figure displays a significant TNF-α release in response to Poly(I:C) stimulation compared to unstimulated ARPE-19 cells. Data are representative of three independent experiments. The bars show mean values, and the error bars represent standard deviations. (n=3, Mann-Whitney *U* test, *=p<0.05)

4.2.2 dsDNA stimulation

As plasmids consist of dsDNA, ARPE-19 were stimulated with transfected dsDNA to assess if dsDNA itself can trigger ARPE-19 cytokine secretion. Cytokine secretion was compared to a control group, treated with Lipofectamine LTX, at five time points (3 h, 12 h, 18 h, 24 h, 48 h) using ELISA. Fig. 18 and Fig. 19 show the concentration of IL-8 and IL-6 produced by ARPE-19 cells following dsDNA stimulation. Stimulation with dsDNA and Lipofectamine LTX induced a slight IL-6 ($p = 0.01$) and a strong IL-8 ($p < 0.001$) release when compared to the control group. For both cytokines, the average peak value of 478 pg/ml (IL-8) and 23 pg/ml (IL-6) was reached at 48 h, which indicates time-dependent cytokine secretion. The elevated IL-6 and IL-8 levels are attributable to dsDNA exposure as the control group did not induce any noticeably increase of these two interleukins. This suggests that plasmids might cause proinflammatory cytokine release, as well. However, dsDNA stimulation did not trigger TNF-α, IFN-β, IFN-α, IL-1β, and CD40L secretion (see Suppl. 1, Suppl. 2, Suppl. 3, Suppl. 4 and Suppl. 5).

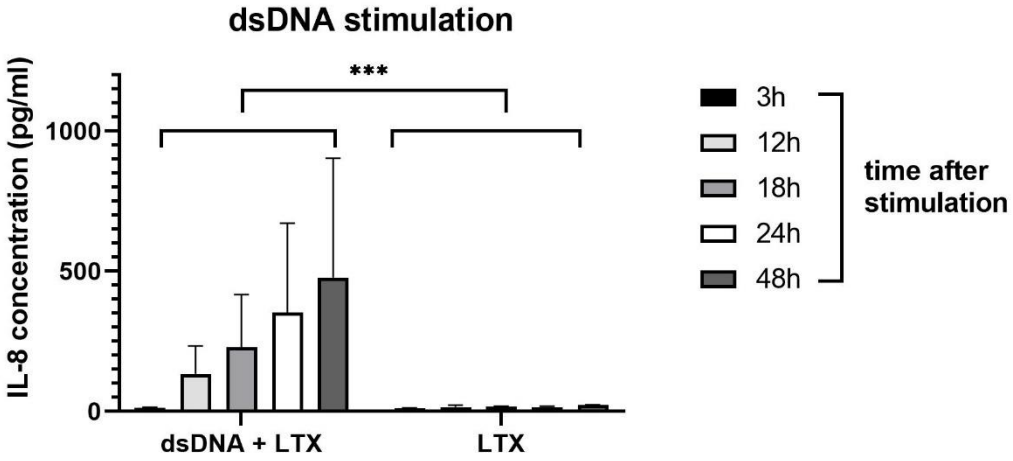

Fig. 18: IL-8 concentration after dsDNA stimulation on ARPE-19 cells.

ARPE-19 cells were stimulated with dsDNA and Lipofectamine LTX. IL-8 concentration of the cells' supernatant was measured by ELISA at five time points (3 h, 12 h, 18 h, 24 h, 48 h). ARPE-19 cells only treated with Lipofectamine LTX were used as a control group. The figure illustrates significantly elevated IL-8 levels in response to dsDNA and Lipofectamine LTX stimulation when compared to the control group. The bars represent mean values, and the error bars show standard deviations of three independent experiments. (n=3, *t*-test, ***=p<0.001)

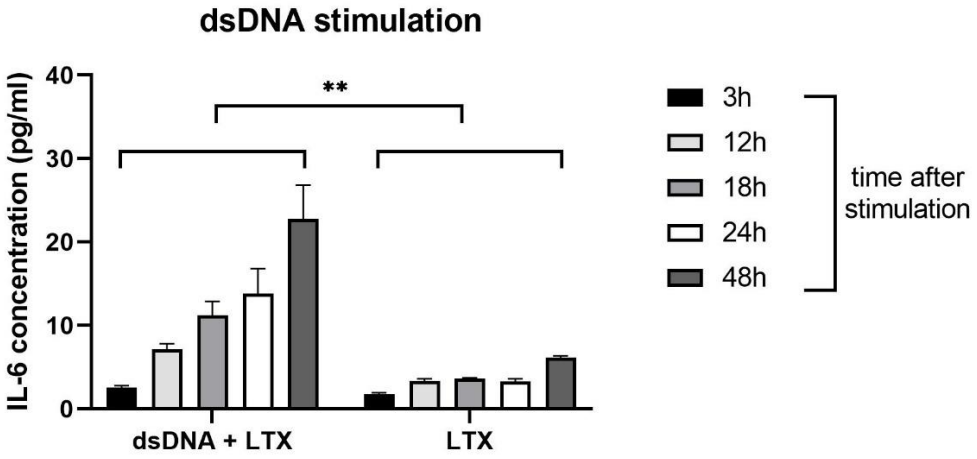

Fig. 19: IL-6 concentration after dsDNA stimulation on ARPE-19 cells.

IL-6 concentration of ARPE-19 cells' supernatant was measured at five time points (3 h, 12 h, 18 h, 24 h, 48 h) after dsDNA stimulation by an ELISA. The figure illustrates a significant IL-6 increase in response to dsDNA and Lipofectamine LTX stimulation comparing to ARPE-19 cells treated with Lipofectamine LTX only. Data are representative of three independent experiments. The bars show mean values, and the error bars represent standard deviations. (n=3, *t*-test, **=p<0.01)

4.3 Assessing plasmid transfection efficacy of different transfection reagents in ARPE-19 cells

The plasmids were delivered into ARPE-19 cells via cationic lipid transfection (Pfromm et al., 2022). Three different transfection reagents (Lipofectamine LTX, Lipofectamine 3000, and a transfection reagent from Altogen Biosystems) were evaluated to maximise the transfection rate. The EGFP-*sp*Cas9 plasmid was selected for optimisation, as its EGFP expression, which can be assessed by fluorescence microscopy, correlates with transfection efficacy. Fig. 20 illustrates one of three plasmid transfections with Lipofectamine LTX. The figure shows an EGFP expression of 33 % and a moderate level of cytotoxicity, such as detached cells, was observed microscopically at 24 h post-transfection.

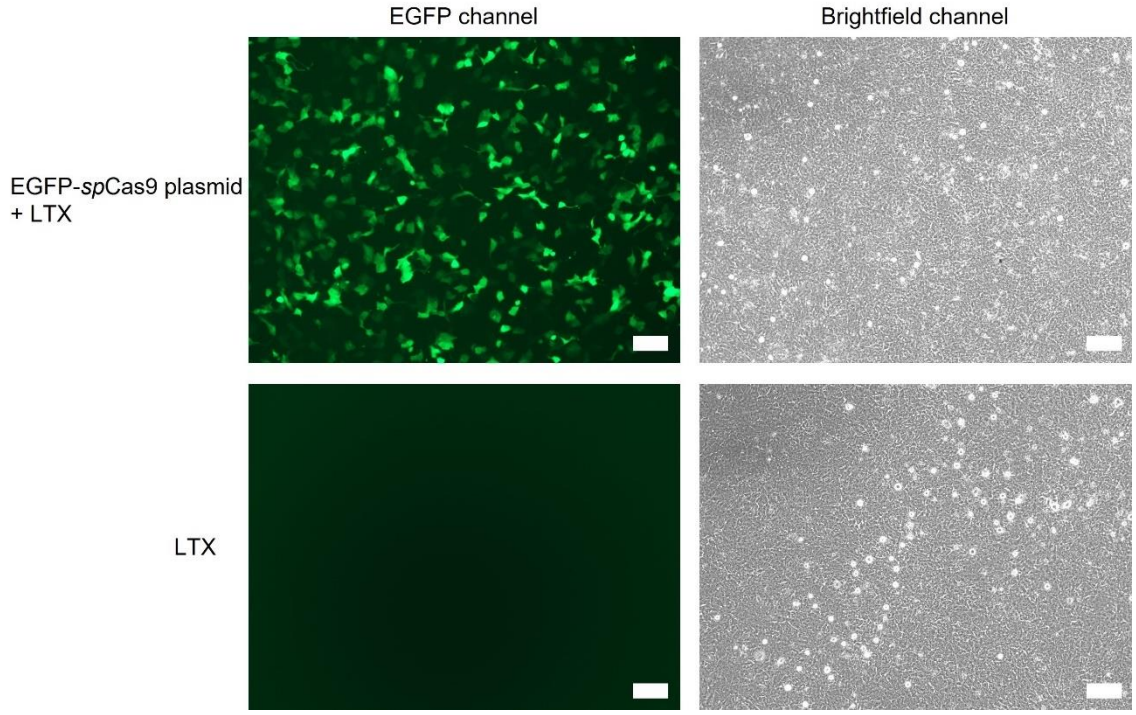

Fig. 20: Cationic lipid transfection of ARPE-19 cells with Lipofectamine LTX.

ARPE-19 cells were transfected with Lipofectamine LTX and EGFP-*sp*Cas9 plasmid. EGFP expression was quantitatively determined with the fluorescence microscope by overlaying the fluorescence image with the brightfield image after 24 h. The transfection efficacy was 33 % according to manual counting by workgroup members. As a control, ARPE-19 cells were treated with Lipofectamine LTX only, in which no EGFP expression was detected. This figure is representative of three independent experiments. Scale bar: 100 µm

Fig. 21 summarises transfection results of three different transfection reagents. The average transfection rate between Lipofectamine LTX (31 %) and Lipofectamine 3000 (26 %) was comparable as no significant differences were detectable. In contrast, only 0.4 % of all cells were transfected by Altogen Biosystems' reagent. Since plasmid transfection with Lipofectamine LTX resulted in a high transfection rate and a moderate toxicity rate, cationic lipid transfection appears as suitable method for assessing Cas9 immunogenicity in ARPE-19 cells. Further transfection experiments were carried out with Lipofectamine LTX.

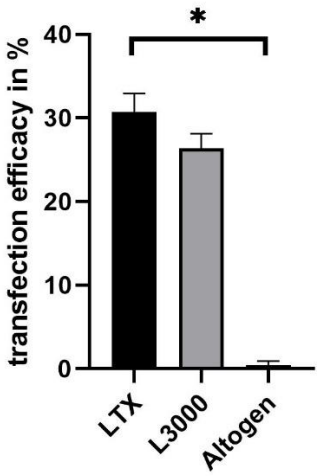

Fig. 21: Cationic lipid-mediated transfection on ARPE-19 cells using different transfection reagents.

The figure shows EGFP-*sp*Cas9 plasmid transfection in ARPE-19 cells with three different transfection reagents (Lipofectamine LTX, Lipofectamine 3000 and Altogen Biosystems' transfection reagent). The bars represent the average transfection efficacy, and the error bars indicate standard deviation of three independent experiments. The transfection efficacy was measured at 24 h post-transfection. The highest transfection efficacy was reached with Lipofectamine LTX and Lipofectamine 3000. (n=3, Kruskal-Wallis-test and pairwise comparisons, *=$p<0.05$)

4.4 ARPE-19 cells express Cas9 after plasmid transfection

ICC was performed to prove Cas9 expression in *sp*Cas9 plasmid transfected cells. Therefore, ARPE-19 cells were transfected with three different plasmids: EGFP-*sp*Cas9 plasmid (positive control), *sp*Cas9 plasmid, and NC plasmid (negative control). Cas9 protein was labelled with a fluorophore which emits a fluorescent signal at 568 nm. Consequently, Cas9 expression was evaluated via

fluorescence microscopy using the AlexaFluor568 channel. Fig. 22 shows the summary of one ICC experiment and is representative of four independent experiments. This confirmed that ARPE-19 cells transfected with *sp*Cas9 plasmid expressed Cas9 protein 24 h after transfection, whereas cells transfected with NC plasmid did not (Pfromm et al., 2022). This experiment indicated that ARPE-19 cells can express Cas9 and proved proper generation of the self-designed *sp*Cas9 plasmid, so that successful *sp*Cas9 plasmid transfection resulted in Cas9 expression (Pfromm et al., 2022). Due to the absence of Cas9 expression in ARPE-19 cells transfected with the NC plasmid, this plasmid was deemed suitable as a negative control plasmid to assess Cas9 immunogenicity in ARPE-19 cells transfected with the *sp*Cas9 plasmid (Pfromm et al., 2022).

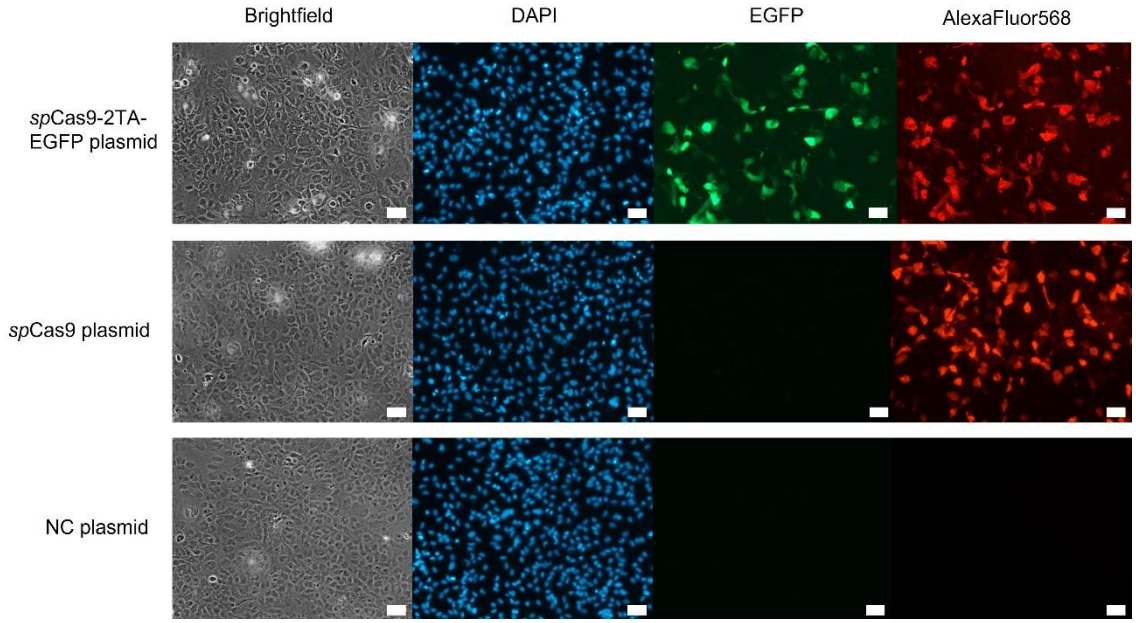

Fig. 22: ARPE-19 cells express Cas9 after plasmid transfection.

ARPE-19 cells were transfected with different plasmids (EGFP-*sp*Cas9, *sp*Cas9, and NC plasmid), represented by three image series. ICC was performed 24 h post-transfection. The right images were taken with the AlexaFluor568 channel. Since the Cas9 protein was labelled with AlexaFluor568 fluorophore, a fluorescence signal indicates Cas9 expression. The DAPI channel, the second column from the left, shows stained DNA, and the EGFP channel displays EGFP expression. ARPE-19 cells expressed Cas9 24 h after EGFP-*sp*Cas9 plasmid or *sp*Cas9 plasmid transfection. NC plasmid transfected cells did not express Cas9, and EGFP signal only occurred in cells treated with EGFP-*sp*Cas9 plasmid. Data are representative of four independent experiments (n = 4) which were all carried out as a control to Cas9 stimulation experiment (see chapter 3.8). Scale bar: 50 µm. Adapted from Pfromm et al. (2022).

4.5 Cas9-induced cyto- and chemokine profile of ARPE-19 cells

The Proteome Profiler Human XL Cytokine Array Kit was used as a screening tool to determine the cytokine concentration of as many cyto- and chemokines as possible so that upregulated immune markers might be quantified later using a more sensitive ELISA. Supernatants of ARPE-19 cells transfected with *sp*Cas9 plasmid and Lipofectamine LTX were compared to a control group transfected with NC plasmid and Lipofectamine LTX, which did not lead to intracellular Cas9 expression. Fig. 23 illustrates the absolute and relative differences of various cyto- and chemokine concentrations between the two groups' supernatants at 24 h after transfection with the respective plasmid. It is shown that a high number of cyto- and chemokines in the Cas9-treated group were upregulated. *Sp*Cas9 plasmid transfection triggered an IL-8 release indicated by an absolute difference of 0.338 and a relative difference of 1.86 when compared to the control (Pfromm et al., 2022). As a second immune marker, CD40L showed the highest increase in relative difference (2.11) in Cas9-treated cells.

This experiment demonstrates that *sp*Cas9 plasmid transfection might induce the secretion of cyto- and chemokines (Pfromm et al., 2022). In this context, IL-8 and CD40L emerge as immune regulators with the highest increase in response to Cas9 expression. To confirm these results, the supernatant concentration of IL-8 and CD40L was determined in three independent experiments and at different time points via ELISA (Pfromm et al., 2022).

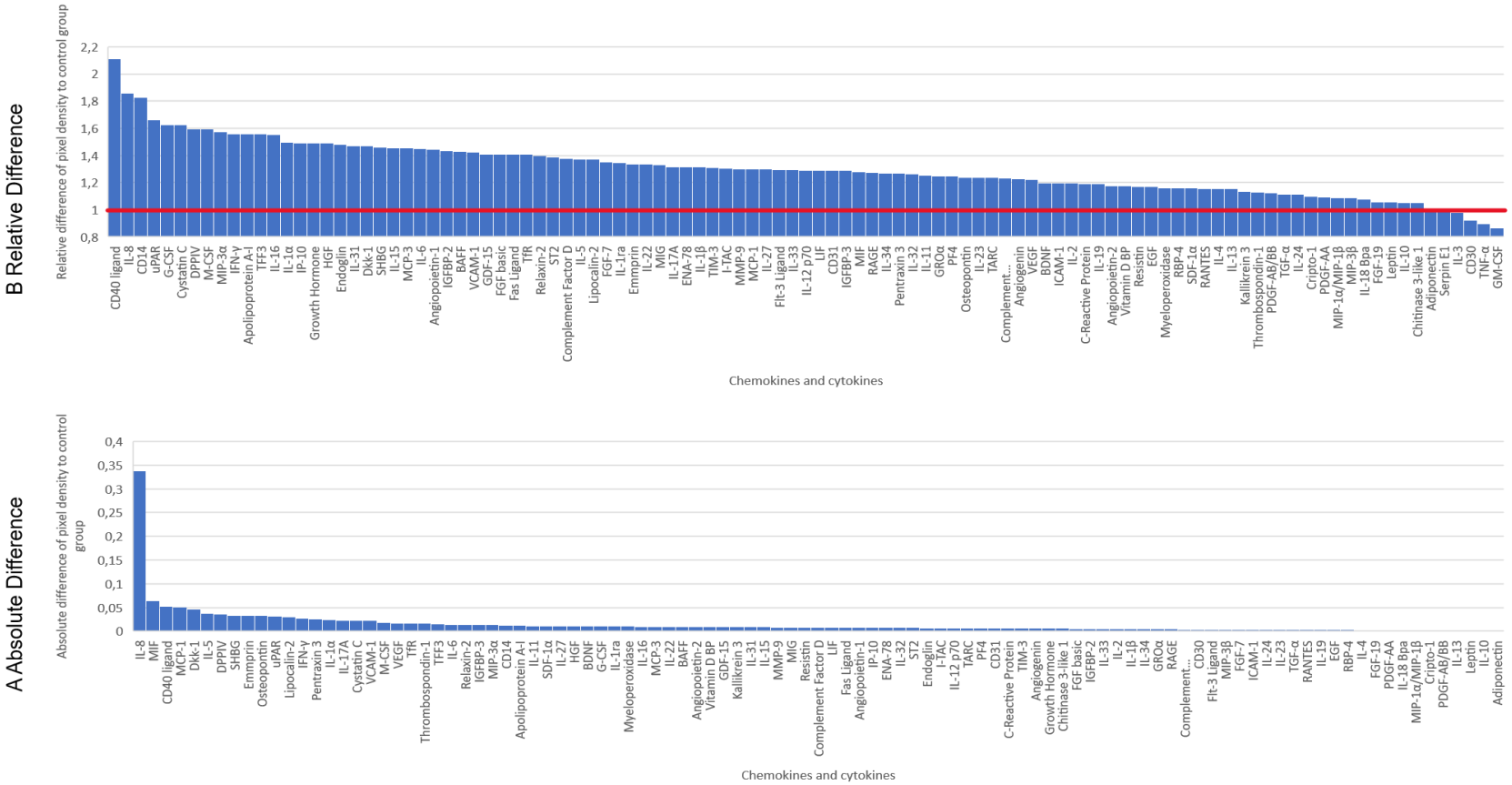

Fig. 23: Absolute and relative differences in Cas9-induced cytokine secretion compared to a control group.

The figure displays the chemo- and cytokine levels produced by ARPE-19 cells 24 h post-transfection with the *sp*Cas9 plasmid in relative and absolute comparison to NC plasmid transfection assessed by Proteome Profiler Array. Cyto- and chemokines are listed on the X-axis, and the Y-axis displays the amount of the relative or absolute difference. The red line marks a relative difference of 1. The figure illustrates a release of IL-8 and CD40L in response to *sp*Cas9 plasmid transfection. The experiment was carried out once. Data adapted from (Pfromm et al., 2022)

4.6 Cas9-induced cytokine production in ARPE-19 cells

ARPE-19 cells were transfected with the *sp*Cas9 plasmid and Lipofectamine LTX to determine the immunogenicity of intracellularly expressed Cas9. Cytokine concentrations measured at five time points (3 h, 12 h, 18 h, 24 h, 48 h) using an ELISA were compared to cytokine measurements from ARPE-19 cells transfected with NC plasmid and Lipofectamine LTX. Fig. 24 displays IL-8 levels after *sp*Cas9 plasmid and NC plasmid transfection at five time points. It is shown, that both *sp*Cas9 plasmid and NC plasmid transfection triggered an IL-8 release by ARPE-19 cells, which significantly increased over time ($p < 0.001$). The average peak value was reached in both groups at 48 h post-transfection: 907.31 pg/ml (*sp*Cas9 plasmid + LTX); 368.94 pg/ml (NC plasmid + LTX). In addition, *sp*Cas9 plasmid transfection induced significantly higher IL-8 concentration ($p = 0.004$) when compared to NC plasmid transfection, indicating a Cas9-enhanced IL-8 secretion.

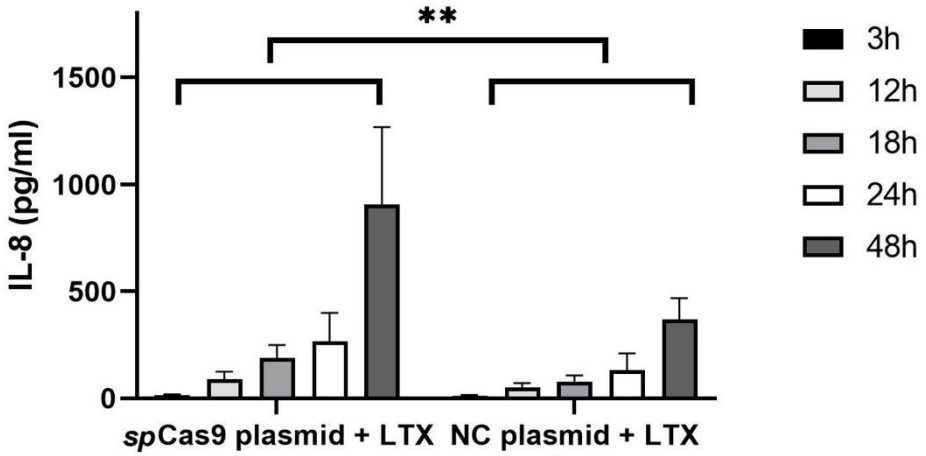

Fig. 24: IL-8 production following Cas9 stimulation of ARPE-19 cells.

The figure highlights the significant IL-8 release from ARPE-19 cells transfected with *sp*Cas9 plasmid and Lipofectamine LTX when compared to the control group, in which ARPE-19 cells were transfected with NC plasmid and Lipofectamine LTX, at five different time points (3 h, 12 h, 18 h, 24 h, and 48 h). The bars represent mean values, and the error bars represent standard deviations of three independent experiments. (n=3, linear regression, **=p<0.01)

Increased CD40L supernatant concentrations of *sp*Cas9 transfected ARPE-19 cells, as observed in chapter 4.5, could not be verified by ELISA as illustrated by Suppl. 1. Besides, *sp*Cas9 plasmid transfection did not trigger IFN-β and IFN-α secretion compared to NC plasmid transfection (see Suppl. 2 and Suppl. 3).

4.7 Immune responses to plasmid-mediated gene transfer

*Sp*Cas9 plasmid and NC plasmid transfected ARPE-19 cells were compared to three control groups to assess whether plasmid-mediated gene transfer itself induced cytokine secretion. ARPE cells were treated either with *sp*Cas9 plasmid (1) or Lipofectamine LTX (2) only, and an unstimulated control group (3) was added. Cytokine levels were assessed at five time points (3 h, 12 h, 18 h, 24 h, and 48 h). Fig. 25 shows an induced IL-8 release of ARPE-19 cells either transfected with *sp*Cas9 or NC plasmid at 18 h, 24 h and 48 h ($p < 0.001$, for both plasmid transfections at all three time points). There was no detectable difference between the controls, indicating that the strong IL-8 secretion was triggered by plasmid-mediated gene transfer. (Pfromm et al., 2022)

To identify co-secreted cytokines, the IL-6 release after *sp*Cas9 and NC plasmid transfection of ARPE-19 cells was also assessed via sandwich ELISA. Fig. 26 displays a strong IL-6 release after both *sp*Cas9 and NC plasmid transfection starting at 12 h post-transfection when compared to an unstimulated control (12 h: *sp*Cas9 plasmid transfection $p = 0.008$; NC plasmid transfection $p = 0.049$; 18 h: *sp*Cas9 plasmid transfection $p < 0.001$; NC plasmid transfection $p = 0.005$; 24 h, 48 h: for both plasmid transfections at both time points $p < 0.001$). There was a stronger IL-6 release seen in ARPE-19 cells transfected with *sp*Cas9 plasmid (48 h: 155.52 pg/ml) when compared to NC plasmid transfection (48 h: 132.62 pg/ml), but the difference was not significant ($p = 0.227$). In addition, no significant differences were detected between the three control groups. The production of further immune markers, CD40L, IFN-β, and IFN-α, was not induced by plasmid transfection (see Suppl. 1, Suppl. 2 and Suppl. 3). This implies that plasmid-mediated gene transfer induced IL-6 and IL-8 but not CD40L, IFN-β, and IFN-α. (Pfromm et al., 2022)

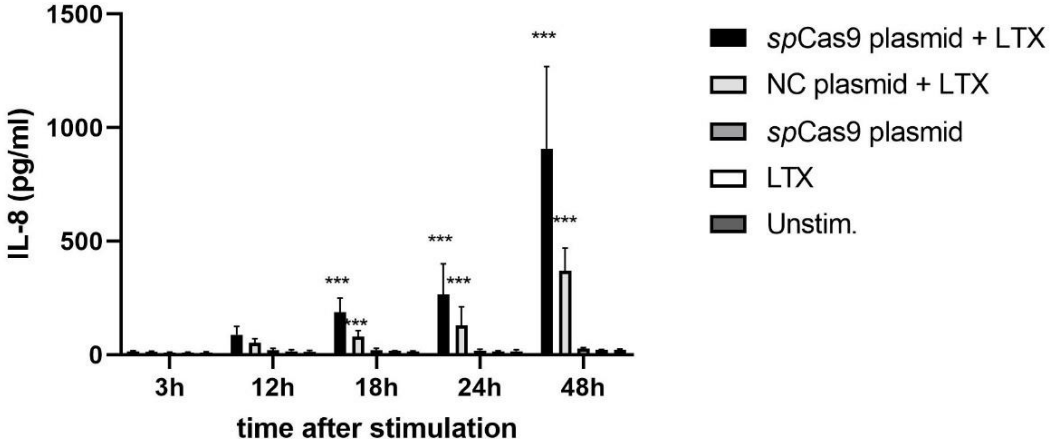

Fig. 25: IL-8 release by ARPE-19 cells after plasmid transfection.

IL-8 levels of *sp*Cas9 plasmid and Lipofectamine LTX transfected ARPE-19 cells were determined at five different time points via ELISA. They were compared to ARPE-19 cells transfected with NC plasmid and Lipofectamine LTX, treated with the *sp*Cas9 plasmid or Lipofectamine LTX only as well as to an unstimulated control. The transfection of the *sp*Cas9 plasmid (*sp*Cas9 plasmid + LTX) and the NC plasmid (NC plasmid + LTX) triggered an IL-8 release. (n=3, one-way ANOVA, Bonferroni, **=p<0.01, ***=p<0.001)

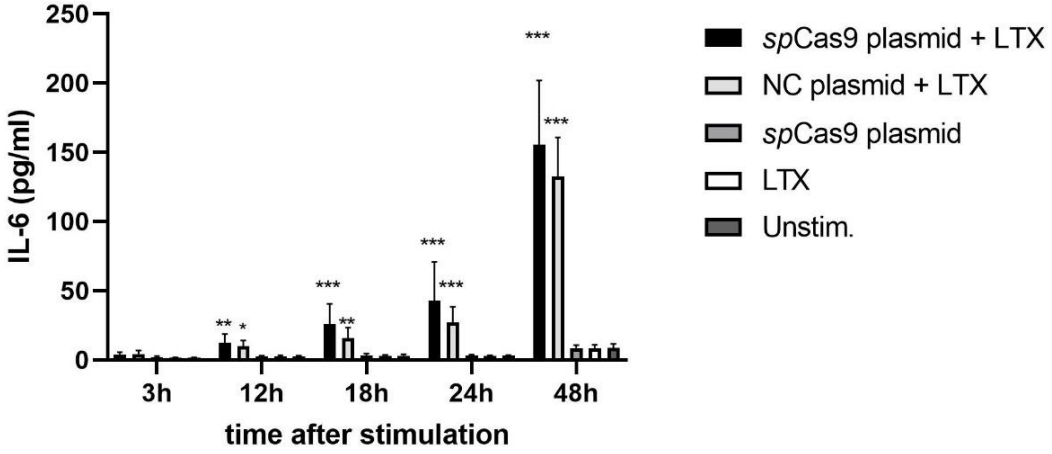

Fig. 26: IL-6 release by ARPE-19 cells after plasmid transfection.

*Sp*Cas9 plasmid (*sp*Cas9 plasmid + LTX) and NC plasmid transfection (NC plasmid + LTX) of ARPE-19 cells triggered a significant IL-6 release. IL-6 levels of plasmid transfected ARPE-19 cells were determined at five different time points via ELISA. These levels were compared to ARPE-19 cells transfected with NC plasmid and Lipofectamine LTX, treated with *sp*Cas9 plasmid or Lipofectamine LTX only as well as to an unstimulated control. No significant difference between *sp*Cas9 and NC plasmid transfected ARPE-19 cells was observed. (n=3, one-way ANOVA, Bonferroni, *=p<0.05, **=p<0.01, ***=p<0.001)

4.8 Presence of IL-8-inducing cytokines in response to Cas9

TNF-α and IL-1β supernatant concentrations were calculated by ELISA at five different time points (3 h, 12 h, 18 h, 24 h, 48 h) to assess whether the detected IL-8 release, as described in chapter 4.6 and 4.7, was triggered by IL-8 inducing cytokines (see chapter 1.6.3.2). Fig. 27 and Fig. 28 demonstrate that *sp*Cas9 plasmid transfected ARPE-19 cells did not secrete significantly elevated TNF-α and IL-1β levels at any time point when compared to NC plasmid transfected ARPE-19 cells. Additionally, plasmid transfection alone, either with the *sp*Cas9 and the NC plasmid, did not induce TNF-α and IL-1β release in ARPE-19 cells in comparison to controls. This suggests that TNF-α and IL-1β are not involved in the immune response of ARPE-19 cells to Cas9 and plasmid transfection.

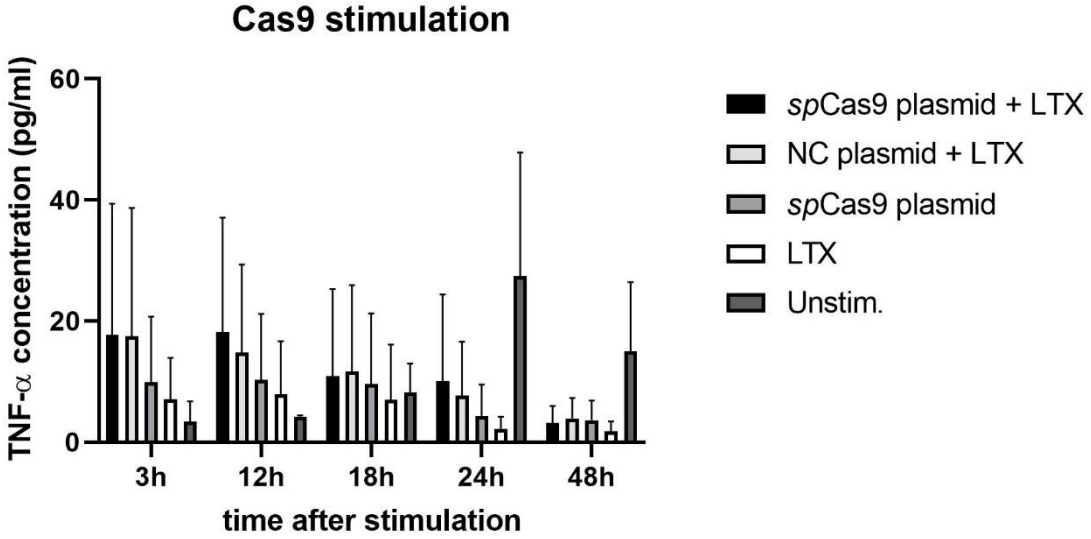

Fig. 27: TNF-α concentration after Cas9 stimulation on ARPE-19 cells.

TNF-α supernatant concentrations of *sp*Cas9 plasmid and Lipofectamine LTX transfected ARPE-19 cells were determined at five different time points (3 h, 12 h, 18 h, 24 h, and 48 h) via ELISA. They were compared to ARPE-19 cells transfected with NC plasmid and Lipofectamine LTX, treated with *sp*Cas9 plasmid or Lipofectamine LTX only as well as to an unstimulated control. No significant TNF-α level differences between all five groups were detected. The bars depict mean values, and the error bars represent standard deviations of three independent experiments. (n=3, one-way ANOVA, Bonferroni)

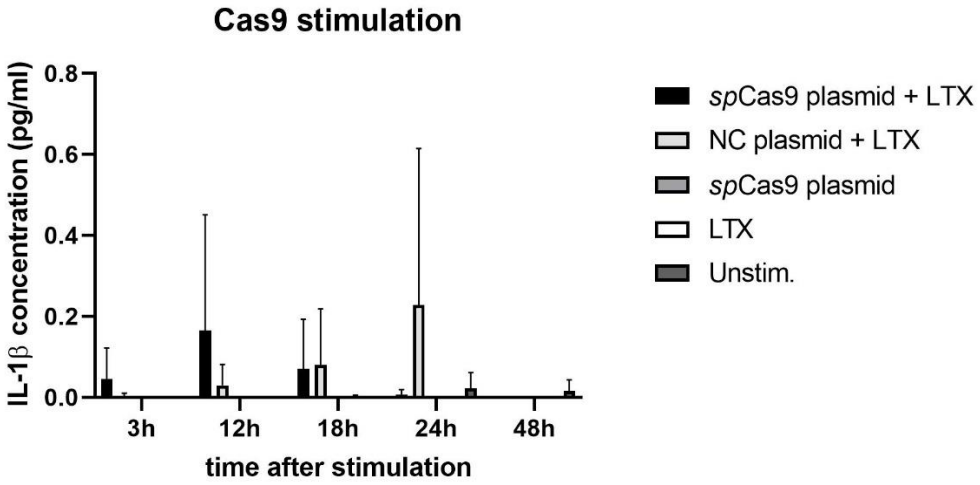

Fig. 28: IL-1β concentration after Cas9 stimulation of ARPE-19 cells.

*Sp*Cas9 plasmid transfection of ARPE-19 cells did not induce an IL-1β release. Cytokine levels were determined at five time points (3 h, 12 h, 18 h, 24 h, and 48 h) using an ELISA. They were compared to ARPE-19 cells transfected with NC plasmid and Lipofectamine LTX, treated with *sp*Cas9 plasmid or Lipofectamine LTX only, as well as to an unstimulated control. The bars represent mean values, and the error bars show standard deviations of three independent experiments. (n=3, one-way ANOVA, Bonferroni)

4.9 Plasmid-mediated gene transfer induced cytotoxicity and upregulation of immunological surface markers

The viability and expression of immunological surface markers of ARPE-19 cells in response to Cas9 and plasmid transfection was determined by flow cytometry. Thus, their cytotoxic and immunological effects are precisely characterised.

4.9.1 Gating strategy and viability rate

To properly assess surface marker expression by flow cytometry, ARPE-19 cells were gated as single, living cells, which is shown in Fig. 29. The results are illustrated by dot plots, in which two different sequences were plotted against each other. The viability rate was determined by plotting FSC-A against 7-AAD, a viability dye, as dead cells emit a more intense 7-AAD fluorescence signal than living cells. This way, viable and dead cells were discriminated to assess the cytotoxic effects of Cas9 and plasmid transfection. (Pfromm et al., 2022)

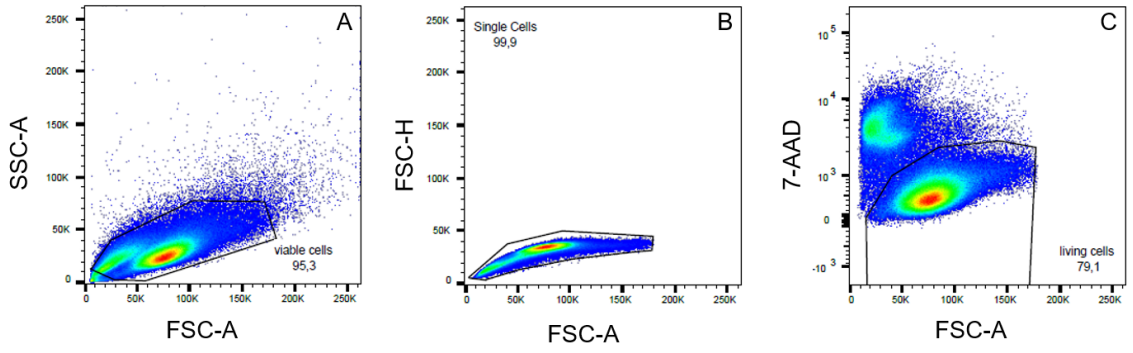

Fig. 29: Gating strategy.

The figure shows a representative example of the gating strategy used for the analysis of immunological surface markers on ARPE-19 cells. In “A”, the forward scatter (FSC), which displays the size of the cells, is plotted against the side scatter (SSC) representing the cells’ granularity. As shown in the figure, minor events, possibly cell debris, as well as very large and highly granulated cells were not included in the analysis. “B” shows single cells and “C” presents another dot plot in which FSC is plotted against 7-AAD. 7-AAD stains dead cells, which allows precise viability rate calculation of the different groups. For the subsequent analysis of immunological surface marker expression, ARPE-19 cells were gated as single, living cells. Adapted from (Pfromm et al., 2022).

To assess the impact of plasmid transfection on cell viability, ARPE-19 cells were transfected with either *sp*Cas9 plasmid or NC plasmid. The viability rates were compared to ARPE-19 cells treated with *sp*Cas9 plasmid or Lipofectamine LTX only or unstimulated cells at 48 h post-transfection. Fig. 30 displays moderate viability rates of *sp*Cas9 (85.2 %) and NC plasmid (86.3 %) transfected ARPE-19 cells, which were significantly reduced when compared to an unstimulated control (*sp*Cas9 plasmid: $p = 0.017$; NC plasmid: $p = 0.032$). As the ratio of living cells did not differ between *sp*Cas9 and NC plasmid transfected cells, cytotoxic effects were likely induced by plasmid-mediated gene transfers rather than by Cas9 expression (Pfromm et al., 2022).

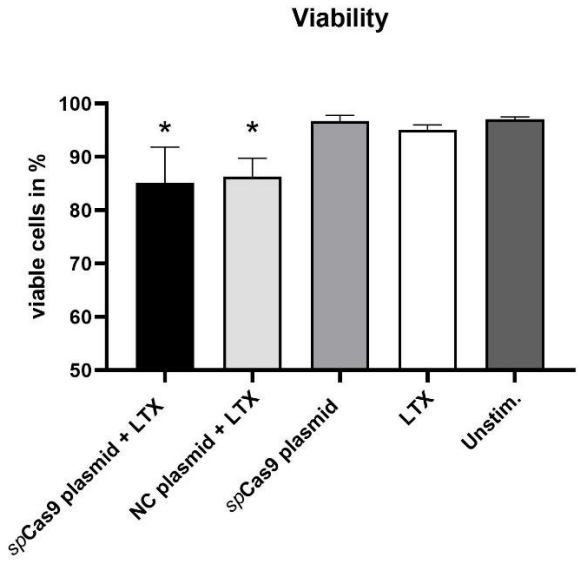

Fig. 30: Plasmid transfection reduces viability rate of ARPE-19 cells.

Viability rates of *sp*Cas9 plasmid and Lipofectamine LTX transfected ARPE-19 cells were determined by flow cytometry at 48 h post-transfection. They were compared to ARPE-19 cells transfected with NC plasmid and Lipofectamine LTX, treated with *sp*Cas9 plasmid or Lipofectamine LTX only as well as to an unstimulated control. *Sp*Cas9 plasmid (spCas9 plasmid + LTX) and NC plasmid transfection (NC plasmid + LTX) significantly reduced the percentage of viable cells when compared to controls. No significant viability rate difference between *sp*Cas9 and NC plasmid transfected ARPE-19 cells was observed. The bars represent mean values, and the error bars show standard deviations of three independent experiments. (n=3, one-way ANOVA, Bonferroni *=p<0.05)

4.9.2 Surface marker expression in ARPE-19 cells

The expression of the surface markers HLA-ABC, HLA-DR, CD59 and CD54 on ARPE-19 in response to *sp*Cas9 plasmid and NC plasmid transfection as well as controls was analysed by flow cytometry, which is displayed by Fig. 31. The detected events of the FACS analysis were displayed in a histogram according to their frequency. The fluorescence intensity is shown on the x-axis and the cell count on the y-axis. Since the ARPE-19 cells were stained with secondary fluorescent antibodies, the fluorescence signal intensity corresponds to existing antigen-antibody binding sites indicating surface molecule expression.

Fig. 31 shows that plasmid transfection, both with *sp*Cas9 and NC plasmid, led to a right shift of the HLA-ABC and CD54 histogram, indicating an increased expression of these surface molecules. This right shift was reproduced as Fig. 32

illustrates the MFI of fluorescent-labelled ABs (HLA-ABC, HLA-DR, CD54, CD59) of three independent experiments. It is shown, that both *sp*Cas9 and NC plasmid transfection increased HLA-ABC (both plasmid transfections: $p < 0.001$) and CD54 (*sp*Cas9 plasmid: $p = 0.004$; NC plasmid: $p = 0.029$) expression on ARPE-19 cells. Compared to NC plasmid transfection, *sp*Cas9 plasmid transfection did not lead to a significant change in the ARPE-19 expression profile of the surface markers. Besides, no significant differences in HLA-DR and CD59 levels were observed between any group. These experiments suggest that plasmid transfection but not the presence of Cas9 triggered an upregulation of HLA-ABC and CD54 expression on ARPE-19 cells. (Pfromm et al., 2022)

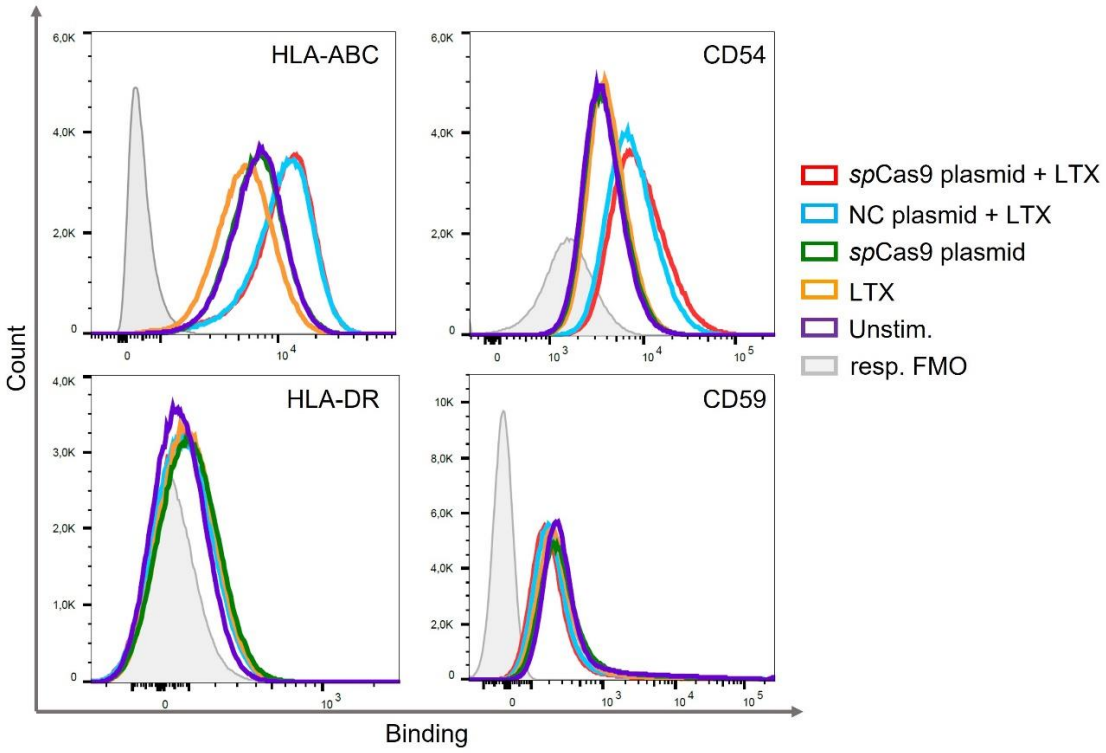

Fig. 31: Histograms of surface marker expression.

The figure illustrates histograms of HLA-ABC, HLA-DR, CD54, and CD59 expression on ARPE-19 cells transfected with *sp*Cas9 plasmid and Lipofectamine LTX. They were compared to ARPE-19 cells transfected with NC plasmid and Lipofectamine LTX, treated with *sp*Cas9 plasmid or Lipofectamine LTX only as well as to an unstimulated control. *Sp*Cas9 and NC plasmid transfection resulted in a right shift of the HLA-ABC and CD54 histograms compared to the control groups, indicating an upregulation of these markers. In contrast, HLA-DR and CD59 histograms showed no differences between any groups. The figure is representative of three independent experiments.

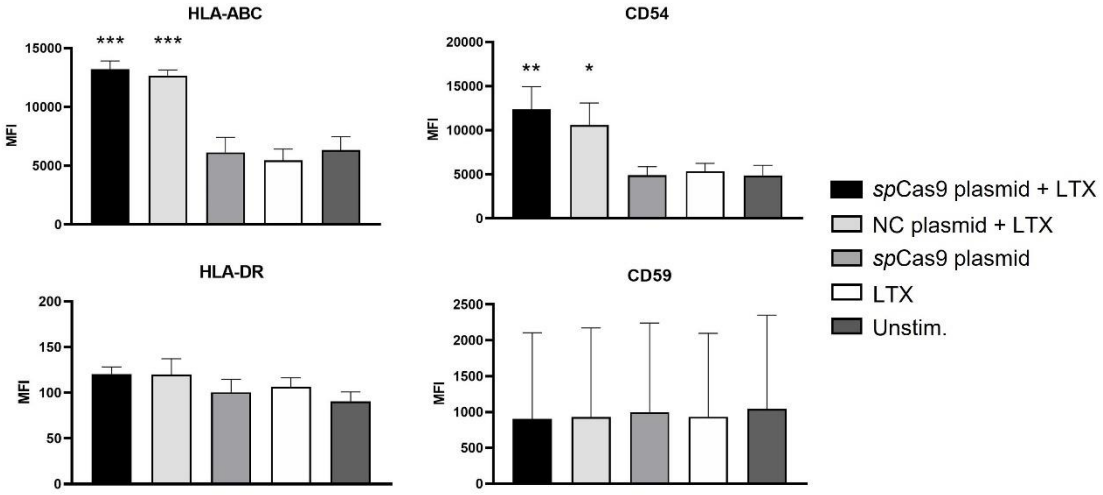

Fig. 32: Plasmid-mediated gene transfer upregulates HLA-ABC and CD54.

The figure displays MFI of fluorescent-labelled ABs indicating the expression of HLA-ABC, HLA-DR, CD54, and CD59 on ARPE-19 cells transfected with *sp*Cas9 plasmid and Lipofectamine LTX. They were compared to ARPE-19 cells transfected with NC plasmid and Lipofectamine LTX, treated with *sp*Cas9 plasmid or Lipofectamine LTX only, as well as to an unstimulated control. *Sp*Cas9 and NC plasmid transfection resulted in a significant upregulation of HLA-ABC and CD54 when compared to control groups. In contrast, HLA-DR and CD59 expression were not significantly increased by plasmid transfection. The bars represent mean values, and the error bars represent standard deviations of three independent experiments. (n=3, one-way ANOVA (HLA-ABC, HLA-DR, CD54), Kruskal-Wallis-test (CD59), *=p<0.05, **=p<0.01, ***=p<0.001)

5 Discussion

CRISPR/Cas9 gene editing systems are a promising and rapidly developing technology that have already been applied in *in vivo* retinal gene therapy studies (Hung et al., 2016a, Jo et al., 2019a, Pfromm et al., 2022). To ensure the safety and efficacy of this technology, the present work was the first to investigate the immunological impact of *sp*Cas9 on human RPE. The assessment of cytokine production in RPE is integral to understand the immunological impact of *sp*Cas9, as cytokines may impede successful gene editing (Bonillo et al., 2022, Cromer et al., 2018, Pfromm et al., 2022). The two research objectives were to assess whether intracellular Cas9 induces a proinflammatory cytokine release in human RPE cells indicating immune response initiation, and whether plasmid transfection is a suitable method for retinal gene therapy delivery from an immunological perspective. It was found that intracellular *sp*Cas9 induced IL-8 secretion in ARPE-19 cells. Additionally, plasmid transfection itself triggered IL-6 and IL-8 secretion as well as an upregulated expression of HLA-ABC and CD54 on human ARPE-19 cells (Pfromm et al., 2022). Moreover, the cell viability rate was significantly reduced after plasmid transfection (Pfromm et al., 2022).

5.1 Limitations of the ARPE-19 *in vitro* model

In this study, ARPE-19 cells, a human non-primary immortalised cell line, were used as a model of human RPE, as they exhibit structural and functional similarities to RPE cells *in vivo*, making ARPE-19 cells suitable for *in vitro* experiments (ATCC, n.d., Dunn et al., 1996). Ablonczy et al. (2011) stated that ARPE-19 cells appropriately mimic aged and pathologic *in vivo* RPE cells, which are potential gene therapy targets. However, since the ARPE-19 cells were not polarised or pigmented in my experiments, some ARPE-19 characteristics may differ from RPE cells *in vivo*. (Biesemeier et al., 2010, Dunn et al., 1998, Luo et al., 2006). Nonetheless, the absence of ARPE-19 pigmentation is advantageous in experiments involving fluorescence, such as FACS, as melanin can extinguish other fluorescence signals (Losi et al., 1993, Samuel et al., 2017). In contrast to post-mitotic RPE cells *in vivo*, ARPE-19 cells are immortalised and divide more

frequently than primary RPE cells. Immortalised cell lines such as ARPE-19 are more readily transfectable than primary cell lines, resulting in higher transfection efficacies (Tseng et al., 1999, Vercauteren et al., 2011). Sufficient transfection efficacies might lead to higher Cas9 expression in ARPE-19 cells, enabling the detection of even slight Cas9 immunological effects. Thus, a limited *in vivo* significance of ARPE-19 cells was accepted, to demonstrate Cas9 immunogenicity as sensitively as possible. However, this model is not able to assess the interaction of the RPE with other retinal immune cells such as resident microglia, which might be relevant to retinal immune responses. Klettner et al. (2014), e.g., demonstrated immunological cross-talk between the RPE and retinal microglia (Bonillo et al., 2022). In subsequent studies, ARPE-19 cells should be manipulated to exhibit additional characteristics of *in vivo* RPE cells, such as polarisation and pigmentation, to maximise their *in vivo* relevance.

5.2 Intracellular *sp*Cas9-induced IL-8 secretion in ARPE-19 cells

Cas9-expressing ARPE-19 cells were shown to secrete IL-8, an indication of *sp*Cas9 immunogenicity. This finding is consistent with Kang et al. (2018), who triggered an immune response in Tohoku hospital pediatrics-1 (THP-1) cells, a human monocytic cell line, and peripheral blood mononuclear cells (PBMCs) via cellular exposure to extracellular *sp*Cas9 proteins (Pfromm et al., 2022). However, THP-1 cells and PBMCs did not express *sp*Cas9 endogenously, since the *sp*Cas9 was applied in protein form and not transfected as plasmid DNA (Kang et al., 2018). The dissimilar delivery of *sp*Cas9 might activate different PRRs, resulting in a varying cytokine secretion, since monocytes secrete proinflammatory macrophage inflammatory protein 3 α (MIP3α), myeloperoxidase (MPO) and CD40L (Bonillo et al., 2022, Kang et al., 2018). The latter was not secreted in response to *sp*Cas9 by ARPE-19 cells. This varying cytokine secretion could be attributable to the different cell types used in the respective study. Nevertheless, both the present study and Kang et al. (2018) demonstrated that *sp*Cas9 induces the secretion of proinflammatory cytokines, indicating *sp*Cas9 immunogenicity in immune and non-immune cells *in vitro*.

Chew et al. (2016) demonstrated *sp*Cas9 immunogenicity with an *in vivo* model, in which *sp*Cas9 plasmids were delivered intramuscularly in mice. As in my project, *sp*Cas9 was endogenously expressed, but was delivered via AAV and electroporation as opposed to cationic lipid transfection (Chew et al., 2016). Chew et al. (2016) detected both a cellular immune response, in terms of myeloid and T cell proliferation, and *sp*Cas9 specific antibodies, indicating a humoral immune reaction (Bonillo et al., 2022). The immune responses were independent of the delivery method and could be linked to the expression of *sp*Cas9. However, no severe tissue damage was observed, suggesting that *sp*Cas9 may be only slightly immunogenic (Chew et al., 2016). This observation is consistent with the results of the present work, as apart from IL-8, no further cytokines were found to be upregulated, indicating relatively low levels of Cas9 immunogenicity.

Cromer et al. (2018) also observed a Cas9-induced cytokine secretion, providing further evidence for Cas9 immunogenicity. Exogenous *sp*Cas9 mRNA, introduced into human CD34+ hematopoietic stem cells by electroporation or AAVs, triggered an IFN-dominant immune response (Cromer et al., 2018). In addition, Cromer et al. (2018) observed an inverse correlation between the severity of the induced immune response and the efficacy of Cas9 gene editing, demonstrating that cytokine production may impede Cas9 gene therapy. (Bonillo et al., 2022, Pfromm et al., 2022)

In conclusion, our results are consistent with the work of Kang et al. (2018) and Cromer et al. (2018), who both showed Cas9-induced cytokine secretion as an indicator of an immune response. Currently, there is no evidence of a destructive nature of these immune reactions as Chew et al. (2016) did not observe severe tissue damage in response to Cas9-induced cytokine secretion. The present work is the first to demonstrate an immune response in RPE cells to *sp*Cas9 expression.

5.2.1 Immunological effects of IL-8 secretion on the retina

IL-8 is a CXC-chemokine, which has a chemotactic, activating effect on neutrophil granulocytes (Baggiolini et al., 1989). The CXC-chemokine binds to the CXCR1-receptor of human neutrophil granulocytes and thereby mediates its effects (Hess et al., 2004, Luster, 1998). IL-8 is secreted chiefly in the early phase of an acute inflammatory response (Kobayashi, 2008, Luster, 1998) and has been implicated with human retinal inflammatory diseases (Aksünger et al., 1997, Jonas et al., 2012, Petrovič et al., 2007, Pfromm et al., 2022). Recruited neutrophil granulocytes, attracted by a local retinal IL-8 secretion, for instance, migrate across the blood-retina barrier to reach the site of inflammation (Elner et al., 1997, Smith et al., 1994). Neutrophils have a proangiogenic effect at the site of inflammation through the secretion of VEGF and may also cause local tissue destruction (Kobayashi, 2008). Additionally, neutrophil granulocytes recruit monocytes to inflamed tissue (Wantha et al., 2013), and are involved in pathogen elimination via the release of reactive oxygen species, peptides, and neutrophil extracellular traps (NETs) (Brinkmann et al., 2004). Zhou et al. (2010) postulated that neutrophil granulocytes play a crucial role in destabilising the outer blood-retina barrier. Furthermore, studies showed that neutrophil granulocytes are involved in retinal inflammation (Ashander et al., 2019, Giese et al., 2003), which is associated with impaired vision (Bonillo et al., 2022, Chen et al., 2018, Kauppinen et al., 2016).

Moreover, due to its angiogenetic properties, IL-8 is involved in neovascularisation processes and induces the expression of various adhesion molecules (Baggiolini et al., 1989, Strieter et al., 1992). Studies demonstrated a weak chemotactic effect of IL-8 on basophilic granulocytes, which was not present on monocytes as well as eosinophil granulocytes (Baggiolini et al., 1995, Krieger et al., 1992, Leonard et al., 1990, Yoshimura et al., 1987). Contradictory studies exist on the chemotactic effect of IL-8 on lymphocytes (Larsen et al., 1989, Leonard et al., 1991). Gesser et al. (1996) demonstrated an influence of IL-8 on CD4+ T cells and highlighted its role in the direct regulation of T cell function. Hess et al. (2004) found that IL-8 only had a chemotactic effect on a small subpopulation of CD8+ T cells expressing the CXCR1 receptor. This finding

could explain the varying results between studies. CXCR1-positive CD8+ T cells were highly cytotoxic and secreted INF-γ (Hess et al., 2004, Pfromm et al., 2022). Since Cas9 is expressed intracellularly, Cas9 peptides might be presented to cytotoxic T cells via MHC I (Simhadri et al., 2018). The recruitment of CXCR1-positive CD8+ T cells to the retina could cause immune-mediated destruction and might lead to elimination of Cas9 expressing cells, preventing a successful gene therapy (Bonillo et al., 2022, Pfromm et al., 2022). This hypothesis should be further investigated in a following project.

Elner et al. (1997) showed a polarised IL-8 secretion by RPE, predominantly basolaterally in the direction of the choroid. As polarised secretion of cytokines was not able to be analysed in the present study, a distinction between apical or basolateral Cas9-induced IL-8 secretion should be investigated in future work to obtain more precise insights into inflammatory processes and consequences. The above-mentioned studies suggest that a Cas9-induced IL-8 response could lead to recruitment of neutrophil granulocytes and highly cytotoxic CD8+ T cells resulting in retinal inflammation.

5.2.2 IL-8 signaling pathways

Elner et al. (1990) found that human RPE cells secrete IL-8 in response to IL-1β, TNF-α, and LPS stimulation. They also demonstrated that IL-1β is the most potent inducer of IL-8 (Elner et al., 1990). Therefore, IL-8 might not be secreted directly in response to Cas9. Instead Cas9 might induce IL-8 stimulating cytokines, such as IL-1β and TNF-α. Hence, IL-1β and TNF-α concentrations were measured in the supernatant of Cas9-stimulated ARPE-19 cells. No significant increase of either cytokine was detected, making it unlikely that the detected IL-8 secretion was induced by IL-1β or TNF-α. However, cytokine production in Cas9-stimulated ARPE-19 cells was first measured at three hours post-stimulation. This might have been too late to detect TNF-α production, since it is often secreted in the early stages of an immune response (Beutler and Cerami, 1989). The present work provides no evidence that the detected IL-8 release was induced by the proinflammatory cytokines TNF-α and IL-1β. Cas9 may induce IL-8 directly via PRR.

Numerous phosphokinases and transcription factors associated with IL-8 secretion from human RPE cells have been identified in recent years. It was found that IL-8 release was activated by intracellular calcium mobilisation and the transcription factor nuclear factor kappa-light-chain-enhancer of activated B cells (NF-κB) was shown to be involved (Yang et al., 2015). Relvas et al. (2009) showed that IL-8 secretion in RPE and ARPE-19 cells was mediated via the extracellular signal-regulated kinase 1 and 2 (ERK1/2) signaling pathway. Tao et al. (2016) identified, in addition to the NF-κB signaling pathway, the involvement of the mitogen-activated protein kinase (MAPK) signaling pathways in the LPS-induced IL-8 secretion of ARPE-19 cells. According to the current state of research, these two signaling pathways are frequent mediators of IL-8 secretion in human RPE (Elner et al., 2006, Relvas et al., 2009, Tao et al., 2016). Therefore, their involvement in Cas9-induced IL-8 secretion should be investigated, which could be achieved using inhibitors or knock-out models of the corresponding signaling pathway. However, it is unusual that *sp*Cas9 should only enhance IL-8 secretion as Tao et al. (2016) demonstrated that MAPK and NF-κB were involved in the RPE secretion of several cytokines. Nevertheless, the identification of the induced signaling pathway is necessary to suppress a potential immune response in a targeted manner (Kang et al., 2018).

5.2.3 Potential *sp*Cas9 PRRs

Human cells recognise pathogens, so-called PAMPs and DAMPs, via PRRs, which induce proinflammatory cytokine and chemokine secretion upon activation (Kawasaki and Kawai, 2014). Due to the method design, it could not be concluded whether the Cas9 DNA sequence, the intracellularly transcribed Cas9 mRNA and/or the intracellularly translated Cas9 protein induced the IL-8 secretion. Consequently, DNA, RNA, and protein sensors should be considered as relevant PRRs of the Cas9 pathogen. The identification of a Cas9 PRR is crucial, as it might enable targeted inhibition designed to suppress a destructive immune response (Liao et al., 2017).

5.2.3.1 RNA sensors

Intracellular RNA sensors may be responsible for the recognition of Cas9 mRNA. Since Cas9 is present intracellularly as mRNA, RNA sensors that detect single-stranded RNA (ssRNA) are more likely to be involved in the recognition of Cas9 than dsRNA sensors.

TLRs represent an essential group of RNA sensors (TLR 3, 7, 8) and PRRs. TLR7 is an intracellular receptor that detects ssRNA. This PRR is located on the endosome, and human RPE cells have been shown to express TLR7, but not to the same extent as dendritic cells (Detrick and Hooks, 2020, Kawasaki and Kawai, 2014, Mancuso et al., 2009, Pfromm et al., 2022). The involvement of TLR7 in retinal inflammatory processes has also been reported (Liao et al., 2017). Adapter proteins like myeloid differentiation primary response 88 (MyD88) are recruited after stimulation of TLR7, which also induces a signal transduction cascade with activation of MAPK and NF-κB resulting in the transcription and secretion of proinflammatory cytokines (Cho, 2013, Kawasaki and Kawai, 2014). Whether TLR7-activation triggers IL-8 secretion is controversial and may depend on the cell type as different cell types were used in different studies (Fukui et al., 2013, Li et al., 2016). However, there is currently no evidence pertaining to whether TLR7 activation in RPE cells induces IL-8 secretion, but TLR7 involvement in the detection of the Cas9 pathogen must still be considered. TLR8 is a further intracellular ssRNA sensor, whose presence in RPE cells is controversial in the literature (Heil et al., 2004, Kumar et al., 2004, Mai et al., 2014). In contrast to Kumar et al. (2004), Mai et al. (2014) detected TLR8 mRNA in RPE cells and attributed the deviating results to the lower passage numbers used by Kumar et al. (2004) and deemed their own results as more reliable. Recently, it was shown that IL-8 is secreted by polymorphonuclear neutrophils (Ehrnström et al., 2020) and HEK293 cells (Pluta et al., 2019) in response to TLR8 activation, which has not yet been demonstrated in human RPE cells. However, since Mai et al. (2014) did not detect TLR8 proteins in human RPE, TLR8 involvement in the detection of Cas9 mRNA in ARPE-19 cells is doubtful. Contrarily, TLR3 has proven to be highly expressed in RPE cells and the presented work also confirmed that ARPE-19 cells responded to the TLR3

agonist Poly(I:C) with IL-6 and IL-8 secretion (Kumar et al., 2004). However, TLR3 predominantly recognises double-stranded RNA motifs (Alexopoulou et al., 2001), which is why the detection of Cas9 mRNA via TLR3 and 8 is unlikely.

RLRs, such as retinoic acid inducible gene-I (RIG-I) and melanoma differentiation-associated gene 5 (MDA5), are another group of intracellular RNA sensors present in RPE cells (Bonillo et al., 2022, Pfromm et al., 2022, Singh et al., 2017, Wörnle et al., 2011). RLRs primarily respond to viral dsRNA and Kimura et al. (2018) found that ssRNA does not induce an RLR signaling cascade. However, Cromer et al. (2018) showed an upregulation of RIG-I on human CD34+ hematopoietic stem cells in response to exogenous *sp*Cas9 mRNA delivery (Bonillo et al., 2022, Pfromm et al., 2022). Therefore, it should be further investigated if RLRs, particularly RIG-I, are involved in the detection of endogenous *sp*Cas9 mRNA.

PRRs include NLRs, with well-known representatives like the NOD-like receptor pyrin domain containing 3 (NLRP3) inflammasome and nucleotide-binding and oligomerisation domain containing 2 (NOD2) (Chen et al., 2017). Currently, there is no evidence of NOD2 expression in the human RPE. Sha et al. (2014) stated that human macrophages use NLRP3 to detect synthetic ssRNA and bacterial RNA constituents, such as mRNA, transfer RNA (tRNA), and ribosomal RNA (rRNA). This finding indicates that NLRP3 is involved in the detection of pathogenic RNA, at least in human macrophages (Sha et al., 2014). The NLRP3 inflammasome was also identified in human RPE cells as well as ARPE-19 cells (Kerur et al., 2013, Wang et al., 2019). Contrarily, Kosmidou et al. (2018) could not verify the presence of NLRP3 in ARPE-19 cells. Since Wang et al. (2019) and Kosmidou et al. (2018) cultivated ARPE-19 cells in different culture media, varying culture conditions may have an impact on NLRP3 expression, but whether or not ARPE-19 cells express NLRP3 remains controversial. The activation of the NLRP3 inflammasome results in the secretion of the proinflammatory cytokines IL-1β and IL-18 (Doyle et al., 2012, Tseng et al., 2013). Since Cas9 did not induce IL-1β secretion in the present study, it is improbable that the NLRP3 inflammasome is responsible for the detection of Cas9 mRNA. However, Doyle et al. (2012) reported only a slight IL-1β release after NLRP3

stimulation of ARPE-19 cells, which is why NLRP3 involvement cannot be excluded by this study due to possibly insufficient assay sensitivity. To further investigate the role of the NLRP3 inflammasome in Cas9 recognition, the protein levels of NLRP3 and IL-18 should be determined in future Cas9 transfection experiments.

5.2.3.2 Protein sensors

The current project demonstrates that ARPE-19 cells express *sp*Cas9 protein after *sp*Cas9 plasmid transfection. The viability rate of 85.2 %, found in cells transfected with *sp*Cas9 plasmid, indicates the presence of *sp*Cas9 protein both intra- and extracellularly. Consequently, intra- as well as extracellular protein sensors might be involved in the Cas9 pathogen detection.

Kang et al. (2018) recently showed that the Cas9 protein acts as a PAMP and induces secretion of proinflammatory cytokines MIP3α, CD40L, and MPO in human monocytes (Bonillo et al., 2022, Pfromm et al., 2022). The authors demonstrated the stimulator of interferon genes (STING), as wells as the signal transducer and activator of transcription 6 (STAT6) to be involved in this process (Bonillo et al., 2022, Kang et al., 2018). However, whether Cas9 is directly detected via STING or other proteins upstream of STING warrants further investigation. STING is mainly involved in the detection of intracellular nucleic acids as well as in immune reactions against bacterial pathogens such as *Streptococcus pyogenes* (Barber, 2015, Gratz et al., 2011). It needs to be clarified which ligands lead to the activation of STING, as its activation results in the secretion of IFN type 1 and proinflammatory cytokines (Barber, 2011). Chen et al. (2011) observed the interaction between STING and STAT6 described by Kang et al. (2018) as well. The observed absence of CD40L secretion in *sp*Cas9-stimulated ARPE-19 cells in the present study does not eliminate STING's involvement in Cas9 recognition, as activation of the STING/STAT6 signaling pathway might lead to varying cell type-dependent cytokine secretion. For this reason, Cas9 protein detection through this signaling pathway in RPE cells should be further examined.

TLR2 is responsible for the detection of a variety of bacterial pathogens (Aliprantis et al., 1999, Takeuchi et al., 1999). This receptor is located on the cell membrane and forms heterodimers with TLR1 and TLR6 to recognise ligands, which have not yet been fully identified (Detrick and Hooks, 2020, Ozinsky et al., 2000, Takeuchi et al., 2001). Hösel et al. (2012) showed that TLR2 detects viral capsids consisting of proteins suggesting that TLR2 might act as a sensor for extracellular proteins such as *sp*Cas9 (Bonillo et al., 2022). The presence of TLR2 on human RPE and ARPE-19 cells was confirmed by Kumar et al. (2004) and Paeng et al. (2015), respectively (Pfromm et al., 2022). Furthermore, Paeng et al. (2015) demonstrated that a TLR2 blockade reduces the expression of IL-8 in LPS-stimulated ARPE-19 cells. Therefore, whether TLR2 recognises the Cas9 protein of dead cells leading to IL-8 secretion should be investigated further.

Chavakis et al. (2003) first categorised the PRR RAGE, which predominantly detects advanced glycation end-products (AGEs) (Teissier and Boulanger, 2019). Besides AGEs, numerous other ligands have been identified, including proteins, such as amphoterin and calgranulin (Hori et al., 1995, Narumi et al., 2015). This protein interaction indicates that RAGE may serve as a sensor of extracellular proteins. Activation of this receptor resulted, similarly to TLRs, in increased expression of NF-κB, which is associated with secretion of proinflammatory cytokines (Bianchi et al., 2010). Since Chang et al. (2017) revealed that RAGE is expressed by ARPE-19 cells and is involved in amphoterin-induced cytokine secretion (Pfromm et al., 2022), it is imperative to investigate whether RAGE is vital in detecting extracellular Cas9 proteins.

Cromer et al. (2018) detected a more vigorous immune response in human CD34+ hematopoietic stem cells triggered by *sp*Cas9 mRNA when compared to *sp*Cas9 RNPs. To discriminate whether Cas9 protein or Cas9 mRNA induce IL-8 secretion, ARPE-19 cells should be transfected with Cas9 RNPs in a further experiment since a subsequent immune response could be isolated to the *sp*Cas9 protein.

5.3 Relevance of plasmid transfection for retinal gene therapy

The present study also poses the question of whether plasmid transfection is a convenient method for future retinal gene therapy, from an immunological perspective. It was shown above that plasmid-mediated gene transfer, but not extracellular plasmid DNA, triggered IL-6 and IL-8 release. Moreover, HLA-ABC and CD54 upregulation, as well as a reduced viability rate after plasmid transfection were observed. The results of this study were determined using established methods such as ELISA and FACS. Plasmid-mediated gene transfer was achieved via cationic lipid transfection. (Pfromm et al., 2022)

5.3.1 Plasmid-mediated gene transfer induced cytokine secretion

Intracellular Cas9 plasmids bear the risk of detection by cytoplasmic DNA sensors leading to cytokine secretion (Muerdter et al., 2018). While plasmid immunogenicity is beneficial in DNA-based vaccination, plasmid-induced cytokine secretion can attenuate the intended effects of gene therapy (Bonillo et al., 2022, Cromer et al., 2018, Pfromm et al., 2022, Xenopoulos and Pattnaik, 2014). The results of the present study support the thesis of plasmid immunogenicity since the *sp*Cas9 plasmid induced cytokine secretion in ARPE-19 cells. IL-6 and IL-8 are inflammatory cytokines that have a prominent role in retinal inflammatory processes (Bonillo et al., 2022, Holtkamp et al., 2001). The role of IL-8 was discussed in detail in chapter 5.2.1.

Studies showed that IL-6 secreted by RPE cells led to the attraction of retinal microglia, and that it plays a chemotactic role on immune cells such as leukocytes (Jo et al., 2019b, Romano et al., 1997). Karkhur et al. (2019) demonstrated that IL-6 plays an integral role in non-infectious uveitis. Plasmid-induced IL-6 and IL-8 release in ARPE-19 cells, therefore, demonstrates a proinflammatory response. In some publications, IL-6 (human PBMCs) and IL-8 (RPE) secretion in response to DNA was also reported (Ebihara et al., 2007, Hartmann and Krieg, 1999). However, the authors used DNA with CpG motifs as a stimulant, not plasmids (Ebihara et al., 2007, Hartmann and Krieg, 1999). (Pfromm et al., 2022)

Nevertheless, the detected plasmid-induced cytokine profile, IL-6 and IL-8, differs from Muerdter et al. (2018) and Mann et al. (2012) who both observed an

IFN type 1 dominated immune response. IFN-α and IFN-β levels were also assessed in this study, but no significant plasmid-induced increase in these cytokines was found in ARPE-19 cells. Muerdter et al. (2018) worked with a different cell line, though, which is why it can be presumed that DNA plasmids trigger cell-type-dependent cytokine secretions. Cytoplasmic DNA could additionally be sensed by different intracellular DNA sensors, inducing varying signaling pathways. Chen et al. (2018) demonstrated that NF-κB and MAPK signaling pathways could mediate IL-6 and IL-8 secretion in ARPE-19 cells, so this should be examined to identify plasmid-induced immune pathways to enable targeted prevention of an immune response (Pfromm et al., 2022).

5.3.2 Reduced viability rates after plasmid transfection

A reduced viability rate was observed after *sp*Cas9 plasmid (85.2 %) and NC plasmid (86.3 %) transfection. In contrast, neither extracellular plasmids nor the transfection reagents alone exhibited cytotoxic effects. Armeanu et al. (2000) and Dokka et al. (2000) also reported moderate cytotoxic effects of cationic lipid transfection, but compared to other transfection methods such as electroporation, the cytotoxicity rates of cationic lipids are comparatively low (Jacobsen et al., 2006). However, it cannot be concluded whether ARPE-19 cells died via apoptotic, pyroptotic or nonapoptotic (necrotic) cell death pathways, which could have triggered an accompanying inflammatory reaction. Nevertheless, Nguyen et al. (2007) stated that cell death of HeLa cells after plasmid transfection with cationic lipids was caused by apoptosis (Pfromm et al., 2022). Apoptosis or programmed cell death tends to have anti-inflammatory effects, whereas necrosis and pyroptosis are associated with inflammation. Necrosis describes an accidental cell death and is characterised by the loss of cell membrane integrity. The inflammatory form of programmed cell death, pyroptosis, occurs particularly after infection with a pathogen and is designed to prevent its spread. Additionally, pyroptosis is dependent on caspase-1, an enzyme involved in IL-1β and IL-18 secretion. (Brennan and Cookson, 2000, Fink and Cookson, 2005, Pfromm et al., 2022)

As IL-1β secretion was not induced by plasmid transfection in the present work, the involvement of a pyroptotic cell death pathway is less likely. Nevertheless, the detected IL-6 and IL-8 secretion could demonstrate an inflammatory response to DAMPs, which are released by dying cells. Therefore, the different cell death signaling pathways should be investigated in further experiments to obtain a detailed insight into the cytotoxic effects of plasmid transfection.

5.3.3 Plasmid-mediated gene transfer induced immune modulators

In the present study, a significantly increased ICAM-1/CD54 expression on ARPE-19 cells, triggered by plasmid transfection, was detected (Pfromm et al., 2022). Similar findings were obtained in two studies, which found increased ICAM-1/CD54 expression could be induced by CpG motifs, a well-known TLR9 agonist (Hartmann and Krieg, 1999, Li et al., 2004). However, Hartmann and Krieg (1999) as well as Li et al. (2004) worked with pulmonary endothelial cells or monocytes instead of RPE cells. In chapter 1.6.3.4 it was outlined that ICAM-1/CD54 is involved in leukocyte migration across the blood-retina barrier, suggesting its upregulation is a further sign of a proinflammatory ARPE-19 cell response to plasmid-based gene therapy (Pfromm et al., 2022).

Plasmid-induced HLA-ABC expression on ARPE-19 cells is a further indication of plasmid immunogenicity (Pfromm et al., 2022). These results correspond to the study by Mann et al. (2012), which showed an increased gene expression profile for co-stimulatory antigen presentation molecules in skeletal muscle after the delivery of a non-coding plasmid (Pfromm et al., 2022). However, the present work is the first to detect such an immune response in the RPE. The reported IL-6 and IL-8 secretion indicates involvement of the innate immune system, whereas HLA-ABC upregulation suggests a link of ARPE-19 cells to the adaptive immune system, as antigens can be presented to CD8+ T cells via HLA-ABC (Bröker et al., 2019). Increased HLA-ABC presence might be desirable in vaccination, but can have severe consequences in gene therapy (Mann et al., 2012).

In plasmid-based gene therapy, proteins such as Cas9 are expressed endogenously and may impact antigen presentation. The endogenous expression of the *sp*Cas9 protein after plasmid transfection could result in MHC I

antigen presentation to CD8+ T cells, which might eliminate gene-edited cells. In case of exogenous delivery, for example via RNPs, the cells could present antigens via MHC II to CD4+ T cells and might induce antibody formation. Hence, the adaptive immune defence may differ between plasmid- and protein-based gene therapy. (Moreno et al., 2019, Neefjes et al., 2011, Simhadri et al., 2018)
The theory of plasmid-induced MHC I antigen presentation is supported by the HLA-ABC and HLA-DR expression profile in ARPE-19 cells reported in the present study.

5.3.4 DNA sensors

Mammalian cells can detect pathogenic DNA with different DNA PRRs, however, not all DNA PRRs will be discussed here, for the sake of clarity. TLR9 is a DNA sensor primarily activated by CpG DNA, and is present endosomally in RPE cells as described in chapter 1.6.3.1 (Bauer et al., 2001, Kumar et al., 2004). Since Mann et al. (2012) observed an upregulation of the TLR9 pathway in response to plasmid DNA, this receptor should be assessed as a potential mediator of the induction of a plasmid-triggered immune reaction (Pfromm et al., 2022).
Absent in melanoma 2 (AIM2) is a cytosolic DNA PRR, which was recently found to be expressed by RPE (Prager et al., 2016). Activation of the AIM2 pathway is associated with IL-1β and IL-18 release (Fernandes-Alnemri et al., 2009). As IL-1β secretion was not detected in the present study in response to plasmid DNA, the participation of AIM2 in the sensing of plasmid DNA in RPE is unlikely. However, AIM2 involvement cannot be ruled out, as IL-18 levels and the expression of AIM2 were not assessed.
Cyclic GMP-AMP synthase (cGAS)-STING represents another relevant DNA sensing pathway. cGAS, which has already been detected in human RPE, recognises cytoplasmic DNA sequences and induces STING activation (Kerur et al., 2018, Pfromm et al., 2022). This STING activation induces TANK-binding kinase-1 (TBK-1), which was found to be critical for plasmid-induced immune responses, leading to a secretion of IFN type 1 and proinflammatory cytokines (Barber, 2011, Ishii et al., 2008, Sun et al., 2013). A further STING-inducing DNA sensor is IFN-γ-inducible 16 (IFI16), which is also present on RPE and its

activation results in an IFN-β response (Chaum et al., 2015, Horan et al., 2013). The lack of IFN-β detection in response to Cas9 transfection in the present work contradicts the involvement of both signaling pathways. However, Ishikawa et al. (2009) demonstrated through the use of a STING knock-out animal model, that the absence of STING weakened the immune response to plasmid DNA vaccination, emphasising its relevance for plasmid-mediated immune reactions. Therefore, DNA sensing by cGAS-STING or IFI16-STING should be regarded as a potential cause of plasmid-triggered immune responses in ARPE-19 cells.

5.3.5 Clinical relevance of *sp*Cas9 plasmids

Cas9 has been applied in DNA plasmid form in several pre-clinical studies on retinal gene therapy (Pfromm et al., 2022). Bakondi et al. (2016) and Wang et al. (2014a) achieved *in vivo* Cas9 plasmid transfection using electroporation. Bakondi et al. (2016) were able to eradicate an autosomal dominant mutation, causing RP, in a rat model using Cas9 plasmids. They further demonstrated an allele-specific knock-down, so that degeneration of the retina could be averted (Bakondi et al., 2016). Wang et al. (2014a) also accomplished *in vivo* gene editing of the murine retina with Cas9 plasmids. Hung et al. (2016a) questioned the feasibility of this delivery method in humans and instead used AAVs for Cas9 transduction. Duan et al. (2016) also discussed that induced DSB in RPE cells are often repaired by NHEJ instead of HDR, making targeted editing less efficient. However, Duan et al. (2016) outlined ways, such as NHEJ inhibitors (Maruyama et al., 2015) or a mutant *sp*Cas9 form (Cong et al., 2013), to possibly circumvent this obstacle (Bonillo et al., 2022). Moreover, Zuris et al. (2015) argue that plasmid DNA entails the risks of long-term exposure, which could induce cellular immune responses (Bonillo et al., 2022, Ruan et al., 2017, Wang et al., 2015). Kim et al. (2017) stated that although a Cas9 enzyme was expressed in cells for more than 32 weeks, no relevant off-target mutations occurred. This indicates that long-term Cas9 expression is not necessarily disadvantageous. Nevertheless, as previously discussed in chapter 5.3.4, intracellular Cas9 plasmids carry the risk of detection by cytoplasmic DNA sensors, inducing cytokine secretion (Mann et al., 2012, Pfromm et al., 2022). The results of our

work support this thesis, since the *sp*Cas9 plasmid induced immune reactions of ARPE-19 cells. The publications of Bakondi et al. (2016) and Wang et al. (2014a) demonstrate the current relevance of Cas9 plasmids in retinal gene therapy. Due to its immunogenicity, DNA plasmid delivery in RPE should be considered with caution. Plasmid transfection must be benchmarked against other conventional types of gene or protein delivery, to assess its relevance in retinal gene therapy.

5.3.6 Cas9 mRNA and protein therapy

Alternatively, Cas9 can be delivered as mRNA. Cas9 mRNA has the benefit of not requiring further transport to the cell nucleus as well as having lower risks concerning long-term Cas9 expression (Zangi et al., 2013, Zuris et al., 2015). Wang et al. (2013) and Yin et al. (2016) have already carried out successful gene editing *in vivo* via Cas9 mRNA. Yin et al. (2016) also observed fewer off-target effects in transient Cas9 expression when compared to long-term viral Cas9 expression. However, different groups independently identified problems with mRNA stability and immunogenicity (Cromer et al., 2018, Van Tendeloo et al., 2007, Zangi et al., 2013, Zuris et al., 2015). Cromer et al. (2018) demonstrated a potent immune response by non-immune primary cells to exogenous Cas9 mRNA, IFN type 1 secretion, as well as increased cytotoxicity, which both had a negative impact on the gene editing efficacy (Bonillo et al., 2022, Pfromm et al., 2022). In contrast, Hendel et al. (2015) reported a lower cytotoxic effect of Cas9 mRNA delivery when compared to Cas9 plasmids. Although Kormann et al. (2011) described that modified mRNA can have lower immunogenicity and higher stability, the use of Cas9 mRNA should be considered with caution from an immunological perspective.

It is feasible to deliver Cas9 as RNPs instead of plasmid form to reduce the risk of long-term immune responses as well as off-target editing related to persistent Cas9 expression (Staahl et al., 2017, Zuris et al., 2015). Hendel et al. (2015) as well as Cromer et al. (2018) found that among Cas9 plasmid, mRNA, and RNP editing, the latter demonstrated the lowest cytotoxic effect suggesting that RNPs are an attractive alternative to Cas9 plasmids. For these reasons, protein-based Cas9 gene therapy has been extensively studied in recent years, and various

research groups were able to deliver RNPs *in vivo* via direct injection or nanoparticles (Bonillo et al., 2022, Simhadri et al., 2018, Staahl et al., 2017, Wang et al., 2016). Since RPE cells are post-mitotic in the human organism, it should be emphasised that Staahl et al. (2017) managed to edit genes in post-mitotic neuronal cells using gene therapy based on RNPs. Cromer et al. (2018) compared the immunogenicity of Cas9 mRNA and RNPs in CD34+ hematopoietic stem cells. Only a slight immune response was found in cells treated with RNPs, but the detected DNA damage induced apoptosis (Bonillo et al., 2022, Cromer et al., 2018). RNP-induced DNA damage was also observed by Haapaniemi et al. (2018) (Bonillo et al., 2022). In contrast, the immune response to Cas9 mRNA was considerably more severe, suggesting that RNPs are more secure and efficient in gene editing (Cromer et al., 2018). Likewise, Staahl et al. (2017) could not detect an immune response of brain microglia to RNPs, which might be relevant for retinal gene therapy as microglia are also present in the eye (Lee et al., 2008). On the contrary, protein-based gene therapy is not entirely immunologically innocuous, as Kang et al. (2018) attributed immunogenicity to the *sp*Cas9 protein (Bonillo et al., 2022, Pfromm et al., 2022). Moreover, due to the relatively rapid degradation of proteins, a repetitive delivery is required, which could lead to a severe secondary immune response to a recurring antigen (Courtenay-Luck et al., 1986, Kok et al., 2013, Moreno et al., 2019). Elimination via cytotoxic T lymphocytes and AB neutralisation can be prevented by using different, non-cross-reactive Cas9 orthologs for each procedure (Moreno et al., 2019). Although Moreno et al. (2019) presented a solution for the secondary immune reactions to RNPs, the issue of the primary immune response, addressed by Kang et al. (2018), remains. Since Staahl et al. (2017) and Kang et al. (2018) used different cell lines in their studies, this may have led to the contradicting results.

From an immunological perspective, RNPs are a promising alternative to DNA plasmids, but their immunological and cytotoxic effects on retinal cells need further investigation.

5.3.7 Clinical relevance of cationic lipid transfection

Plasmids and proteins can be transfected by cationic lipids, a non-viral gene transfer method. In the present study, cationic lipid-mediated plasmid transfection was used to deliver Cas9 into ARPE-19 cells. A transfection efficacy of 31 % was obtained, which was accompanied by a moderate cytotoxic effect (see chapter 5.3.2). Vercauteren et al. (2011) found that ARPE-19 cells are a more convenient gene delivery target than primary RPE cells, which is likely due to the higher mitosis rates of the immortalised cell line (Tseng et al., 1999). Plasmids enter the cytoplasm via endocytosis and subsequently require transport into the nucleus before transcription into the corresponding mRNA (Yin et al., 2014). In dividing cells such as ARPE-19 cells, this takes place predominantly in the S phase, as the nuclear membrane breaks down during mitosis (Männistö et al., 2005, Tseng et al., 1999). Since *in vivo* RPE cells are post-mitotic, Cas9 gene expression after cationic lipid transfection would likely be marginal, as Ludtke et al. (2002) showed that plasmid DNA was transferred into the nucleus of non-dividing cells, but with far less efficacy than in dividing cells. However, Hangai et al. (1996) and Masuda et al. (1996) managed to introduce genes into RPE *in vivo* by intravitreal as well as subretinal injection of liposomes. Collectively, cationic-lipid-mediated plasmid transfection is not the method of choice for retinal gene therapy and requires further development to reduce immunogenicity and improve transfection efficacy in primary RPE cells (Bonillo et al., 2022, Koirala et al., 2013).

In addition to non-viral vectors, viral vectors such as AAV can be used to deliver *sp*Cas9 to target cells. Hung et al. (2016a) and Jo et al. (2019a) transduced retinal cells and RPE cells, respectively, via AVV and reported successful gene editing (Pfromm et al., 2022). However, there are limitations of AAV-based gene therapy, such as immunogenicity and a limited packaging capacity (~4.7 kbp) making delivery of genes, such as *ABCA4* (Stargardt's disease, 6.8 kbp) and *GRP98* (Usher syndrome, 18.9 kbp), challenging (Bonillo et al., 2022, Lipinski et al., 2013, Reichel et al., 2017). The dual AAV system was developed, in which two AAVs are combined to apply the gene machinery, increasing packaging capacity (Bonillo et al., 2022, Truong et al., 2015). However, *GRP98* exceeds even the packaging capacity of the dual AAV system, suggesting AAVs are not

suitable for the treatment of every retinal disorder in the diverse field of IRDs (Bonillo et al., 2022, Koirala et al., 2013, Lipinski et al., 2013). Thus, it is advisable to further improve non-viral gene therapy vectors such as liposomes to ensure that several gene delivery methods are available and can be tailored to their respective retinal disorders.

5.4 Conclusion

The data gathered in this doctoral thesis provides evidence that both Cas9 gene transfer and plasmid-mediated gene therapy can induce retinal immune reactions. Consequently, the hypothesis that Cas9 is a facultative immunogen is confirmed. The present study also demonstrates that plasmid-based retinal gene therapy poses immunological risks (Pfromm et al., 2022). To further assess these risks, experiments could be repeated with primary RPE cells to increase the *in vivo* significance of the results. Additionally, the immunogenicity of the *sp*Cas9 plasmid, mRNA, and protein specifically, should be assessed in a further project. Moreover, a comparison of *sp*Cas9 with other promising Cas9 orthologues, such as *sa*Cas9 and *cj*Cas9, in terms of immunogenicity, is indicated. The findings of the present thesis may have a significant impact on the current developments of retinal gene therapy, as immune reactions can mitigate relevant gene editing effects (Bonillo et al., 2022, Cromer et al., 2018, Pfromm et al., 2022). Thus, immune suppression may facilitate the success of retinal gene therapy for IRDs, leading to the preservation of vision for affected patients.

6 Summary

CRISPR/Cas9 enables precise DNA sequence modifications and represents a potential cure for inherited retinal diseases (IRDs). It has been shown that Cas9 triggers immune responses which significantly impair gene editing efficacy. We aim to study the immunogenicity of plasmid-mediated gene transfer and expression of Cas9 on the human retinal pigment epithelium (RPE) *in vitro*.

For this purpose, an immortalised RPE cell line was transfected with a self-designed Cas9-coding (*sp*Cas9) plasmid via cationic lipofection. The immunomodulatory surface marker expression and inflammatory cytokine concentrations were compared between *sp*Cas9 plasmid and non-coding (NC) plasmid transfected RPE cells to assure that potential immune responses could be ascribed to Cas9. To assess the immunogenicity of plasmid-mediated gene transfer, the same immunological parameters were compared between plasmid transfected and non-transfected RPE cells, which were exposed to either cationic lipids or plasmids only.

Transfection of an *sp*Cas9 plasmid induced a significant IL-8 secretion ($p = 0.004$) in RPE cells, suggesting that the inflammatory response seen in the RPE cells was triggered by either the Cas9 DNA sequence, Cas9 mRNA, and/or the subsequently produced Cas9 protein. The supernatant of plasmid transfected RPE cells exhibited increased IL-6 ($p < 0.001$) and IL-8 levels ($p < 0.001$) when compared to non-transfected RPE cells. An upregulation of HLA-ABC ($p < 0.001$) and ICAM-1/CD54 expression ($p < 0.001$) as well as a reduced viability rate (85.2 %) of plasmid-transfected RPE was detected using FACS analysis.

The data of this study indicates that Cas9 plasmid-mediated gene transfer has immunogenic potential. Further research is required to assess the role of pattern-recognition receptors and signaling pathways in Cas9 pathogen detection, and the impact of the induced immune responses on gene editing efficacy. These results are highly relevant to the safety of CRISPR/Cas9-based gene therapy as a potential treatment for IRDs.

7 Zusammenfassung

CRISPR/Cas9 ermöglicht präzise Modifizierungen am menschlichen Genom und stellt eine potenziell kurative Option für erbliche Netzhauterkrankungen dar. Vorarbeiten zeigen, dass Cas9 Immunreaktionen auslöst, die die Wirksamkeit der Genmodifizierung signifikant beeinträchtigen. Wir vermuten, dass der Plasmid-mediierte Gentransfer und die Expression von Cas9 eine inflammatorische Immunantwort im humanen retinalen Pigmentepithel (RPE) *in vitro* hervorrufen.

Hierzu wurde eine immortalisierte RPE-Zelllinie mit einem eigenständig entwickelten Cas9 codierenden (*sp*Cas9) Plasmid über kationische Lipofektion transfiziert. Die Expression von immunmodulatorischen Oberflächenmarkern sowie die inflammatorische Zytokinkonzentrationen des Zellüberstandes wurden RPE-Zellen gegenübergestellt, die, anstelle des *sp*Cas9 Plasmids, mit einem nicht codierenden (NC) Plasmid transfiziert wurden. Auf diese Weise konnte die Immunogenität des Cas9 beurteilt werden. Um die Immunantwort der RPE-Zellen auf den Plasmid-mediierten Gentransfer zu bestimmen, wurden die oben genannten immunologischen Parameter zusätzlich zwischen Plasmid-transfizierten und nicht-transfizierten RPE-Zellen, die entweder nur den kationischen Lipiden oder den Plasmiden ausgesetzt waren, verglichen.

Die Transfektion des *spCas9* Plasmids induzierte eine signifikante IL-8 Sekretion ($p = 0{,}004$) der RPE-Zellen, was suggeriert, dass die inflammatorische Reaktion der RPE-Zellen entweder durch die Cas9 DNA-Sequenz, die Cas9 mRNA und/oder das Cas9 Protein ausgelöst wurde. Der Zellüberstand Plasmid-transfizierter RPE-Zellen wies, verglichen mit nicht-transfizierten RPE-Zellen, erhöhte IL-6 ($p < 0{,}001$) und IL-8 Spiegel ($p < 0{,}001$) auf. In der FACS Analyse wurde eine erhöhte Expression von HLA-ABC ($p < 0{,}001$) und ICAM-1/CD54 ($p < 0{,}001$) sowie eine reduzierte Viabilitätsrate (85,2 %) des Plasmid-transfizierten RPE detektiert.

Die Daten dieser Studie weisen darauf hin, dass der Plasmid-mediierte Gentransfer von Cas9 ein immunogenes Potenzial besitzt. Es bedarf weiterer Forschung über die Beteiligung von Pattern-Recognition-Rezeptoren und

Signalwege an der Pathogen-Detektion sowie die Auswirkungen der induzierten Immunreaktion auf die Wirksamkeit der Genmodifizierung. Die vorliegenden Ergebnisse sind bedeutsam für die Sicherheit der CRISPR/Cas9-basierten Gentherapie zur möglichen Behandlung erblicher Netzhauterkrankungen.

8 List of publications

Teile der vorliegenden Dissertationsschrift wurden bereits veröffentlicht:

Authors: Bonillo, M.; Pfromm, J.K.; Fischer, M.D.
Title: Challenges to gene editing approaches in the retina
Journal: Klinische Monatsblätter für Augenheilkunde
Year: 2022
Acknowledgement: Reproduced with permission from Thieme.

Authors: Pfromm, J.K.; Bonillo, M.; Dauletbekov, D.; Bucher, K.; Fischer, M.D.
Title: Plasmid-mediated gene transfer of Cas9 induces vector-related but not *Sp*Cas9-related immune responses in human retinal pigment epithelial cells
Journal: Scientific reports
Year: 2022
Acknowledgement: Reproduced with permission from Springer Nature.

9 List of references

Aaij, C. & Borst, P. 1972. The gel electrophoresis of DNA. *Biochimica et Biophysica Acta (BBA)-Nucleic Acids and Protein Synthesis,* 269**,** 192-200.

Abcam. n.d. *Immunocytochemistry and immunofluorescence protocol* [Online]. Available: https://www.abcam.com/protocols/immunocytochemistry-immunofluorescence-protocol [Accessed 17.04.2020].

Ablonczy, Z., Dahrouj, M., Tang, P. H., et al. 2011. Human retinal pigment epithelium cells as functional models for the RPE in vivo. *Investigative ophthalmology & visual science,* 52**,** 8614-8620.

Adamis, A., Shima, D., Yeo, K.-T., et al. 1993. Synthesis and secretion of vascular permeability factor/vascular endothelial growth factor by human retinal pigment epithelial cells. *Biochemical and biophysical research communications,* 193**,** 631-638.

Addgene. n.d.-a. *Agarose gel electrophoresis* [Online]. Available: https://www.addgene.org/protocols/gel-electrophoresis/ [Accessed 19.09.2019].

Addgene. n.d.-b. *DNA ligation* [Online]. Available: https://www.addgene.org/protocols/dna-ligation/ [Accessed 20.09.2019].

Ahmado, A., Carr, A.-J., Vugler, A. A., et al. 2011. Induction of differentiation by pyruvate and DMEM in the human retinal pigment epithelium cell line ARPE-19. *Investigative ophthalmology & visual science,* 52**,** 7148-7159.

Aksünger, A., Or, M., Okur, H., et al. 1997. Role of interleukin 8 in the pathogenesis of proliferative vitreoretinopathy. *Ophthalmologica,* 211**,** 223-225.

Alexopoulou, L., Holt, A. C., Medzhitov, R., et al. 2001. Recognition of double-stranded RNA and activation of NF-κB by Toll-like receptor 3. *Nature,* 413**,** 732-738.

Aliprantis, A. O., Yang, R.-B., Mark, M. R., et al. 1999. Cell activation and apoptosis by bacterial lipoproteins through toll-like receptor-2. *Science,* 285**,** 736-739.

Altogen. n.d. *ARPE-19 Transfection Kit (Retinal Pigment Epithelium)* [Online]. Available: https://altogen.com/product/arpe-19-transfection-reagent-renal-adenocarcinoma/ [Accessed 16.04.2020].

Ansari, A. M., Ahmed, A. K., Matsangos, A. E., et al. 2016. Cellular GFP toxicity and immunogenicity: potential confounders in in vivo cell tracking experiments. *Stem Cell Reviews and Reports,* 12**,** 553-559.

Armbrecht, M. 2013. *Detektion von Kontaminationen in DNA und Protein-Proben durch photometrische Messungen* [Online]. Available: https://www.eppendorf.com/product-media/doc/de/59828/Eppendorf_Detection_Application-Note_279_BioPhotometer-D30_Detection-contamination-DNA-protein-samples-photometric-measurements.pdf [Accessed 13.04.2020].

Armeanu, S., Pelisek, J., Krausz, E., et al. 2000. Optimization of nonviral gene transfer of vascular smooth muscle cells in vitro and in vivo. *Molecular Therapy,* 1**,** 366-375.

Ashander, L. M., Lie, S., Ma, Y., et al. 2019. Neutrophil Activities in Human Ocular Toxoplasmosis: An In Vitro Study With Human Cells. *Investigative ophthalmology & visual science,* 60**,** 4652-4660.

Atcc. n.d. *ARPE-19 (ATCC® CRL-2302™)* [Online]. Available: https://www.lgcstandards-atcc.org/products/all/CRL-2302.aspx?geo_country=de [Accessed 23.09.2019].

Baehr, W., Palczweski, K., Wu, S. M., et al. 2003. The retinoid cycle and retina disease. *Vision research (Oxford),* 43.

Baggiolini, M., Walz, A. & Kunkel, S. 1989. Neutrophil-activating peptide-1/interleukin 8, a novel cytokine that activates neutrophils. *The Journal of clinical investigation,* 84**,** 1045-1049.

Baggiolini, M., Loetscher, P. & Moser, B. 1995. Interleukin-8 and the chemokine family. *International journal of immunopharmacology,* 17**,** 103-108.

Bakondi, B., Lv, W., Lu, B., et al. 2016. In vivo CRISPR/Cas9 gene editing corrects retinal dystrophy in the S334ter-3 rat model of autosomal dominant retinitis pigmentosa. *Molecular Therapy,* 24**,** 556-563.

Ban, Y. & Rizzolo, L. J. 2000. Differential regulation of tight junction permeability during development of the retinal pigment epithelium. *American Journal of Physiology-Cell Physiology,* 279**,** C744-C750.

Barber, G. N. 2011. Innate immune DNA sensing pathways: STING, AIMII and the regulation of interferon production and inflammatory responses. *Current opinion in immunology,* 23**,** 10-20.

Barber, G. N. 2015. STING: infection, inflammation and cancer. *Nature Reviews Immunology,* 15**,** 760-770.

Bauer, S., Kirschning, C. J., Häcker, H., et al. 2001. Human TLR9 confers responsiveness to bacterial DNA via species-specific CpG motif recognition. *Proceedings of the national academy of sciences,* 98**,** 9237-9242.

Bd Biosciences. n.d.-a. *Brilliant stain buffer* [Online]. Available: https://www.bdbiosciences.com/ds/pm/tds/566349.pdf [Accessed 30.04.2020].

Bd Biosciences. n.d.-b. *BD FACSCanto™ II* [Online]. Available: https://www.bdbiosciences.com/en-in/instruments/research-instruments/research-cell-analyzers/facscanto-ii [Accessed 29.04.2020].

Bennett, C. F., Chiang, M.-Y., Chan, H., et al. 1992. Cationic lipids enhance cellular uptake and activity of phosphorothioate antisense oligonucleotides. *Molecular pharmacology,* 41**,** 1023-1033.

Benson, M. T., Shepherd, L., Rees, R. C., et al. 1992. Production of interleukin-6 by human retinal pigment epithelium in vitro and its regulation by other cytokines. *Current eye research,* 11**,** 173-179.

Beutler, B. & Cerami, A. 1989. The biology of cachectin/TNF--a primary mediator of the host response. *Annual review of immunology,* 7**,** 625-655.

Bian, Z.-M., Field, M. G., Elner, S. G., et al. 2018. Distinct CD40L receptors mediate inflammasome activation and secretion of IL-1β and MCP-1 in cultured human retinal pigment epithelial cells. *Experimental eye research,* 170**,** 29-39.

Bianchi, R., Giambanco, I. & Donato, R. 2010. S100B/RAGE-dependent activation of microglia via NF-κB and AP-1: Co-regulation of COX-2 expression by S100B, IL-1β and TNF-α. *Neurobiology of aging,* 31**,** 665-677.

Bibb, C. & Young, R. W. 1974. Renewal of fatty acids in the membranes of visual cell outer segments. *The Journal of cell biology,* 61**,** 327-343.

Biesemeier, A., Kreppel, F., Kochanek, S., et al. 2010. The classical pathway of melanogenesis is not essential for melanin synthesis in the adult retinal pigment epithelium. *Cell and tissue research,* 339**,** 551-560.

Biolegend. n.d. *ELISA MAX™ Standard Set Human IL-8* [Online]. Available: https://www.biolegend.com/en-us/products/human-il-8-elisa-max-standard-5663 [Accessed 26.09.2019].

Biorad. n.d. *Antibody titration* [Online]. Available: https://www.bio-rad-antibodies.com/flow-cytometry-antibody-titration.html [Accessed 30.04.2020].

Birnboim, H. C. & Doly, J. 1979. A rapid alkaline extraction procedure for screening recombinant plasmid DNA. *Nucleic Acids Research,* 7**,** 1513-1523.

Blaauwgeers, H. G., Holtkamp, G. M., Rutten, H., et al. 1999. Polarized vascular endothelial growth factor secretion by human retinal pigment epithelium and localization of vascular endothelial growth factor receptors on the inner choriocapillaris: evidence for a trophic paracrine relation. *The American journal of pathology,* 155**,** 421-428.

Bonillo, M., Pfromm, J. & Fischer, M. D. 2022. Challenges to gene editing approaches in the retina. *Klinische Monatsblätter für Augenheilkunde*.

Booij, J. C., Florijn, R. J., Ten Brink, J. B., et al. 2005. Identification of mutations in the AIPL1, CRB1, GUCY2D, RPE65, and RPGRIP1 genes in patients with juvenile retinitis pigmentosa. *Journal of medical genetics,* 42**,** e67-e67.

Bora, N. S., Gobleman, C. L., Atkinson, J. P., et al. 1993. Differential expression of the complement regulatory proteins in the human eye. *Investigative ophthalmology & visual science,* 34**,** 3579-3584.

Boulton, M. & Wassell, J. 1998. Ageing of the human retinal pigment epithelium. *In:* Coscas, G. & Piccolino, F. C. (eds.) *Retinal Pigment Epithelium and Macular Diseases.* Dordrecht: Springer Netherlands.

Boulton, M. & Dayhaw-Barker, P. 2001. The role of the retinal pigment epithelium: topographical variation and ageing changes. *Eye,* 15**,** 384-389.

Brandstetter, C., Holz, F. G. & Krohne, T. U. 2015. Complement component C5a primes retinal pigment epithelial cells for inflammasome activation by lipofuscin-mediated photooxidative damage. *Journal of Biological Chemistry,* 290**,** 31189-31198.

Brennan, M. A. & Cookson, B. T. 2000. Salmonella induces macrophage death by caspase-1-dependent necrosis. *Molecular microbiology,* 38**,** 31-40.

Brinkmann, V., Reichard, U., Goosmann, C., et al. 2004. Neutrophil extracellular traps kill bacteria. *science,* 303**,** 1532-1535.

Bröker, B., Schütt, C. & Fleischer, B. 2019. Wie erkennen die Immunzellen ein Antigen? . *Grundwissen Immunologie.* Springer Spektrum, Berlin, Heidelberg.

Cao, W., Tombran-Tink, J., Elias, R., et al. 2001. In vivo protection of photoreceptors from light damage by pigment epithelium–derived factor. *Investigative ophthalmology & visual science,* 42**,** 1646-1652.

Chang, Y.-C., Lin, C.-W., Hsieh, M.-C., et al. 2017. High mobility group B1 up-regulates angiogenic and fibrogenic factors in human retinal pigment epithelial ARPE-19 cells. *Cellular Signalling,* 40**,** 248-257.

Chaplin, D. D. 2010. Overview of the immune response. *Journal of allergy and clinical immunology,* 125**,** S3-S23.

Charlesworth, C. T., Deshpande, P. S., Dever, D. P., et al. 2019. Identification of preexisting adaptive immunity to Cas9 proteins in humans. *Nature Medicine,* 25**,** 249-254.

Chaum, E., Winborn, C. S. & Bhattacharya, S. 2015. Genomic regulation of senescence and innate immunity signaling in the retinal pigment epithelium. *Mammalian Genome,* 26**,** 210-221.

Chavakis, T., Bierhaus, A., Al-Fakhri, N., et al. 2003. The pattern recognition receptor (RAGE) is a counterreceptor for leukocyte Integrins a novel pathway for inflammatory cell recruitment. *The Journal of experimental medicine,* 198**,** 1507-1515.

Chen, H., Sun, H., You, F., et al. 2011. Activation of STAT6 by STING is critical for antiviral innate immunity. *Cell,* 147**,** 436-446.

Chen, N., Xia, P., Li, S., et al. 2017. RNA sensors of the innate immune system and their detection of pathogens. *IUBMB life,* 69**,** 297-304.

Chen, X., Han, R., Hao, P., et al. 2018. Nepetin inhibits IL-1β induced inflammation via NF-κB and MAPKs signaling pathways in ARPE-19 cells. *Biomedicine & Pharmacotherapy,* 101**,** 87-93.

Chesnoy, S. & Huang, L. 2000. Structure and function of lipid-DNA complexes for gene delivery. *Annu Rev Biophys Biomol Struct,* 29**,** 27-47.

Chew, W. L., Tabebordbar, M., Cheng, J. K. W., et al. 2016. A multifunctional AAV–CRISPR–Cas9 and its host response. *Nature Methods,* 13**,** 868-874.

Chikhlikar, P., De Arruda, L. B., Agrawal, S., et al. 2004. Inverted terminal repeat sequences of adeno-associated virus enhance the antibody and CD8+ responses to a HIV-1 p55Gag/LAMP DNA vaccine chimera. *Virology,* 323**,** 220-232.

Cho, P. 2013. *The role of microRNAs in the early life human innate immune response.* University of British Columbia.

Cho, S. W., Kim, S., Kim, Y., et al. 2014. Analysis of off-target effects of CRISPR/Cas-derived RNA-guided endonucleases and nickases. *Genome research,* 24**,** 132-141.

Clinicaltrials.Gov. n.d.-a. *Single Ascending Dose Study in Participants With LCA10* [Online]. Available: https://clinicaltrials.gov/ct2/show/NCT03872479?term=NCT03872479&draw=2&rank=1 [Accessed 28.09.2020 2020].

Clinicaltrials.Gov. n.d.-b. *A Study to Evaluate Efficacy, Safety, Tolerability and Exposure After a Repeat-dose of Sepofarsen (QR-110) in LCA10*

(ILLUMINATE) [Online]. Available: https://clinicaltrials.gov/ct2/show/NCT03913143?term=NCT03913143&draw=2&rank=1 [Accessed 28.09.2020 2020].

Clinicaltrials.Gov. n.d.-c. *A Study to Evaluate the Safety and Tolerability of QR-1123 in Subjects With Autosomal Dominant Retinitis Pigmentosa Due to the P23H Mutation in the RHO Gene (AURORA)* [Online]. Available: https://clinicaltrials.gov/ct2/show/NCT04123626?term=NCT04123626&draw=2&rank=1 [Accessed 28.09.2020 2020].

Cong, L., Ran, F. A., Cox, D., et al. 2013. Multiplex genome engineering using CRISPR/Cas systems. *Science,* 339**,** 819-823.

Constable, I. J., Pierce, C. M., Lai, C.-M., et al. 2016. Phase 2a randomized clinical trial: safety and post hoc analysis of subretinal rAAV. sFLT-1 for wet age-related macular degeneration. *EBioMedicine,* 14**,** 168-175.

Courtenay-Luck, N. S., Epenetos, A. A., Moore, R., et al. 1986. Development of primary and secondary immune responses to mouse monoclonal antibodies used in the diagnosis and therapy of malignant neoplasms. *Cancer research,* 46**,** 6489-6493.

Cousins, S., Mccabe, M., Danielpour, D., et al. 1991. Identification of transforming growth factor-beta as an immunosuppressive factor in aqueous humor. *Investigative ophthalmology & visual science,* 32**,** 2201-2211.

Crane, I. J. & Liversidge, J. Mechanisms of leukocyte migration across the blood–retina barrier. Seminars in immunopathology, 2008. Springer, 165-177.

Cromer, M. K., Vaidyanathan, S., Ryan, D. E., et al. 2018. Global transcriptional response to CRISPR/Cas9-AAV6-based genome editing in CD34+ hematopoietic stem and progenitor cells. *Molecular Therapy,* 26**,** 2431-2442.

Crudele, J. M. & Chamberlain, J. S. 2018. Cas9 immunity creates challenges for CRISPR gene editing therapies. *Nature Communications,* 9**,** 3497.

Dawson, D., Volpert, O., Gillis, P., et al. 1999. Pigment epithelium-derived factor: a potent inhibitor of angiogenesis. *Science,* 285**,** 245-248.

Detrick, B. & Hooks, J. J. 2020. The RPE Cell and the Immune System. *In:* Klettner, A. K. & Dithmar, S. (eds.) *Retinal Pigment Epithelium in Health and Disease.* Cham: Springer International Publishing.

Dokka, S., Toledo, D., Shi, X., et al. 2000. Oxygen radical-mediated pulmonary toxicity induced by some cationic liposomes. *Pharmaceutical research,* 17**,** 521-525.

Doyle, S. L., Campbell, M., Ozaki, E., et al. 2012. NLRP3 has a protective role in age-related macular degeneration through the induction of IL-18 by drusen components. *Nature medicine,* 18**,** 791-798.

Duan, Y., Ma, G., Huang, X., et al. 2016. The clustered, regularly interspaced, short palindromic repeats-associated endonuclease 9 (CRISPR/Cas9)-created MDM2 T309G mutation enhances vitreous-induced expression of MDM2 and proliferation and survival of cells. *Journal of Biological Chemistry,* 291**,** 16339-16347.

Dunn, K., Aotaki-Keen, A., Putkey, F., et al. 1996. ARPE-19, a human retinal pigment epithelial cell line with differentiated properties. *Experimental eye research,* 62**,** 155-170.

Dunn, K. C., Marmorstein, A. D., Bonilha, V. L., et al. 1998. Use of the ARPE-19 cell line as a model of RPE polarity: basolateral secretion of FGF5. *Investigative ophthalmology & visual science,* 39**,** 2744-2749.

Ebihara, N., Chen, L., Tokura, T., et al. 2007. Distinct functions between toll-like receptors 3 and 9 in retinal pigment epithelial cells. *Ophthalmic research,* 39**,** 155-163.

Ehrnström, B., Kojen, J. F., Giambelluca, M., et al. 2020. TLR8 and complement C5 induce cytokine release and thrombin activation in human whole blood challenged with Gram-positive bacteria. *Journal of Leukocyte Biology,* 107**,** 673-683.

Elner, S. G., Delmonte, D., Bian, Z.-M., et al. 2006. Differential expression of retinal pigment epithelium (RPE) IP-10 and interleukin-8. *Experimental eye research,* 83**,** 374-379.

Elner, V., Strieter, R., Elner, S., et al. 1990. Neutrophil chemotactic factor (IL-8) gene expression by cytokine-treated retinal pigment epithelial cells. *The American journal of pathology,* 136**,** 745.

Elner, V. M., Burnstine, M. A., Strieter, R. M., et al. 1997. Cell-associated human retinal pigment epithelium interleukin-8 and monocyte chemotactic protein-1: immunochemical and in-situ hybridization analyses. *Experimental eye research,* 65**,** 781-789.

Engvall, E. & Perlmann, P. 1971. Enzyme-linked immunosorbent assay (ELISA) quantitative assay of immunoglobulin G. *Immunochemistry,* 8**,** 871-874.

Enoch, J., Mcdonald, L., Jones, L., et al. 2019. Evaluating whether sight is the most valued sense. *JAMA ophthalmology,* 137**,** 1317-1320.

Eurofins. n.d.-a. *Power read DNA sequencing service* [Online]. Available: https://www.eurofinsgenomics.com/en/products/dna-sequencing/power-reads/ [Accessed 26.04.2020].

Eurofins. n.d.-b. *Mix2Seq* [Online]. Available: https://www.eurofinsgenomics.eu/en/custom-dna-sequencing/eurofins-services/mix2seq/ [Accessed 23.09.2019].

European Medicines Agency. 2018. *New gene therapy for rare inherited disorder causing vision loss recommended for approval* [Online]. Available: https://www.ema.europa.eu/en/news/new-gene-therapy-rare-inherited-disorder-causing-vision-loss-recommended-approval [Accessed 11.08.2020].

Fang, I.-J. & Trewyn, B. G. 2012. Application of mesoporous silica nanoparticles in intracellular delivery of molecules and proteins. *Methods in enzymology.* Elsevier.

Felgner, P. L., Gadek, T. R., Holm, M., et al. 1987. Lipofection: a highly efficient, lipid-mediated DNA-transfection procedure. *Proceedings of the National Academy of Sciences,* 84**,** 7413-7417.

Fernandes-Alnemri, T., Yu, J.-W., Datta, P., et al. 2009. AIM2 activates the inflammasome and cell death in response to cytoplasmic DNA. *Nature,* 458**,** 509-513.

Fink, S. L. & Cookson, B. T. 2005. Apoptosis, pyroptosis, and necrosis: mechanistic description of dead and dying eukaryotic cells. *Infection and immunity,* 73**,** 1907-1916.

Fishman-Lobell, J., Rudin, N. & Haber, J. 1992. Two alternative pathways of double-strand break repair that are kinetically separable and independently modulated. *Molecular and cellular biology,* 12**,** 1292-1303.

Frackman, S., Kobs, G., Simpson, D., et al. 1998. Betaine and DMSO: enhancing agents for PCR. *Promega notes,* 65**,** 27-29.

Frambach, D. A., Roy, C. E., Valentine, J. L., et al. 1989. Precocious retinal adhesion is affected by furosemide and ouabain. *Current eye research,* 8**,** 553-556.

Frey, J. 2019. *Die Wirkung des Tyrosinkinase-Inhibitors Crenolanib auf autoaktive Isoformen der Rezeptortyrosinkinase KIT.* University of Tuebingen.

Frucht, D. M., Fukao, T., Bogdan, C., et al. 2001. IFN-γ production by antigen-presenting cells: mechanisms emerge. *Trends in immunology,* 22**,** 556-560.

Fu, Y., Foden, J. A., Khayter, C., et al. 2013. High-frequency off-target mutagenesis induced by CRISPR-Cas nucleases in human cells. *Nature biotechnology,* 31**,** 822-826.

Fukui, A., Ohta, K., Nishi, H., et al. 2013. Interleukin-8 and CXCL10 expression in oral keratinocytes and fibroblasts via Toll-like receptors. *Microbiology and immunology,* 57**,** 198-206.

Fukuoka, Y., Strainic, M. & Medof, M. 2003. Differential cytokine expression of human retinal pigment epithelial cells in response to stimulation by C5a. *Clinical & Experimental Immunology,* 131**,** 248-253.

Gaforio, J., Serrano, M., Algarra, I., et al. 2002. Phagocytosis of apoptotic cells assessed by flow cytometry using 7-Aminoactinomycin D. *Cytometry: The Journal of the International Society for Analytical Cytology,* 49**,** 8-11.

Geneious. n.d. *Primer design and testing* [Online]. Available: https://www.geneious.com/features/primer-design/ [Accessed 13.04.2020].

Gesser, B., Lund, M., Lohse, N., et al. 1996. IL-8 induces T cell chemotaxis, suppresses IL-4, and up-regulates IL-8 production by CD4+ T cells. *Journal of leukocyte biology,* 59**,** 407-411.

Giese, M. J., Rayner, S. A., Fardin, B., et al. 2003. Mitigation of neutrophil infiltration in a rat model of early Staphylococcus aureus endophthalmitis. *Investigative ophthalmology & visual science,* 44**,** 3077-3082.

Gratz, N., Hartweger, H., Matt, U., et al. 2011. Type I interferon production induced by Streptococcus pyogenes-derived nucleic acids is required for host protection. *PLoS Pathog,* 7**,** e1001345.

Grehn, F. 2019. Retinopathie pigmentosa. *Augenheilkunde.* Springer.

Griffith, T. S., Brunner, T., Fletcher, S. M., et al. 1995. Fas ligand-induced apoptosis as a mechanism of immune privilege. *Science,* 270**,** 1189-1192.

Haapaniemi, E., Botla, S., Persson, J., et al. 2018. CRISPR–Cas9 genome editing induces a p53-mediated DNA damage response. *Nature medicine,* 24**,** 927-930.

Hahn, W. C., Menu, E., Bothwell, A., et al. 1992. Overlapping but nonidentical binding sites on CD2 for CD58 and a second ligand CD59. *Science,* 256**,** 1805-1807.

Hall, M. O., Bok, D. & Bacharach, A. 1969. Biosynthesis and assembly of the rod outer segment membrane system. Formation and fate of visual pigment in the frog retina. *Journal of molecular biology,* 45**,** 397-406.

Hamann, S., La Cour, M., Lui, G. M., et al. 2000. Transport of protons and lactate in cultured human fetal retinal pigment epithelial cells. *Pflügers Archiv,* 440**,** 84-92.

Hangai, M., Kaneda, Y., Tanihara, H., et al. 1996. In vivo gene transfer into the retina mediated by a novel liposome system. *Investigative ophthalmology & visual science,* 37**,** 2678-2685.

Harik, S. I., Kalaria, R. N., Whitney, P. M., et al. 1990. Glucose transporters are abundant in cells with" occluding" junctions at the blood-eye barriers. *Proceedings of the National Academy of Sciences,* 87**,** 4261-4264.

Hartmann, G. & Krieg, A. 1999. CpG DNA and LPS induce distinct patterns of activation in human monocytes. *Gene therapy,* 6**,** 893-903.

He, Z., Proudfoot, C., Whitelaw, C. B. A., et al. 2016. Comparison of CRISPR/Cas9 and TALENs on editing an integrated EGFP gene in the genome of HEK293FT cells. *Springerplus,* 5**,** 814.

Heier, J. S., Kherani, S., Desai, S., et al. 2017. Intravitreous injection of AAV2-sFLT01 in patients with advanced neovascular age-related macular degeneration: a phase 1, open-label trial. *The Lancet,* 390**,** 50-61.

Heil, F., Hemmi, H., Hochrein, H., et al. 2004. Species-specific recognition of single-stranded RNA via toll-like receptor 7 and 8. *Science,* 303**,** 1526-1529.

Hendel, A., Bak, R. O., Clark, J. T., et al. 2015. Chemically modified guide RNAs enhance CRISPR-Cas genome editing in human primary cells. *Nature biotechnology,* 33**,** nbt. 3290.

Hess, C., Means, T. K., Autissier, P., et al. 2004. IL-8 responsiveness defines a subset of CD8 T cells poised to kill. *Blood,* 104**,** 3463-3471.

Holtkamp, G., Kijlstra, A., Peek, R., et al. 2001. Retinal pigment epithelium-immune system interactions: cytokine production and cytokine-induced changes. *Progress in retinal and eye research,* 20**,** 29-48.

Holtkamp, G. M., Van Rossem, M. & De Vos, A. 1998. Polarized secretion of IL-6 and IL-8 by human retinal pigment epithelial cells. *Clinical & Experimental Immunology,* 112**,** 34-43.

Hooks, J. J., Nagineni, C. N., Hooper, L. C., et al. 2008. IFN-β provides immuno-protection in the retina by inhibiting ICAM-1 and CXCL9 in retinal pigment epithelial cells. *The Journal of Immunology,* 180**,** 3789-3796.

Horan, K. A., Hansen, K., Jakobsen, M. R., et al. 2013. Proteasomal degradation of herpes simplex virus capsids in macrophages releases DNA to the cytosol for recognition by DNA sensors. *The Journal of Immunology,* 190**,** 2311-2319.

Hori, O., Brett, J., Slattery, T., et al. 1995. The receptor for advanced glycation end products (RAGE) is a cellular binding site for amphoterin mediation of neurite outgrowth and co-expression of rage and amphoterin in the

developing nervous system. *Journal of biological chemistry,* 270**,** 25752-25761.
Hösel, M., Broxtermann, M., Janicki, H., et al. 2012. Toll-like receptor 2–mediated innate immune response in human nonparenchymal liver cells toward adeno-associated viral vectors. *Hepatology,* 55**,** 287-297.
Hsu, P. D., Scott, D. A., Weinstein, J. A., et al. 2013. DNA targeting specificity of RNA-guided Cas9 nucleases. *Nature biotechnology,* 31**,** 827.
Hughes, B. A., Miller, S. S. & Machen, T. E. 1984. Effects of cyclic AMP on fluid absorption and ion transport across frog retinal pigment epithelium. Measurements in the open-circuit state. *The Journal of general physiology,* 83**,** 875-899.
Hung, S. S., Chrysostomou, V., Li, F., et al. 2016a. AAV-mediated CRISPR/Cas gene editing of retinal cells in vivo. *Investigative ophthalmology & visual science,* 57**,** 3470-3476.
Hung, S. S., Mccaughey, T., Swann, O., et al. 2016b. Genome engineering in ophthalmology: application of CRISPR/Cas to the treatment of eye disease. *Progress in retinal and eye research,* 53**,** 1-20.
Invivogen. n.d.-a. *dsDNA-EC* [Online]. Available: https://www.invivogen.com/dsdna-ec [Accessed].
Invivogen. n.d.-b. *Poly(I:C) HMW* [Online]. Available: https://www.invivogen.com/polyic-hmw [Accessed 25.09.2019].
Invivogen. n.d.-c. *HEK-BlueTM IFN-α/β cells* [Online]. Available: https://www.invivogen.com/sites/default/files/invivogen/old/PDF/HEK_Blue_IFNab_TDS.pdf [Accessed 24.09.2019].
Ishida, K., Panjwani, N., Cao, Z., et al. 2003. Participation of pigment epithelium in ocular immune privilege. 3. Epithelia cultured from iris, ciliary body, and retina suppress T-cell activation by partially non-overlapping mechanisms. *Ocular immunology and inflammation,* 11**,** 91-105.
Ishii, K. J., Kawagoe, T., Koyama, S., et al. 2008. TANK-binding kinase-1 delineates innate and adaptive immune responses to DNA vaccines. *Nature,* 451**,** 725-729.
Ishikawa, H., Ma, Z. & Barber, G. N. 2009. STING regulates intracellular DNA-mediated, type I interferon-dependent innate immunity. *Nature,* 461**,** 788-792.
Iyama, T. & Wilson Iii, D. M. 2013. DNA repair mechanisms in dividing and non-dividing cells. *DNA repair,* 12**,** 620-636.
Iyer, V., Shen, B., Zhang, W., et al. 2015. Off-target mutations are rare in Cas9-modified mice. *Nature methods,* 12**,** 479.
Jacobsen, F., Mertens-Rill, J., Beller, J., et al. 2006. Nucleofection: a new method for cutaneous gene transfer? *BioMed Research International,* 2006.
Jaffe, G. J., Van Le, L., Valea, F., et al. 1992. Expression of interleukin-1α, interleukin-1β, and an interleukin-1 receptor antagonist in human retinal pigment epithelial cells. *Experimental eye research,* 55**,** 325-335.
Jinek, M., Chylinski, K., Fonfara, I., et al. 2012. A Programmable Dual-RNA–Guided DNA Endonuclease in Adaptive Bacterial Immunity. *Science,* 337**,** 816-821.

Jo, D. H., Song, D. W., Cho, C. S., et al. 2019a. CRISPR-Cas9–mediated therapeutic editing of Rpe65 ameliorates the disease phenotypes in a mouse model of Leber congenital amaurosis. *Science advances,* 5**,** eaax1210.

Jo, D. H., Yun, J. H., Cho, C. S., et al. 2019b. Interaction between microglia and retinal pigment epithelial cells determines the integrity of outer blood-retinal barrier in diabetic retinopathy. *Glia,* 67**,** 321-331.

Jonas, J. B., Tao, Y., Neumaier, M., et al. 2012. Cytokine concentration in aqueous humour of eyes with exudative age-related macular degeneration. *Acta ophthalmologica,* 90**,** e381-e388.

Jørgensen, A., Junker, N., Kæstel, C. G., et al. 2001. Superantigen presentation by human retinal pigment epithelial cells to T cells is dependent on CD2–CD58 and CD18–CD54 molecule interactions. *Experimental eye research,* 73**,** 723-733.

Kang, R., Zhu, S., Zeh, H., et al. 2018. The STING-STAT6 pathway drives Cas9-induced host response in human monocytes. *Biochemical and biophysical research communications,* 506**,** 278-283.

Kanuga, N., Winton, H. L., Beauchéne, L., et al. 2002. Characterization of genetically modified human retinal pigment epithelial cells developed for in vitro and transplantation studies. *Investigative ophthalmology & visual science,* 43**,** 546-555.

Karkhur, S., Hasanreisoglu, M., Vigil, E., et al. 2019. Interleukin-6 inhibition in the management of non-infectious uveitis and beyond. *Journal of ophthalmic inflammation and infection,* 9**,** 1-14.

Kauppinen, A., Paterno, J. J., Blasiak, J., et al. 2016. Inflammation and its role in age-related macular degeneration. *Cellular and Molecular Life Sciences,* 73**,** 1765-1786.

Kawasaki, T. & Kawai, T. 2014. Toll-like receptor signaling pathways. *Frontiers in immunology,* 5**,** 461.

Kerur, N., Hirano, Y., Tarallo, V., et al. 2013. TLR-independent and P2X7-dependent signaling mediate Alu RNA-induced NLRP3 inflammasome activation in geographic atrophy. *Investigative ophthalmology & visual science,* 54**,** 7395-7401.

Kerur, N., Fukuda, S., Banerjee, D., et al. 2018. cGAS drives noncanonical-inflammasome activation in age-related macular degeneration. *Nature medicine,* 24**,** 50.

Kielbassa, C., Roza, L. & Epe, B. 1997. Wavelength dependence of oxidative DNA damage induced by UV and visible light. *Carcinogenesis,* 18**,** 811-816.

Kieleczawa, J. 2006. Fundamentals of sequencing of difficult templates—an overview. *Journal of biomolecular techniques: JBT,* 17**,** 207.

Kim, E., Koo, T., Park, S. W., et al. 2017. In vivo genome editing with a small Cas9 orthologue derived from Campylobacter jejuni. *Nature Communications,* 8**,** 14500.

Kimura, S., Matsumiya, T., Shiba, Y., et al. 2018. The Essential Role of Double-Stranded RNA–Dependent Antiviral Signaling in the Degradation of Nonself Single-Stranded RNA in Nonimmune Cells. *The Journal of Immunology,* 201**,** 1044-1052.

Kirsanov, K. I., Lesovaya, E. A., Yakubovskaya, M. G., et al. 2010. SYBR Gold and SYBR Green II are not mutagenic in the Ames test. *Mutation Research/Genetic Toxicology and Environmental Mutagenesis,* 699**,** 1-4.

Kiser, P. D., Golczak, M., Maeda, A., et al. 2012. Key enzymes of the retinoid (visual) cycle in vertebrate retina. *Biochimica et Biophysica Acta (BBA)-Molecular and Cell Biology of Lipids,* 1821**,** 137-151.

Kleinstiver, B. P., Pattanayak, V., Prew, M. S., et al. 2016. High-fidelity CRISPR–Cas9 nucleases with no detectable genome-wide off-target effects. *Nature,* 529**,** 490-495.

Klettner, A., Hamann, T., Schlüter, K., et al. 2014. Retinal pigment epithelium cells alter the pro-inflammatory response of retinal microglia to TLR-3 stimulation. *Acta ophthalmologica,* 92**,** e621-e629.

Kobayashi, Y. 2008. The role of chemokines in neutrophil biology. *Front Biosci,* 13**,** 2400-7.

Koirala, A., Conley, S. M. & Naash, M. I. 2013. A review of therapeutic prospects of non-viral gene therapy in the retinal pigment epithelium. *Biomaterials,* 34**,** 7158-7167.

Kok, C. Y., Cunningham, S. C., Carpenter, K. H., et al. 2013. Adeno-associated virus-mediated rescue of neonatal lethality in argininosuccinate synthetase-deficient mice. *Molecular Therapy,* 21**,** 1823-1831.

Kormann, M. S., Hasenpusch, G., Aneja, M. K., et al. 2011. Expression of therapeutic proteins after delivery of chemically modified mRNA in mice. *Nature biotechnology,* 29**,** 154-157.

Kosmidou, C., Efstathiou, N. E., Hoang, M. V., et al. 2018. Issues with the specificity of immunological reagents for NLRP3: implications for age-related macular degeneration. *Scientific reports,* 8**,** 1-12.

Krieger, M., Brunner, T., Bischoff, S., et al. 1992. Activation of human basophils through the IL-8 receptor. *The Journal of Immunology,* 149**,** 2662-2667.

Kumar, M. V., Nagineni, C. N., Chin, M. S., et al. 2004. Innate immunity in the retina: Toll-like receptor (TLR) signaling in human retinal pigment epithelial cells. *Journal of neuroimmunology,* 153**,** 7-15.

Kumaran, N., Michaelides, M., Smith, A. J., et al. 2018. Retinal gene therapy. *British Medical Bulletin,* 126**,** 13-25.

Kwon, W. & Freeman, S. A. 2020. Phagocytosis by the retinal pigment epithelium: recognition, resolution, recycling. *Frontiers in Immunology***,** 2985.

Labat-Moleur, F., Steffan, A.-M., Brisson, C., et al. 1996. An electron microscopy study into the mechanism of gene transfer with lipopolyamines. *Gene therapy,* 3**,** 1010.

Lakowicz, J. 1999. *Principles of fluorescence spectroscopy. Kluwer Academic, New York,* New York, Springer US.

Larsen, C. G., Anderson, A. O., Appella, E., et al. 1989. The neutrophil-activating protein (NAP-1) is also chemotactic for T lymphocytes. *Science,* 243**,** 1464-1466.

Latella, M. C., Di Salvo, M. T., Cocchiarella, F., et al. 2016. In vivo editing of the human mutant rhodopsin gene by electroporation of plasmid-based CRISPR/Cas9 in the mouse retina. *Molecular Therapy-Nucleic Acids,* 5**,** e389.

Lebedev, A. V., Paul, N., Yee, J., et al. 2008. Hot start PCR with heat-activatable primers: a novel approach for improved PCR performance. *Nucleic acids research,* 36**,** e131-e131.

Lee, J. E., Liang, K. J., Fariss, R. N., et al. 2008. Ex vivo dynamic imaging of retinal microglia using time-lapse confocal microscopy. *Investigative ophthalmology & visual science,* 49**,** 4169-4176.

Lee, P. Y., Costumbrado, J., Hsu, C.-Y., et al. 2012. Agarose gel electrophoresis for the separation of DNA fragments. *JoVE (Journal of Visualized Experiments)***,** e3923.

Leonard, E., Skeel, A., Yoshimura, T., et al. 1990. Leukocyte specificity and binding of human neutrophil attractant/activation protein-1. *The Journal of Immunology,* 144**,** 1323-1330.

Leonard, E. J., Yoshimura, T., Tanaka, S., et al. 1991. Neutrophil recruitment by intradermally injected neutrophil attractant/activation protein-1. *Journal of investigative dermatology,* 96**,** 690-694.

Li, J.-F., Norville, J. E., Aach, J., et al. 2013. Multiplex and homologous recombination–mediated genome editing in Arabidopsis and Nicotiana benthamiana using guide RNA and Cas9. *Nature biotechnology,* 31**,** 688-691.

Li, J., Ma, Z., Tang, Z.-L., et al. 2004. CpG DNA-mediated immune response in pulmonary endothelial cells. *American Journal of Physiology-Lung Cellular and Molecular Physiology,* 287**,** L552-L558.

Li, Q., Miller, R., Han, P.-Y., et al. 2008. Intraocular route of AAV2 vector administration defines humoral immune response and therapeutic potential. *Molecular vision,* 14**,** 1760.

Li, S.-W., Wang, C.-Y., Jou, Y.-J., et al. 2016. SARS coronavirus papain-like protease inhibits the TLR7 signaling pathway through removing Lys63-linked polyubiquitination of TRAF3 and TRAF6. *International journal of molecular sciences,* 17**,** 678.

Liang, X., Potter, J., Kumar, S., et al. 2015. Rapid and highly efficient mammalian cell engineering via Cas9 protein transfection. *Journal of biotechnology,* 208**,** 44-53.

Liao, Y.-R., Li, Z.-J., Zeng, P., et al. 2017. TLR7 deficiency contributes to attenuated diabetic retinopathy via inhibition of inflammatory response. *Biochemical and biophysical research communications,* 493**,** 1136-1142.

Lin, S.-R., Yang, H.-C., Kuo, Y.-T., et al. 2014. The CRISPR/Cas9 system facilitates clearance of the intrahepatic HBV templates in vivo. *Molecular Therapy-Nucleic Acids,* 3**,** e186.

Lino, C. A., Harper, J. C., Carney, J. P., et al. 2018. Delivering CRISPR: a review of the challenges and approaches. *Drug delivery,* 25**,** 1234-1257.

Lipinski, D. M., Thake, M. & Maclaren, R. E. 2013. Clinical applications of retinal gene therapy. *Progress in retinal and eye research,* 32**,** 22-47.

Liu, J. & Shui, S.-L. 2016. Delivery methods for site-specific nucleases: Achieving the full potential of therapeutic gene editing. *Journal of Controlled Release,* 244**,** 83-97.

Liversidge, J., Sewell, H. & Forrester, J. 1988. Human retinal pigment epithelial cells differentially express MHC class II (HLA, DP, DR and DQ) antigens

in response to in vitro stimulation with lymphokine or purified IFN-gamma. *Clinical and experimental immunology,* 73**,** 489.
Liversidge, J., Sewell, H. & Forrester, J. 1990. Interactions between lymphocytes and cells of the blood-retina barrier: mechanisms of T lymphocyte adhesion to human retinal capillary endothelial cells and retinal pigment epithelial cells in vitro. *Immunology,* 71**,** 390.
Losi, A., Bedotti, R., Brancaleon, L., et al. 1993. Porphyrin-melanin interaction: effect on fluorescence and non-radiative relaxations. *Journal of Photochemistry and Photobiology B: Biology,* 21**,** 69-76.
Ludtke, J. J., Sebestyén, M. G. & Wolff, J. A. 2002. The effect of cell division on the cellular dynamics of microinjected DNA and dextran. *Molecular Therapy,* 5**,** 579-588.
Luo, Y., Zhuo, Y., Fukuhara, M., et al. 2006. Effects of culture conditions on heterogeneity and the apical junctional complex of the ARPE-19 cell line. *Investigative ophthalmology & visual science,* 47**,** 3644-3655.
Luster, A. D. 1998. Chemokines—chemotactic cytokines that mediate inflammation. *New England Journal of Medicine,* 338**,** 436-445.
Machitani, M., Sakurai, F., Wakabayashi, K., et al. 2017. Inhibition of CRISPR/Cas9-mediated genome engineering by a type I interferon-induced reduction in guide RNA expression. *Biological and Pharmaceutical Bulletin,* 40**,** 272-277.
Maecker, H. T. & Trotter, J. 2006. Flow cytometry controls, instrument setup, and the determination of positivity. *Cytometry Part A: the journal of the International Society for Analytical Cytology,* 69**,** 1037-1042.
Maeder, M. L. & Gersbach, C. A. 2016. Genome-editing technologies for gene and cell therapy. *Molecular Therapy,* 24**,** 430-446.
Mai, K., Chui, J. J., Di Girolamo, N., et al. 2014. Role of toll-like receptors in human iris pigment epithelial cells and their response to pathogen-associated molecular patterns. *Journal of Inflammation,* 11**,** 20.
Majtner, T. 2015. *Texture-Based Image Description in Fluorescence Microscopy.* PH.D., Masaryk University.
Makhoul, M., Bruyns, C., Edimo, W. S. E., et al. 2012. TNFα suppresses IFNγ-induced MHC class II expression on retinal pigmented epithelial cells cultures. *Acta ophthalmologica,* 90**,** e38-e42.
Mancuso, G., Gambuzza, M., Midiri, A., et al. 2009. Bacterial recognition by TLR7 in the lysosomes of conventional dendritic cells. *Nature immunology,* 10**,** 587-594.
Mandel, M. & Higa, A. 1970. Calcium-dependent bacteriophage DNA infection. *Journal of molecular biology,* 53**,** 159-162.
Mann, C., Anguela, X., Montane, J., et al. 2012. Molecular signature of the immune and tissue response to non-coding plasmid DNA in skeletal muscle after electrotransfer. *Gene Therapy,* 19**,** 1177-1186.
Männistö, M., Rönkkö, S., Mättö, M., et al. 2005. The role of cell cycle on polyplex-mediated gene transfer into a retinal pigment epithelial cell line. *The Journal of Gene Medicine: A cross‐disciplinary journal for research on the science of gene transfer and its clinical applications,* 7**,** 466-476.

Markoulatos, P., Siafakas, N. & Moncany, M. 2002. Multiplex polymerase chain reaction: a practical approach. *Journal of clinical laboratory analysis,* 16**,** 47-51.

Maruyama, T., Dougan, S. K., Truttmann, M. C., et al. 2015. Increasing the efficiency of precise genome editing with CRISPR-Cas9 by inhibition of nonhomologous end joining. *Nature biotechnology,* 33**,** 538-542.

Masuda, I., Matsuo, T., Yasuda, T., et al. 1996. Gene transfer with liposomes to the intraocular tissues by different routes of administration. *Investigative ophthalmology & visual science,* 37**,** 1914-1920.

Max Planck Gesellschaft. n.d. *Arbeitsweise von CRISPR-Cas9* [Online]. Available: https://www.mpg.de/11032932/crispr-cas9-mechanismus [Accessed 03.05.2020].

Medawar, P. B. 1948. Immunity to homologous grafted skin. III. The fate of skin homographs transplanted to the brain, to subcutaneous tissue, and to the anterior chamber of the eye. *British journal of experimental pathology,* 29**,** 58.

Merck Millipore. n.d. *KOD hot start polymerase* [Online]. Available: https://www.sigmaaldrich.com/catalog/product/mm/71086?lang=de&region=DE [Accessed].

Miceli, M. V., Liles, M. R. & Newsome, D. A. 1994. Evaluation of oxidative processes in human pigment epithelial cells associated with retinal outer segment phagocytosis. *Experimental Cell Research,* 214**,** 242-249.

Moreno, A. M., Palmer, N., Alemán, F., et al. 2019. Immune-orthogonal orthologues of AAV capsids and of Cas9 circumvent the immune response to the administration of gene therapy. *Nature biomedical engineering***,** 1-11.

Muerdter, F., Boryń, Ł. M., Woodfin, A. R., et al. 2018. Resolving systematic errors in widely used enhancer activity assays in human cells. *Nature methods,* 15**,** 141.

Müller, M., Lee, C. M., Gasiunas, G., et al. 2016. Streptococcus thermophilus CRISPR-Cas9 systems enable specific editing of the human genome. *Molecular Therapy,* 24**,** 636-644.

Muller, U., Steinhoff, U., Reis, L., et al. 1994. Functional role of type I and type II interferons in antiviral defense. *Science,* 264**,** 1918-1921.

Mullis, K., Faloona, F., Scharf, S., et al. Specific enzymatic amplification of DNA in vitro: the polymerase chain reaction. Cold Spring Harbor symposia on quantitative biology, 1986. Cold Spring Harbor Laboratory Press, 263-273.

Narumi, K., Miyakawa, R., Ueda, R., et al. 2015. Proinflammatory proteins S100A8/S100A9 activate NK cells via interaction with RAGE. *The Journal of Immunology,* 194**,** 5539-5548.

Neefjes, J., Jongsma, M. L., Paul, P., et al. 2011. Towards a systems understanding of MHC class I and MHC class II antigen presentation. *Nature Reviews Immunology,* 11**,** 823-836.

Neta, R., Vogel, S. N., Sipe, J. D., et al. 1988. Comparison of in vivo effects of human recombinant IL 1 and human recombinant IL 6 in mice. ARMED FORCES RADIOBIOLOGY RESEARCH INST BETHESDA MD.

New England Biolabs. n.d.-a. *Alkaline phosphatse, calf intestinal* [Online]. Available: https://www.neb.com/products/m0290-alkaline-phosphatase-calf-intestinal-cip#Protocols,%20Manuals%20&%20Usage [Accessed 20.09.2019].
New England Biolabs. n.d.-b. *NEBcloner: Restriction enzyme double digestion MluI-HF, NsiI-HF* [Online]. Available: http://nebcloner.neb.com/#!/protocol/re/double/NsiI-HF,MluI-HF [Accessed 19.09.2019].
New England Biolabs. n.d.-c. *NEBcloner: Restriction enzyme single digestion BspEI* [Online]. Available: http://nebcloner.neb.com/#!/protocol/re/single/BspEI [Accessed 19.09.2019].
New England Biolabs. n.d.-d. *T4 DNA ligase* [Online]. Available: https://international.neb.com/products/m0202-t4-dna-ligase#Citations%20&%20Technical%20Literature [Accessed 20.09.2019].
New England Biolabs. n.d.-e. *Restriction enzyme digestion* [Online]. Available: https://international.neb.com/applications/cloning-and-synthetic-biology/dna-preparation/restriction-enzyme-digestion [Accessed 19.09.2019].
Newsome, D., Dobard, E., Liles, M., et al. 1990. Human retinal pigment epithelium contains two distinct species of superoxide dismutase. *Investigative ophthalmology & visual science,* 31**,** 2508-2513.
Nguyen, L. T., Atobe, K., Barichello, J. M., et al. 2007. Complex formation with plasmid DNA increases the cytotoxicity of cationic liposomes. *Biological and Pharmaceutical Bulletin,* 30**,** 751-757.
Ogata, N., Wang, L., Jo, N., et al. 2001. Pigment epithelium derived factor as a neuroprotective agent against ischemic retinal injury. *Current eye research,* 22**,** 245-252.
Ozinsky, A., Underhill, D. M., Fontenot, J. D., et al. 2000. The repertoire for pattern recognition of pathogens by the innate immune system is defined by cooperation between toll-like receptors. *Proceedings of the National Academy of Sciences,* 97**,** 13766-13771.
Paeng, S. H., Park, W. S., Jung, W.-K., et al. 2015. YCG063 inhibits Pseudomonas aeruginosa LPS-induced inflammation in human retinal pigment epithelial cells through the TLR2-mediated AKT/NF-κB pathway and ROS-independent pathways. *International journal of molecular medicine,* 36**,** 808-816.
Peddle, C. F. & Maclaren, R. E. 2017. Focus: genome editing: the application of CRISPR/Cas9 for the treatment of retinal diseases. *The Yale journal of biology and medicine,* 90**,** 533.
Perez, V. L. & Caspi, R. R. 2015. Immune mechanisms in inflammatory and degenerative eye disease. *Trends in immunology,* 36**,** 354-363.
Petrovič, M. G., Korošec, P., Košnik, M., et al. 2007. Vitreous levels of interleukin-8 in patients with proliferative diabetic retinopathy. *American journal of ophthalmology,* 143**,** 175-176.
Pfromm, J. K., Bonillo, M., Dauletbekov, D., et al. 2022. Plasmid-mediated gene transfer of Cas9 induces vector-related but not SpCas9-related immune

responses in human retinal pigment epithelial cells. *Scientific reports,* 12**,** 1-14.

Planck, S., Dang, T., Graves, D., et al. 1992. Retinal pigment epithelial cells secrete interleukin-6 in response to interleukin-1. *Investigative ophthalmology & visual science,* 33**,** 78-82.

Planck, S. R., Huang, X.-N., Robertson, J. E., et al. 1993. Retinal pigment epithelial cells produce interleukin-1 β and granulocyte-macrophage colony-stimulating factor in response to interleukin-1α. *Current eye research,* 12**,** 205-212.

Platts, K. E., Benson, M. T., Rennie, I. G., et al. 1995. Cytokine modulation of adhesion molecule expression on human retinal pigment epithelial cells. *Investigative ophthalmology & visual science,* 36**,** 2262-2269.

Pluta, L., Yousefi, B., Damania, B., et al. 2019. Endosomal TLR-8 Senses microRNA-1294 Resulting in the Production of NFκB Dependent Cytokines. *Frontiers in immunology,* 10.

Portillo, J.-a. C., Van Grol, J., Zheng, L., et al. 2008. CD40 mediates retinal inflammation and neurovascular degeneration. *The Journal of Immunology,* 181**,** 8719-8726.

Portillo, J.-a. C., Corcino, Y. L., Miao, Y., et al. 2017. CD40 in retinal Müller cells induces P2X7-dependent cytokine expression in macrophages/microglia in diabetic mice and development of early experimental diabetic retinopathy. *Diabetes,* 66**,** 483-493.

Prager, P., Hollborn, M., Steffen, A., et al. 2016. P2Y1 receptor signaling contributes to high salt-induced priming of the NLRP3 inflammasome in retinal pigment epithelial cells. *PLoS One,* 11**,** e0165653.

Qiagen. 2018. *QIAquick spin handbook* [Online]. Available: https://www.qiagen.com/se/products/discovery-and-translational-research/dna-rna-purification/dna-purification/dna-clean-up/qiaquick-gel-extraction-kit/#resources [Accessed 19.09.2019].

Qiagen. n.d.-a. *Key Steps In Plasmid Purification Protocols* [Online]. Available: https://www.qiagen.com/de/service-and-support/learning-hub/technologies-and-research-topics/plasmid-resource-center/key-steps-in-the-plasmid-purification-protocols/ [Accessed 01.10.19].

Qiagen. n.d.-b. *EndoFree Plasmid Kits* [Online]. Available: https://www.qiagen.com/jp/products/top-sellers/endofree-plasmid-kits/#orderinginformation [Accessed 27.04.2020].

R&D Systems. n.d.-a. *Use of Proteome Profiler Arrays with LI-COR Detection* [Online]. Available: https://www.rndsystems.com/resources/technical/use-proteome-profiler-arrays-li-cor-detection [Accessed 26.09.2019].

R&D Systems. n.d.-b. *Proteome Profiler Human XL Cytokine Array Kit* [Online]. Available: https://www.rndsystems.com/products/proteome-profiler-human-xl-cytokine-array-kit_ary022 [Accessed 26.09.2019].

Rädler, J. O., Koltover, I., Salditt, T., et al. 1997. Structure of DNA-cationic liposome complexes: DNA intercalation in multilamellar membranes in distinct interhelical packing regimes. *Science,* 275**,** 810-814.

Ran, F. A., Hsu, P. D., Lin, C.-Y., et al. 2013. Double nicking by RNA-guided CRISPR Cas9 for enhanced genome editing specificity. *Cell,* 154**,** 1380-1389.

Ran, F. A., Cong, L., Yan, W. X., et al. 2015. In vivo genome editing using Staphylococcus aureus Cas9. *Nature,* 520**,** 186-191.

Reichel, F. F., Dauletbekov, D. L., Klein, R., et al. 2017. AAV8 can induce innate and adaptive immune response in the primate eye. *Molecular Therapy,* 25**,** 2648-2660.

Relvas, L. J. M., Bouffioux, C., Marcet, B., et al. 2009. Extracellular Nucleotides and Interleukin-8 Production by ARPE Cells: Potential Role of Danger Signals in Blood–Retinal Barrier Activation. *Investigative ophthalmology & visual science,* 50**,** 1241-1246.

Renshaw, S. 2017. Immunohistochemistry and Immunocytochemistry. *In:* Renshaw, S. (ed.) *Immunohistochemistry and immunocytochemistry : essential methods.* 2 ed. Chichester, West Sussex, UK: Wilex Blackwell.

Roberts, W. G. & Palade, G. E. 1995. Increased microvascular permeability and endothelial fenestration induced by vascular endothelial growth factor. *Journal of cell science,* 108**,** 2369-2379.

Røkke, G., Korvald, E., Pahr, J., et al. 2014. BioBrick Assembly Standards and Techniques and Associated Software Tools. *In:* Valla, S. & Lale, R. (eds.) *DNA cloning and assembly methods.* Totowa: Humana Press.

Romano, G., Micheli, P., Pacilio, C., et al. 2000. Latest developments in gene transfer technology: achievements, perspectives, and controversies over therapeutic applications. *Stem cells,* 18**,** 19-39.

Romano, M., Sironi, M., Toniatti, C., et al. 1997. Role of IL-6 and its soluble receptor in induction of chemokines and leukocyte recruitment. *Immunity,* 6**,** 315-325.

Rouet, P., Smih, F. & Jasin, M. 1994. Introduction of double-strand breaks into the genome of mouse cells by expression of a rare-cutting endonuclease. *Molecular and cellular biology,* 14**,** 8096-8106.

Ruan, G.-X., Barry, E., Yu, D., et al. 2017. CRISPR/Cas9-mediated genome editing as a therapeutic approach for Leber congenital amaurosis 10. *Molecular Therapy,* 25**,** 331-341.

Russell, S., Bennett, J., Wellman, J. A., et al. 2017. Efficacy and safety of voretigene neparvovec (AAV2-hRPE65v2) in patients with RPE65-mediated inherited retinal dystrophy: a randomised, controlled, open-label, phase 3 trial. *The Lancet,* 390**,** 849-860.

Russell, S. R., Drack, A. V., Cideciyan, A. V., et al. 2020. Results of a phase 1b/2 trial of intravitreal (IVT) sepofarsen (QR-110) antisense oligonucleotide in Leber congenital amaurosis 10 (LCA10) due to p. Cys998X mutation in the CEP290 gene. *Investigative Ophthalmology & Visual Science,* 61**,** 866-866.

Sack, U., Tarnok, A. & Rothe, G. 2006. *Zelluläre Diagnostik: Grundlagen, Methoden und klinische Anwendungen der Durchflusszytometrie; 163 Tabellen*, Karger Medical and Scientific Publishers.

Sakuma, T., Masaki, K., Abe-Chayama, H., et al. 2016. Highly multiplexed CRISPR-Cas9-nuclease and Cas9-nickase vectors for inactivation of hepatitis B virus. *Genes to Cells,* 21**,** 1253-1262.

Sambrook, J., Fritsch, E. F. & Maniatis, T. 1989. *Molecular cloning: a laboratory manual*, Cold spring harbor laboratory press.

Samuel, W., Jaworski, C., Postnikova, O. A., et al. 2017. Appropriately differentiated ARPE-19 cells regain phenotype and gene expression profiles similar to those of native RPE cells. *Molecular vision,* 23**,** 60.

Sanger, F., Nicklen, S. & Coulson, A. R. 1977. DNA sequencing with chain-terminating inhibitors. *Proceedings of the national academy of sciences,* 74**,** 5463-5467.

Schmid, I., Uittenbogaart, C. H. & Giorgi, J. V. 1994. Sensitive method for measuring apoptosis and cell surface phenotype in human thymocytes by flow cytometry. *Cytometry: The Journal of the International Society for Analytical Cytology,* 15**,** 12-20.

Schönbeck, U. & Libby, P. 2001. The CD40/CD154 receptor/ligand dyadRID="†" ID="†" Review. *Cellular and Molecular Life Sciences CMLS,* 58**,** 4-43.

Schroder, K., Hertzog, P. J., Ravasi, T., et al. 2004. Interferon-γ: an overview of signals, mechanisms and functions. *Journal of leukocyte biology,* 75**,** 163-189.

Schumann, J., Ehring, F., Göhde, W., et al. 1971. Impulscytophotometrie der DNS in Hauttumoren. *Archiv für klinische und experimentelle Dermatologie,* 239**,** 377-389.

Sha, W., Mitoma, H., Hanabuchi, S., et al. 2014. Human NLRP3 inflammasome senses multiple types of bacterial RNAs. *Proceedings of the National Academy of Sciences,* 111**,** 16059-16064.

Sigma-Aldrich. 2014. *GenEluteTM plasmid miniprep kit* [Online]. St. Louis: Sigma-aldrich,. Available: https://www.sigmaaldrich.com/content/dam/sigma-aldrich/docs/Sigma/Bulletin/pln70bul.pdf [Accessed 23.09.2019].

Sigma-Aldrich. n.d. *GenElute™ Plasmid Miniprep Kit* [Online]. Available: https://webcache.googleusercontent.com/search?q=cache:1_NCO-z5gQgJ:https://www.sigmaaldrich.com/content/dam/sigma-aldrich/docs/Sigma/Bulletin/pln70bul.pdf+&cd=1&hl=de&ct=clnk&gl=de [Accessed 27.04.2020].

Simhadri, V. L., Mcgill, J., Mcmahon, S., et al. 2018. Prevalence of pre-existing antibodies to CRISPR-associated nuclease Cas9 in the USA population. *Molecular Therapy-Methods & Clinical Development,* 10**,** 105-112.

Singh, P. K., Guest, J.-M., Kanwar, M., et al. 2017. Zika virus infects cells lining the blood-retinal barrier and causes chorioretinal atrophy in mouse eyes. *JCI insight,* 2.

Smith, C., Abalde-Atristain, L., He, C., et al. 2015. Efficient and allele-specific genome editing of disease loci in human iPSCs. *Molecular Therapy,* 23**,** 570-577.

Smith, D., Lee, E. K., Saloupis, P., et al. 1994. Role of neutrophils in breakdown of the blood-retinal barrier following intravitreal injection of platelet-activating factor. *Experimental eye research,* 59**,** 425-432.

Staahl, B. T., Benekareddy, M., Coulon-Bainier, C., et al. 2017. Efficient genome editing in the mouse brain by local delivery of engineered Cas9 ribonucleoprotein complexes. *Nature biotechnology,* 35**,** 431-434.

Stephenson, F. H. 2003. *Calculations for Molecular Biology and Biotechnology : A Guide to Mathematics in the Laboratory,* Amsterdam, Academic Press.
Stratagene. n.d. *XL10-Gold® ultracompetent cells* [Online]. Available: https://www.chem-agilent.com/pdf/strata/200314.pdf [Accessed 20.09.2019].
Strauss, O. 2005. The retinal pigment epithelium in visual function. *Physiological reviews,* 85**,** 845-881.
Streilein, J. W. 1997. Regulation of ocular immune responses. *Eye,* 11**,** 171-175.
Streilein, J. W. 2003. Ocular immune privilege: the eye takes a dim but practical view of immunity and inflammation. *Journal of leukocyte biology,* 74**,** 179-185.
Strieter, R., Kunkel, S., Elner, V., et al. 1992. Interleukin-8. A corneal factor that induces neovascularization. *The American journal of pathology,* 141**,** 1279.
Sun, L., Wu, J., Du, F., et al. 2013. Cyclic GMP-AMP synthase is a cytosolic DNA sensor that activates the type I interferon pathway. *Science,* 339**,** 786-791.
Sung, C.-H., Davenport, C. M., Hennessey, J. C., et al. 1991. Rhodopsin mutations in autosomal dominant retinitis pigmentosa. *Proceedings of the National Academy of Sciences,* 88**,** 6481-6485.
Suzuki, K., Tsunekawa, Y., Hernandez-Benitez, R., et al. 2016. In vivo genome editing via CRISPR/Cas9 mediated homology-independent targeted integration. *Nature,* 540**,** 144-149.
Takeuchi, O., Hoshino, K., Kawai, T., et al. 1999. Differential roles of TLR2 and TLR4 in recognition of gram-negative and gram-positive bacterial cell wall components. *Immunity,* 11**,** 443-451.
Takeuchi, O., Kawai, T., Mühlradt, P. F., et al. 2001. Discrimination of bacterial lipoproteins by Toll-like receptor 6. *International immunology,* 13**,** 933-940.
Tanihara, H., Yoshida, M. & Yoshimura, N. 1992. Tumor necrosis factor-α gene is expressed in stimulated retinal pigment epithelial cells in culture. *Biochemical and biophysical research communications,* 187**,** 1029-1034.
Tao, L., Qiu, Y., Fu, X., et al. 2016. Angiotensin-converting enzyme 2 activator diminazene aceturate prevents lipopolysaccharide-induced inflammation by inhibiting MAPK and NF-κB pathways in human retinal pigment epithelium. *Journal of neuroinflammation,* 13**,** 35.
Taylor, A. W., Streilein, J. W. & Cousins, S. W. 1992. Identification of alpha-melanocyte stimulating hormone as a potential immunosuppressive factor in aqueous humor. *Current eye research,* 11**,** 1199-1206.
Tecan. 2008. *Infinite 200* [Online]. Available: http://lbk.fe.uni-lj.si/ic/wp-content/uploads/2017/09/Tecan_Infinite200.pdf [Accessed 30.06.2020].
Tecan. 2011. *NanoQuant Plate* [Online]. Available: https://ww3.tecan.com/mandant/files/doc/219/NanoQuant_FAQ_Sheet_LayV1.pdf [Accessed 30.06.2020].
Teissier, T. & Boulanger, É. 2019. The receptor for advanced glycation end-products (RAGE) is an important pattern recognition receptor (PRR) for inflammaging. *Biogerontology***,** 1-23.

Thermo Fisher Scientific. n.d.-a. *Overview of ELISA* [Online]. Available: https://www.thermofisher.com/de/de/home/life-science/protein-biology/protein-biology-learning-center/protein-biology-resource-library/pierce-protein-methods/overview-elisa.html [Accessed 03.10.19].

Thermo Fisher Scientific. n.d.-b. *How Cationic Lipid Mediated Transfection Works* [Online]. Available: https://www.thermofisher.com/de/de/home/references/gibco-cell-culture-basics/transfection-basics/gene-delivery-technologies/cationic-lipid-mediated-delivery/how-cationic-lipid-mediated-transfection-works.html [Accessed 24.09.2019].

Thermo Fisher Scientific. n.d.-c. *Lipofectamine 3000 Reagent* [Online]. Available: https://www.thermofisher.com/de/de/home/brands/product-brand/lipofectamine/lipofectamine-3000.html [Accessed 16.04.2020].

Thermo Fisher Scientific. n.d.-d. *Pierce™ TMB Substrate Kit* [Online]. Available: https://www.thermofisher.com/order/catalog/product/34021#/34021 [Accessed 03.10.19].

Thermo Fisher Scientific. n.d.-e. *Lipofectamine LTX with Plus Reagent* [Online]. Available: https://www.thermofisher.com/de/de/home/brands/product-brand/lipofectamine/lipofectamine-ltx-reagent.html [Accessed 16.04.2020].

Truong, D.-J. J., Kühner, K., Kühn, R., et al. 2015. Development of an intein-mediated split–Cas9 system for gene therapy. *Nucleic Acids Research,* 43**,** 6450-6458.

Tseng, W.-C., Haselton, F. R. & Giorgio, T. D. 1999. Mitosis enhances transgene expression of plasmid delivered by cationic liposomes. *Biochimica et Biophysica Acta (BBA)-Gene Structure and Expression,* 1445**,** 53-64.

Tseng, W. A., Thein, T., Kinnunen, K., et al. 2013. NLRP3 inflammasome activation in retinal pigment epithelial cells by lysosomal destabilization: implications for age-related macular degeneration. *Investigative ophthalmology & visual science,* 54**,** 110-120.

U.S. Food and Drug Administration. 2017. *FDA approves novel gene therapy to treat patients with a rare form of inherited vision loss* [Online]. Available: https://www.fda.gov/news-events/press-announcements/fda-approves-novel-gene-therapy-treat-patients-rare-form-inherited-vision-loss [Accessed 11.08.2020].

Van Bilsen, K., Van Hagen, P. M., Bastiaans, J., et al. 2011. The neonatal Fc receptor is expressed by human retinal pigment epithelial cells and is downregulated by tumour necrosis factor-alpha. *British journal of ophthalmology,* 95**,** 864-868.

Van Tendeloo, V. F., Ponsaerts, P. & Berneman, Z. N. 2007. mRNA-based gene transfer as a tool for gene and cell therapy. *Current opinion in molecular therapeutics,* 9**,** 423.

Vercauteren, D., Piest, M., Van Der Aa, L. J., et al. 2011. Flotillin-dependent endocytosis and a phagocytosis-like mechanism for cellular internalization of disulfide-based poly (amido amine)/DNA polyplexes. *Biomaterials,* 32**,** 3072-3084.

Von Lintig, J., Kiser, P. D., Golczak, M., et al. 2010. The biochemical and structural basis for trans-to-cis isomerization of retinoids in the chemistry of vision. *Trends in biochemical sciences,* 35**,** 400-410.

Vugler, A., Carr, A.-J., Lawrence, J., et al. 2008. Elucidating the phenomenon of HESC-derived RPE: anatomy of cell genesis, expansion and retinal transplantation. *Experimental neurology,* 214**,** 347-361.

Wagner, D. L., Amini, L., Wendering, D. J., et al. 2019. High prevalence of Streptococcus pyogenes Cas9-reactive T cells within the adult human population. *Nature medicine,* 25**,** 242-248.

Wang, D., Mou, H., Li, S., et al. 2015. Adenovirus-mediated somatic genome editing of Pten by CRISPR/Cas9 in mouse liver in spite of Cas9-specific immune responses. *Human gene therapy,* 26**,** 432-442.

Wang, H., Yang, H., Shivalila, C. S., et al. 2013. One-step generation of mice carrying mutations in multiple genes by CRISPR/Cas-mediated genome engineering. *Cell,* 153**,** 910-918.

Wang, L., Schmidt, S., Larsen, P. P., et al. 2019. Efficacy of novel selective NLRP3 inhibitors in human and murine retinal pigment epithelial cells. *Journal of Molecular Medicine,* 97**,** 523-532.

Wang, M., Zuris, J. A., Meng, F., et al. 2016. Efficient delivery of genome-editing proteins using bioreducible lipid nanoparticles. *Proceedings of the National Academy of Sciences,* 113**,** 2868-2873.

Wang, S., Sengel, C., Emerson, M. M., et al. 2014a. A gene regulatory network controls the binary fate decision of rod and bipolar cells in the vertebrate retina. *Developmental cell,* 30**,** 513-527.

Wang, X., Moghimi, B., Zolotukhin, I., et al. 2014b. Immune tolerance induction to factor IX through B cell gene transfer: TLR9 signaling delineates between tolerogenic and immunogenic B cells. *Molecular Therapy,* 22**,** 1139-1150.

Wang, Y., Bian, Z.-M., Yu, W.-Z., et al. 2010. Induction of interleukin-8 gene expression and protein secretion by C-reactive protein in ARPE-19 cells. *Experimental eye research,* 91**,** 135-142.

Wantha, S., Alard, J.-E., Megens, R. T., et al. 2013. Neutrophil-derived cathelicidin promotes adhesion of classical monocytes. *Circulation research,* 112**,** 792-801.

Wörnle, M., Merkle, M., Wolf, A., et al. 2011. Inhibition of TLR3-mediated proinflammatory effects by Alkylphosphocholines in human retinal pigment epithelial cells. *Investigative Ophthalmology & Visual Science,* 52**,** 6536-6544.

Wu, W., Tang, L., D'amore, P. A., et al. 2017. Application of CRISPR-Cas9 in eye disease. *Experimental eye research,* 161**,** 116-123.

Wu, Z., Yang, H. & Colosi, P. 2010. Effect of genome size on AAV vector packaging. *Molecular Therapy,* 18**,** 80-86.

Xenopoulos, A. & Pattnaik, P. 2014. Production and purification of plasmid DNA vaccines: is there scope for further innovation? *Expert review of vaccines,* 13**,** 1537-1551.

Yang, I.-H., Wong, J.-H., Chang, C.-M., et al. 2015. Involvement of intracellular calcium mobilization in IL-8 activation in human retinal pigment epithelial cells. *Investigative ophthalmology & visual science,* 56**,** 761-769.

Yang, P., Tyrrell, J., Han, I., et al. 2009. Expression and modulation of RPE cell membrane complement regulatory proteins. *Investigative ophthalmology & visual science,* 50**,** 3473-3481.

Yin, H., Kanasty, R. L., Eltoukhy, A. A., et al. 2014. Non-viral vectors for gene-based therapy. *Nature Reviews Genetics,* 15**,** 541-555.

Yin, H., Song, C.-Q., Dorkin, J. R., et al. 2016. Therapeutic genome editing by combined viral and non-viral delivery of CRISPR system components in vivo. *Nature biotechnology,* 34**,** 328-333.

Yoshimura, T., Matsushima, K., Tanaka, S., et al. 1987. Purification of a human monocyte-derived neutrophil chemotactic factor that has peptide sequence similarity to other host defense cytokines. *Proceedings of the National Academy of Sciences,* 84**,** 9233-9237.

Zangi, L., Lui, K. O., Von Gise, A., et al. 2013. Modified mRNA directs the fate of heart progenitor cells and induces vascular regeneration after myocardial infarction. *Nature biotechnology,* 31**,** 898-907.

Zetsche, B., Volz, S. E. & Zhang, F. 2015. A split-Cas9 architecture for inducible genome editing and transcription modulation. *Nature Biotechnology,* 33**,** 139-142.

Zhou, J., He, S., Zhang, N., et al. 2010. Neutrophils compromise retinal pigment epithelial barrier integrity. *Journal of Biomedicine and Biotechnology,* 2010.

Zhou, R. & Caspi, R. R. 2010. Ocular immune privilege. *F1000 biology reports,* 2.

Zuris, J. A., Thompson, D. B., Shu, Y., et al. 2015. Cationic lipid-mediated delivery of proteins enables efficient protein-based genome editing in vitro and in vivo. *Nature biotechnology,* 33**,** 73-80.

10 Appendix

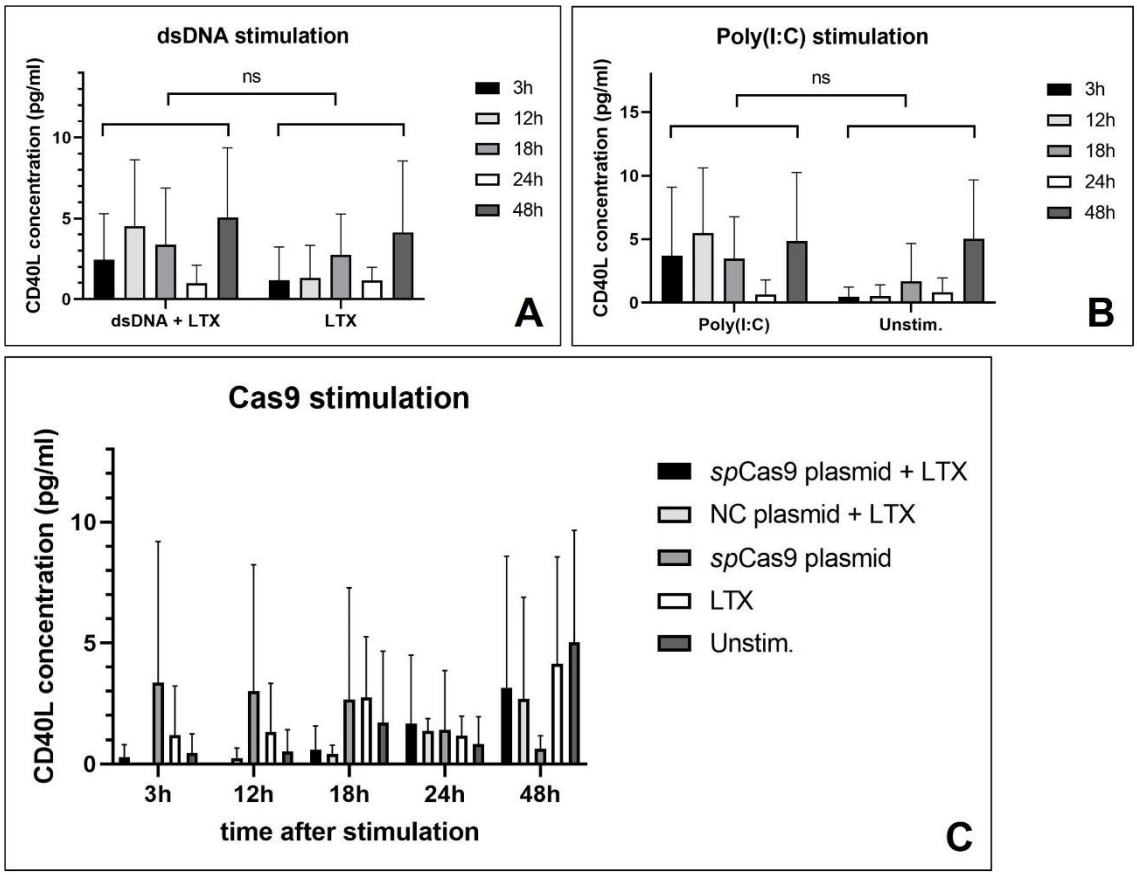

Suppl. 1: CD40L concentration after Cas9, dsDNA and Poly(I:C) stimulation on ARPE-19 cells.

The figure shows CD40L supernatant concentrations of dsDNA (A), Poly(I:C) (B) and Cas9 (C) stimulated ARPE-19 cells compared to controls. CD40L levels were measured at five different time points after stimulation (3 h, 12 h, 18 h, 24 h, and 48 h) by an ELISA. Neither dsDNA, Poly(I:C) nor Cas9 resulted in an increased CD40L release. The bars represent mean values, and the error bars show standard deviations of three independent experiments. (n=3, *t*-test (A,B), Kruskal-Wallis-test and pairwise comparisons (C), ns = not significant)

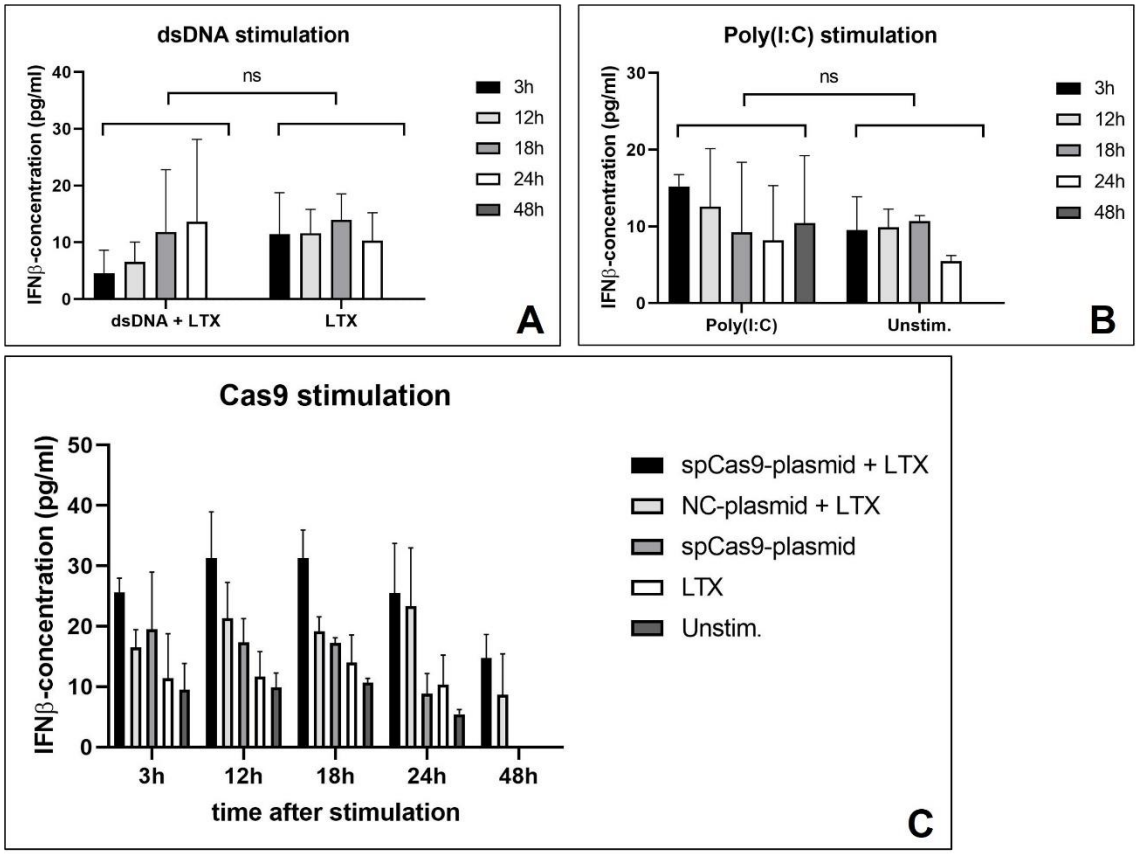

Suppl. 2: IFN-β concentration after Cas9, dsDNA and Poly(I:C) stimulation on ARPE-19 cells.

DsDNA (A), Poly(I:C) (B) and Cas9 (C) stimulation did not induce a significant IFN-β release of ARPE-19 cells when compared to control groups. IFN-β levels were measured at five different time points after stimulation (3 h, 12 h, 18 h, 24 h, and 48 h) using an ELISA. The bars represent mean values, and the error bars represent standard deviations of three independent experiments. (n=3, *t*-test (A,B), Kruskal-Wallis-test and pairwise comparisons (C), ns = not significant)

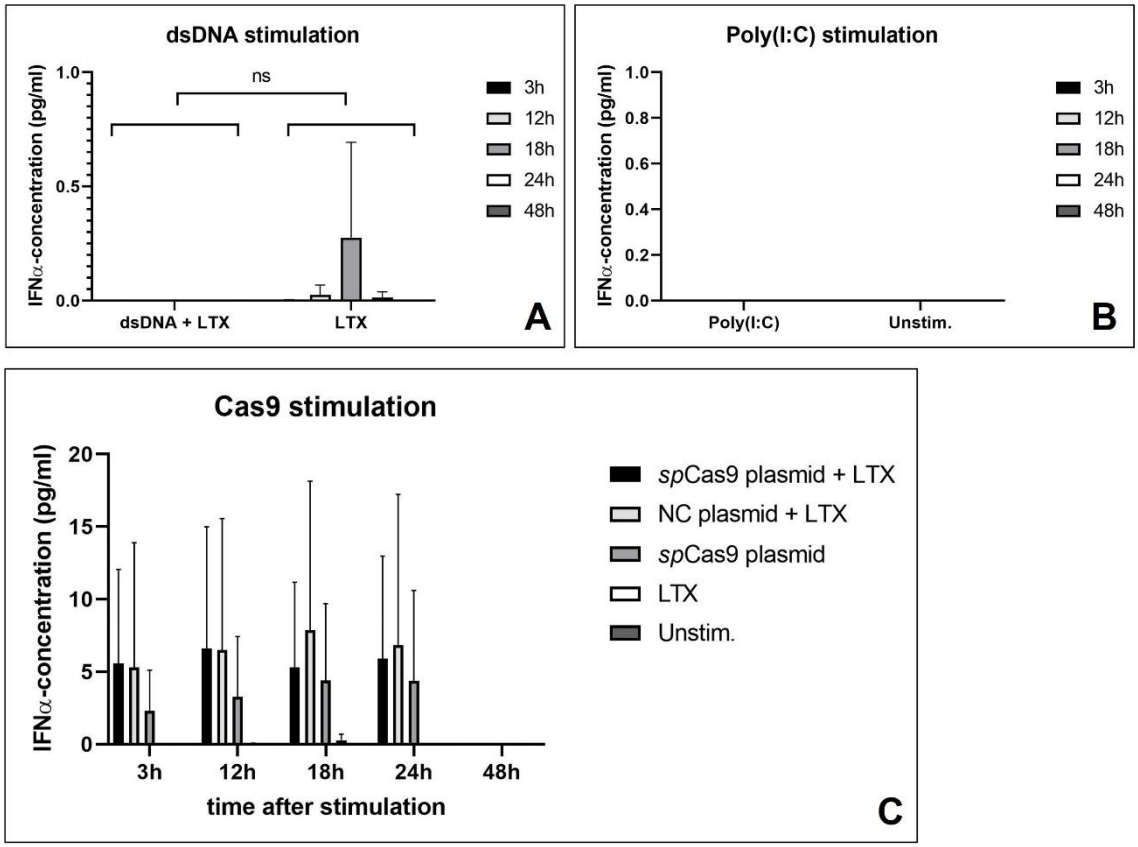

Suppl. 3: IFN-α concentration after Cas9, dsDNA and Poly(I:C) stimulation on ARPE-19 cells.

The figure displays IFN-α supernatant levels of dsDNA (A), Poly(I:C) (B) and Cas9 (C) stimulated ARPE-19 when compared to control groups. IFN-α concentrations were determined at 3 h, 12 h, 18 h, 24 h, and 48 h post-stimulation by an ELISA. None of the three stimulants triggered a significant IFN-α release. The bars represent mean values, and the error bars represent standard deviations of three independent experiments. (n=3, Mann-Whitney *U* test (A,B), Kruskal-Wallis-test and pairwise comparisons(C), ns = not significant)

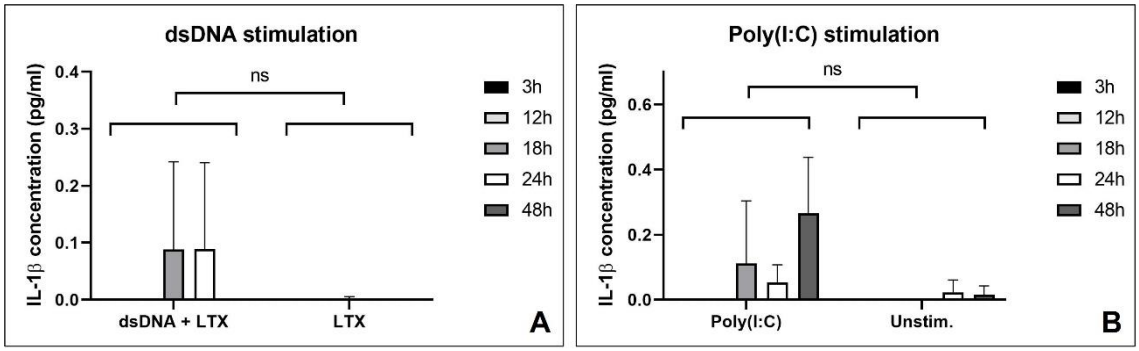

Suppl. 4: IL-1β concentration after dsDNA and Poly(I:C) stimulation on ARPE-19 cells.

ARPE-19 cells did not secrete significant levels of IL-1β in response to dsDNA (A) and Poly(I:C) (B) stimulation when compared to control groups. IL-1β levels were assessed at five different time points after stimulation (3 h, 12 h, 18 h, 24 h, and 48 h) using an ELISA. The bars show mean values, and the error bars represent standard deviations of three independent experiments. (n=3, Mann-Whitney *U* test (A,B), ns = not significant)

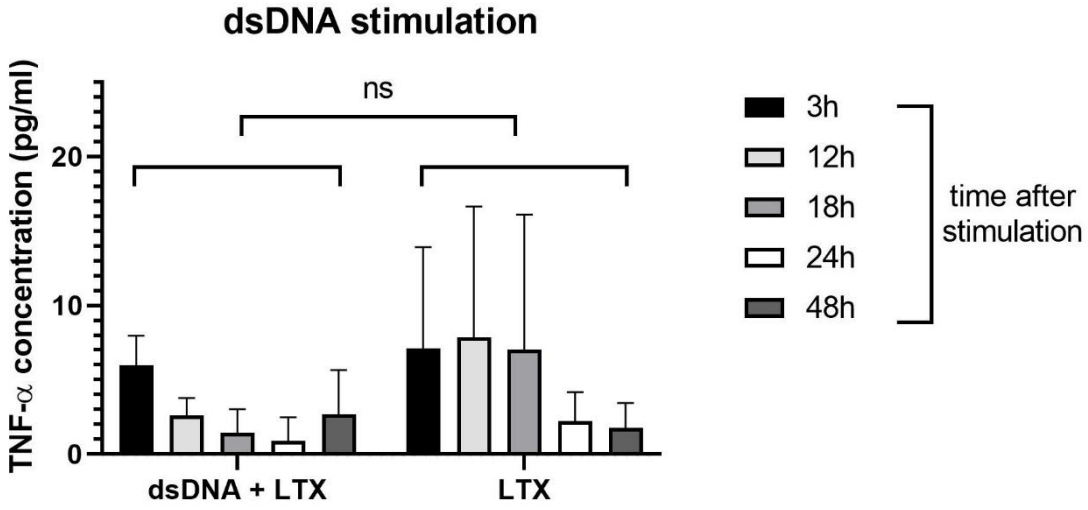

Suppl. 5: TNF-α concentration after dsDNA stimulation on ARPE-19 cells.

The figure displays TNF-α supernatant concentrations of dsDNA stimulated ARPE-19 compared to a control group (LTX). TNF-α levels were measured at five different time points after stimulation (3 h, 12 h, 18 h, 24 h, and 48 h). Poly(I:C) stimulation did not trigger an increased TNF-α release. Data are representative of three independent experiments. The bars show mean values, and the error bars represent standard deviations. (n=3, *t*-test, ns = not significant)

11 Erklärung zum Eigenanteil

Die Arbeit wurde am Forschungsinstitut für Augenheilkunde in Tübingen unter Betreuung von Frau Dr. Kirsten Bucher, Herrn Dr. Daniyar Dauletbekov und Herrn Prof. Dr. Dr. M. Dominik Fischer durchgeführt.
Die Konzeption der Studie erfolgte in Zusammenarbeit mit Frau Dr. Kirsten Bucher, Herrn Dr. Daniyar Dauletbekov und Herrn Prof. Dr. Dr. M. Dominik Fischer.

Sämtliche Versuche wurden von mir eigenständig durchgeführt. Allein die FACS-Analyse mittels FACSCanto und FlowJo wurde in Zusammenarbeit mit Frau Dr. Kristin Bieber (Core Facility Flow Cytometry, Universitätsklinikum Tübingen) und Frau Dr. Kirsten Bucher durchgeführt.

Die statistische Auswertung erfolgte nach Beratung durch Herrn Prof. Dr. Peter Martus (Institut für Klinische Epidemiologie und angewandte Biometrie, Tübingen) durch mich.

Ich versichere, das Manuskript selbstständig verfasst zu haben und keine weiteren als die von mir angegebenen Quellen verwendet zu haben.

Die Publikation, die Teile dieser Doktorarbeit enthält, wurde zusammen mit Frau Julia Pfromm unter Anleitung von Herrn Prof. Dr. Dr. M. Dominik Fischer selbständig verfasst. Die Korrektur des Manuskriptes erfolgte ebenfalls durch Herrn Prof. Dr. Dr. M. Dominik Fischer.

Tübingen, den 17.02.2022

12 Danksagung

An dieser Stelle möchte ich allen beteiligten Personen meinen großen Dank aussprechen, die mich bei der Anfertigung meiner Dissertation unterstützt haben.

Mein besonderer Dank gilt Herrn Prof. Dr. Dr. M. Fischer für die ausgezeichnete Betreuung und hilfreiche Unterstützung bei der Umsetzung der gesamten Arbeit.

Außerdem möchte ich mich bei meinen Kollegen Dr. Kirsten Bucher, Julia Pfromm, Oksana Faul, Dr. Daniyar Dauletbekov und Eduardo Rodríguez Bocanegra für die exzellente Zusammenarbeit bedanken.

Auch möchte ich Dr. Kristin Bieber (Core Facility Flow Cytometry, Universitätsklinikum Tübingen) meinen Dank aussprechen, die mich insbesondere bei meinen FACS-Experimenten hervorragend unterstützt hat. Für die methodische Beratung möchte ich mich bei Prof. Dr. Peter Martus (Institut für Klinische Epidemiologie und angewandte Biometrie, Tübingen) herzlich bedanken.

Meiner Familie, meiner Freundin und meinen Freunden danke ich für ihre Geduld und Ermutigungen während der Arbeit an meiner Dissertation.